UAlg

UNIVERSIDADE DO ALGARVE

Searching for continental related sediment in Algarve continental shelf sedimentary record as a tool to identify tsunami deposits

Jacqueline Santos

Master in Marine and Coastal Systems

Faro

(2022)

UAlg

UNIVERSIDADE DO ALGARVE

Searching for continental related sediment in Algarve continental shelf sedimentary record as a tool to identify tsunami deposits

Jacqueline Santos

Master in Marine and Coastal Systems

Supervisor: Dra. Teresa Drago (IPMA, IDL)

Profª Dra. Delminda Moura (UALG, CIMA)

Faro

(2022)

Declaração de autoria de trabalho / Declaration of Authorship of work

Searching for continental related sediment in Algarve continental shelf sedimentary record as a tool to identify tsunami deposits

Declaro ser a autora deste trabalho, que é original e inédito. Autores e trabalhos consultados estão devidamente citados no texto e constam da listagem de referências incluída.

I declare to be the author of this work, which is original and unpublished. Authors and works consulted are duly cited in the text and are included in the list of references.

_____

Jacqueline Santos

Faro, 24 of February 2022

Copyright

A Universidade do Algarve reserva para si o direito, em conformidade com o disposto no Código do Direito de Autor e dos Direitos Conexos, de arquivar, reproduzir e publicar a obra, independentemente do meio utilizado, bem como de a divulgar através de repositórios científicos e de admitir a sua cópia e distribuição para fins meramente educacionais ou de investigação e não comerciais, conquanto seja dado o devido crédito ao autor e editor respetivos.

The University of Algarve reserves the right, in accordance with the provisions of the Code of the Copyright Law and related rights, to file, reproduce and publish the work, regardless of the used mean, as well as to disseminate it through scientific repositories and to allow its copy and distribution for purely educational or research purposes and non-commercial purposes, although be given due credit to the respective author and publisher.

Acknowledgment

Abstract

Records of earthquakes and associated tsunamis are particularly important in a tectonic active zone as it is Portugal, especially the Algarve coast. Studies of geological records allow assessing the information about undocumented tsunami events beyond a wider time frame than historical records. Most of the existing studies are focused especially on onshore deposits but in later years, offshore studies were developed, regarding their better preservation. In this scope, this work aims to add a new proxy to the results of the subtask WP2.2 of the ASTARTE project which the object was to characterize tsunami deposits at continental shelf sedimentary record off Quarteira-Faro coast. The objective of the present work is identify continental related sediments, that may likely to be transported by tsunami backwash. Detailed studies of the texture and sand mineralogical composition of the Algarve coastal zone and of some previously determined potential "high energy events" layers defined in the scope of the subtask WP2.2 in ASTARTE project (core MW107) were performed and compared. Two types of sand mineralogical compositions were identified in both studied layers and in coastal sites, in particular, those from Vale do Lobo and Forte Novo cliffs. They were named "iron-coated quartz", and "orange clay aggregates". Their presence in the ASTARTE defined layers coincides with the increased mean grain-size, molluscs, and the lower or absence of mica in these layers, which with other proxies data resulting from ASTARTE project (subtask WP2.2) support the related tsunami nature. Although only the topwards layer (Layer 4) coincides with the known 1755 Lisbon tsunami, the Layer 3 and Layer 1 might be potentially related to a high energy event. Future work should aim to study the sand mineralogical composition of the entire core to define the background sedimentation and confirm if the variations of continental related material from the local coastal areas are associated to high energy events. In addition, its also suggested to study more cores from the ASTARTE project (subtask WP2.2) for lateral correlation and it is further recommended to date above and below the layers of potential high energy events, to determine if the material was deposit immediately after the event or if it is the result of subsequent remobilization and transport in the inner shelf.

Keywords: Tsunami deposits offshore; continental shelf; historical tsunamis events; sand mineralogical composition; Algarve

Resumo Alargado

Os registos de terramotos e tsunamis são particularmente importantes numa zona tectónicamente activa como é Portugal, e particularmente no caso da costa algarvia. No entanto, estender esses registos para além de um período de tempo mais alargado do que os registos históricos, só é possível se se recorrer ao registo geológico. A maior parte dos estudos realizados têm sido em depósitos litorais, mas nos últimos anos foram estudados registos sedimentares da plataforma continental e de maiores profundidades atendendo à sua melhor preservação.

A maioria dos estudos de depósitos tsunami estão concentrados em terra, especialmente devido à proximidade na recolha das amostras, embora seja mais susceptível de modificação (por exemplo, erosão, acção antrópica), comparado com uma melhor preservação e continuidade daqueles localizados no mar. A identificação de depósitos de tsunami é uma tarefa difícil, sendo que a melhor abordagem é a existência de um estudo multidisciplinar envolvendo vários tipos de análises, nomeadamente, sedimentológicas, geoquímicas, geofísicas e paleontológicas.

A presente dissertação vem no seguimento do trabalho efetuado no projeto ASTARTE (subtarefa WP2.2) (2013-2015) cujo objetivo era precisamente a identificação e caracterização de eventos de tsunami com base no estudo do registo sedimentar da plataforma continental do sul de Portugal (Algarve). O estudo efetuado durante o projeto possibilitou a identificação de possíveis níveis compatíveis com eventos de alta energia para os quais é necessário efetuar um estudo mais detalhado. Esses níveis foram definidos no projeto ASTARTE através de assinaturas sedimentológicas, como a variação na distribuição do tamanho dos grãos; geoquímica (XRF) e por parâmetros magnéticos que sugeriram um regime de sedimentação de alta energia. Neste âmbito, este trabalho visa precisamente adicionar mais alguma informação há já existente, tendo por objeto de estudo, uma sondagem da plataforma continental amostrada ao largo da costa de Faro-Quarteira a uma profundidade de cerca de 57 m, numa zona de sedimentos finos. Nesta sondagem tinham sido definidos 4 níveis, que no presente trabalho foram nomeados da base para o topo como Layer 1, Layer 2, Layer 3 e Layer 4. De referir ainda que os níveis definidos foram estendidos em 5 cm para profundidades abaixo e acima, com o objetivo de se detetar alguma diferença entre o nível definido e o resto da sondagem (background). Esta extensão dos níveis definidos, está referida como 5 cm abaixo e 5 cm acima. Foi então realizado uma análise detalhada da textura e composição mineralógica da areia do troço costeiro localizado entre Faro e Armação da Pêra, com o objetivo de pesquisar a existência de um indicador terrígeno comum presente nos sedimentos desta zona e dos níveis referidos acima. Partiu-se do princípio que a existência deste indicador mineralógico na sondagem em estudo poderia estar relacionado com o transporte do continente para a plataforma por ondas de retorno de tsunamis.

De uma maneira geral, os sedimentos da zona costeira estudada (arribas, dunas e praias) são constituídos maioritamente por sedimentos terrígenos, com a predominância de quartzo, quartzo com pátina de ferro e agregados de argila alaranjada. Com base nestes resultados, foram definidos como indicadores continentais, os componentes mineralógicos, nomeados como "quartzo com pátina de ferro" e "agregados alaranjados", especialmente presentes nas arribas de Vale do Lobo e Forte Novo. Estes indicadores foram encontrados posteriormente na sondagem, nos níveis acima referidos principalmente nos níveis 1 e 3. O

nível 1 apresentou o "quartzo com pátina de ferro" em diversas profundidades, enquanto o nível 3 apresentou "agregados alaranjados", num menor número de profundidades porém com maior representatividade, até cerca de 24% da amostra total no nível a 32 cm.

Se se adicionar estes resultados aos obtidos com os resultantes das análises efetuadas no projeto ASTARTE (subtarefa WP2.2), nomeadamente, o aumento da média granulométrica, o aumento de um input terrrígeno dado pela relação Fe/Ca, enriquecimento em moluscos e aumento da percentagem de mica no topo dos níveis definidos reforça a hipótese de se estar em presença de depósitos relacionados com eventos de alta energia.

De acordo com as datações obtidas por AMS C^{14} parece haver uma clara relação entre o nível 4 e o tsunami de Lisboa de 1755, o que já foi colocado em evidência no trabalho de Kümmerer et al. (2020). Quanto aos níveis 1 e 3 acima referidos, estes estão datados de 4155 e 3348 e de 1461 e 806. Apesar de não existir registo histórico de tsunami nessas datas, o nível 1 foi datado num período similar a uma unidade possivelmente relacionada a um evento de alta energia desconhecido ao sudoeste de Portugal nos trabalhos de Reicherter et al., 2019, Bellanova et al., 2019 e Feist et al., 2020.

Os resultados obtidos nessa dissertação suportam a hipótese que, dos 4 níveis definidos pela subtarefa WP2.2 no projeto ASTARTE, 3 poderão estar possívelmente associados a eventos de alta energia, sendo um deles compatível em idade com o tsunami de 1755.

Os resultados mostraram ainda que, o estudo da composição mineralógica da areia das zonas costeiras, permitiu apoiar a hipótese da existência de um transporte de material do continente para a plataforma continental, o que juntamente com os dados resultantes do projeto ASTARTE (subtarefa WP2.2) apoia a ideia de se estar em presença de níveis relacionados com eventos de alta energia. No entanto, a identificação e caracterização de depósitos de tsunami "offshore" tem sempre inerente algumas incertezas, ao contrário de estudos "onshore". Como sugestão, sugere-se que em futuros trabalhos, aquilo que se fez, que foi estender a análise mineralógica realizada 5 centímetros acima e abaixo, se estenda a toda a sondagem, para melhor confirmar se os aumentos verificados existem efetivamente e unicamente nos níveis observados ou se acontecem em mais níveis. Outra proposta, está relacionada com a importância de estudar mais sondagens da subtarefa WP2.2 do projeto ASTARTE, para observar se existe variação da composição mineralógica em diferentes profundidades e confirmar a existência de material transportado da zona costeira durante eventos de alta energia para a plataforma continental. Igualmente, sugere-se a realização de mais datações, nomeadamente dos níveis acima e abaixo dos níveis estudados, para assim compreender se o material foi depositado imediatamente após o transporte ou se é o resultado de remobilizações.

Palavras chave: Depósitos de tsunami offshore; plataforma continental; eventos históricos tsunamis; composição mineralógica da areia; Algarve

Contents

List of Figures

List of Tables

LIST OF ABBREVIATIONS

ASTARTE   European Project Assessment, Strategy, and Risk Reduction for Tsunamis in Europe

ADL   ASTARTE defined layers

ICQ   Iron-coated quartz

MSCL   Multisensor core logger

OCA   Orange clay aggregates

NI   Non identified

XRD   X-ray diffraction

XRF   X-ray fluorescence

MW   Mower

BCE   Before Commom Era

CE   Common Era

1.INTRODUCTION

Tsunamis are high energy events that cause damages to coastal areas in several ways. In addition to the devastating effects on the coast, they also impact the livelihoods of the local habitants. The effects of several tsunami events around the world, such as the 2004 Indian Ocean Tsunami, the 2009 South Pacific Tsunami and the 2011 Tohoku-Oki Tsunami, have increased worldwide interest in the cause of the destruction of these events and led to an increase in studies of tsunami impacts.

Portugal is a region susceptible to earthquakes that can generate tsunamis due to the proximity of the Eurasian and African plate boundaries, named by Azores-Gibraltar (Bezzeghoud and Borges, 2003). Major earthquakes in Portugal have been caused by seismic activity generated in the Southwest Iberian Margin, including the 1755 earthquake (Zitellini et al., 2004). The documented records of tsunami events are only available until a certain time frame, and only the study of the geological record can provide access to information over a wider time frame than the documented records. Therefore, understanding the sedimentological tsunami signatures is relevant to access information about the magnitude and time interval of these events (Dawson and Shi, 2000).

The majority of tsunami based geological evidence studies are still broadly made onshore, especially because of the proximal availability of sites, although it is more susceptible to modification (e.g. erosion, anthropic action), contrasting with a better preservation and continuity of those located offshore (Dawson and Stewart, 2008). In the coastal areas of Portugal, geological evidence of tsunamigenic depositions of 1755 Lisbon Tsunami have been detected by several authors in different localizations such as Boca do Rio (Dawson et al., 1995; Hindson and Andrade, 1999; Costa et al., 2012; Font et al., 2013; Vigliotti et al., 2019; Feist et al., 2019), Martinhal (Kortekass and Dawson, 2007) Salgados lowland (Costa et al., 2012; Costa et al., 2016; Moreira et al., 2017), and Ria Formosa (Andrade et al., 2004). The number of studies contrast with few studies dedicated to the identification and characterization of tsunami deposits in the continental shelf sedimentary record (Abrantes et al., 2008; Quintela et al., 2016; Kümmerer et al., 2020, Feist et al., 2020).

The present work follows the results of a previous project on tsunamis in the Northeast Atlantic and Mediterranean (NEAM), entitled "Assessment, Strategy, and Risk Reduction

for Tsunamis in Europe (ASTARTE)" (EU project - FP7-ENV2013 6.4-3, no. 603839) aimed to achieve a higher level of tsunami resilience in the NEAM region. One of the sub-tasks of the work package 2 – Long term recurrence of tsunami (WP2.2) was focused on search for past tsunami events based on the continental shelf sedimentary record study in an attempt to contribute to the assessment of the long-term recurrence of these events in the northeast Atlantic region. Six sediment cores located off the Algarve coast were analyzed using different methodologies, including X-ray core imaging, photo, magnetic analysis (magnetic susceptibility), sedimentological analysis (grain size, carbonates, and organic matter) and geochemical analysis (X-ray fluorescence). This study identified, for each studied core, some layers that may correspond, eventually, to high energy events with the necessity of further studies to confirm this hypothesis. In this scope, the focus of the present work is to study in detail the 4 layers detected in the core Mower 107 (MW107), aiming to search for evidence of terrigenous material transported from the coast to the continental shelf that could be related to tsunami backwash.

1.2. Objectives

The layers potentially related with high energy events identified in the MW107 core of Algarve continental shelf sedimentary record by the ASTARTE project sub-task WP2.2 needed a more detailed investigation in order to be confirmed (or not). Therefore, this thesis aims to search for evidence of terrigenous material transported from the continent to the continental shelf based on the sand mineralogical composition between the defined layers and the coastal sediments from Faro-Armação da Pêra section.

The work herein is related with the knowledge that tsunami backwash can transport large amounts of sediment from coastal areas towards offshore. Ergo, the recognition of specific continental related material in the continental shelf sedimentary record is an complementary approach, to add to other multiproxies for the identification of tsunami deposits in continental shelf sedimentary records.

Overall, this thesis aims to answer the following questions: i) Is there any mineralogical proxy that could be used as an indicator of coastal material contribution? ii) And is it possible to detect this proxy in the studied core, transported from the coast by high energy events? iii) And finally, how to know that these events could be tsunami related?

2. LITERATURE REVIEW

2.1 Historical Tsunami events in Portugal

Portugal has been affected by several seismic events over the years due to its proximity to the boundary between the Eurasian and African Plates, known as Azores-Gibraltar fracture. The region of the SW Iberian margin shows an important seismic activity (Zitellini et al., 2004) and is responsible for the origin of the main earthquakes that occurred off the coast in Portugal (Baptista and Miranda, 2009). In Portugal, most of the studies have been focused on investigating the seismic sources of these events, as well the hydrodynamics and effects of the tsunami inundation (Baptista et al., 1998a; Baptista et al., 2007; Zitellini et al., 2001; Omira et al., 2011; Ramalho et al., 2018). Several extreme historic wave events were reported in the coastal areas of Portugal (Table 1), but the confirmation and magnitude of some events are still under contention (Baptista and Miranda, 2009).

Table 1. Information about tsunami events in Portugal. n.i.- non-identified. Calibrated Ages (years): BCE-Before Common Era; AD-Anno Domini. Table adapted from Baptista and Miranda (2009). Intensity based on Papadopoulos and Imamura scale (2001). Realiability scale: 0 (tsunami not realizable), 4 (tsunami verified). u.n. – unknown.

Date	Source Location		Tsunami Intensity	Reliability of the event
	Lat (N)	Lon(E)		
60 BCE	36.00	-10.70	VII	3
382 CE	36.00	-09.50	VI	3
January 26, 1531	38.90	-09.00	VII	4
December 27, 1722	37.02	-07.48	VI	4
November 1, 1755	36.70	-09.80	XI	4
November 16, 1755	43.40	-11.00	III	2
March 29, 1756	38.70	-9.20	III	2
March 31, 1761	34.50	-13.00	XI	4
December 18, 1926	38.70	-9.20	IV	4
November 18, 1929	44.50	-56.30	II	4
March 4, 1930	32.65	-16.97	VIII	4
November 25, 1941	37.42	-19.01	II	4
February 28, 1969	36.01	-10.57	III	4
July 17, 1969	u.n.	u.n.	II	4
May 26, 1975	35.90	-17.50	II	4

According to the historical records of Portugal, referred to in the catalogue (Baptista and Miranda, 2009), the earliest event was in 60 BCE. Brito (1597, in Andrade et al., 2016) and Mendonça (1758, in Baptista and Miranda, 2009) have described this event as a remarkable earthquake that affected the coastal areas of Portugal and Galicia. However, the information about this event is limited. The intensity attributed to this tsunami event was VII (Baptista and Miranda, 2009), and the location of the epicenter was postulated to have derived off the Portuguese coast (Moreira, 1988 in Baptista et al., 1998a).

The 382 CE earthquake and tsunami have a lack of information regarding the effects of this event. The tsunami intensity attributed to this event was VI (Baptista and Miranda, 2009). Andrade et al. (2016), in a study of the sedimentological evidence of tsunamis in the coastal area of the Algarve (Portugal), suggested dismissing the events of 60 BCE and 382 from the tsunami catalogues due to the absence of detailed information in the historical records.

Observations in January of 1531 reported that the earthquake caused floods in the riverbanks of Tagus, destruction in Spain and Morocco, and more than 1000 fatalities in Lisbon (Galbis, 1932). This event has attributed an intensity of VII, which is classified as an event that can cause severe damages (Baptista and Miranda, 2009). Mendonça, (1758 in Abrantes et al., 2008), described this event even more catastrophic than the 1755 Lisbon tsunami. The modelling study by Miranda et al. (2012), suggested the Vila Franca de Xira fault as a possible source of the earthquake and the tsunami controversy as described by Galbis (1932), that the tsunami only affected boats inside the estuary.

On December 27, 1722, the Algarve, Lisbon, and Seville was impacted by an earthquake (Baptista and Miranda, 2007). A study couple of multichannel seismic processes and tsunami modelling, proposed magnitude of $Mw = 6.5$ and that the epicentre was located close to the Algarve shore in the submarine area (Baptista et al., 2007). However, there is no specific evidence that this earthquake generated a tsunami.

The tsunami of November 1, 1755 was described by several authors as the most destructive event in Europe (Baptista et al., 1998b). The estimated magnitude of the earthquake by Solares and Aroyo (2004), is $Mw = 8.5 \pm 0.3$. Estimated tsunami parameters suggested that the tsunami waves were higher than 10 m in the southwest of Portugal (Cape of São Vicente) and 15 m in Cadiz, Spain (Baptista et al., 1998b). Several sources for the

earthquake event have been discussed (Baptista et al., 1998b; Zitellini et al., 2001; Omira et al., 2009; Ramalho et al., 2018), and it is most often suggested in the southwest of continental Portugal. Baptista and Miranda (2009), classified this event as a devastating tsunami with intensity XI, and is considered the strongest event in Europe.

The effects of the 1761 CE earthquake were felt in Portugal, United Kingdom, Ireland, and other areas besides (Baptista and Miranda, 2009). The magnitude of this earthquake was proposed through the historical information and backward ray tracing methods as magnitude around 8.5 and it is considered that the tsunami caused destruction in the Portuguese coast (Baptista et al., 2006; Baptista and Miranda, 2009).

Andrade et al. (2016) studied the stratigraphical and chronological evidence of high energy events to confirm the flooding events that affected the Algarve coast. The results of this study suggested reviewing the intensities attributed to the tsunami events of 1722 and 1761, and that the 60 BCE and 382 CE tsunami events should be excluded from the tsunami catalogues. The recent tsunami events of 1926, 1929, 1930, 1941, 1969, and 1975 were detected by the tide gauge stations in the Portuguese coastal areas and were classified with intensities of II, III and IV, which were lower compared to the historical tsunamis, except the event of 1930 (Baptista and Miranda, 2009). The intensities from I to IV are not associated with damage (Papadopoulos and Imamura, 2001).

2.2. State of art tsunami proxies in the geologica9l record offshore

After the 2004 Indian Ocean tsunami, the 2009 South Pacific Tsunami and the 2011 Tohoku-Oki Tsunami, the interest in tsunami events evolved due to their destructive nature. Thereby, the number of publications on different aspects of tsunamis began to increase (Feldens et al., 2009; Srinivasalu et al., 2010; Sakuna et al., 2012; Milker et al., 2013; Veerasingam et al., 2014). The identification of tsunami deposits offshore is not an easy task. Several studies have explored a wide variety of methods and proxies to investigate and identify related tsunami layers in the sedimentary continental shelf cover (Table 2). Among them, we can include variations in textural and composition of the sediments (Abrantes et al., 2008; Smedile et al., 2011; Sakuna et al., 2012), statistical variations, such as calibration of the sediments (Sakuna et al., 2012; Tyuleneva et al., 2018), geochemical elements (Tyuleneva et al., 2018; Riou et al., 2020b), seismic profiles (Riou et al., 2020b), foraminifera associations (Pilarczyk et al., 2020), allochthonous material, such as shells

(Toyofuku et al., 2014; Puga-Bernabéu and Aguirre, 2017) or foraminifera (Quintela et al., 2016), quartz microtextural analysis (e.g. Kümmerer et al., 2020), magnetic properties (van den Bergh et al., 2003; Veerasingam et al., 2004; Abrantes et al., 2008; Kümmerer et al., 2020), X-rays of the sedimentary core (Noda et al., 2007; Ikehara et al., 2014), and Biomarkers, such as n-alkanes and polycyclic aromatic hydrocarbons (Bellanova et al., 2019).

Indeed, the texture of the offshore tsunami deposits are usually characterized by coarser grain-size (Veerasingam et al., 2014, Tyuleneva et al., 2018) in a fining up sequence (van den Bergh et al., 2003; Goodman-Tchernov et al., 2009) related with the decrease of hydrodynamic energy during the tsunami layer deposition, which allows the particles in suspension to settle down (Jagodziński et al., 2009). Noda et al. (2007) found a decrease of very fine sand which is transported offshore, in a study off Hokkaido Island (Japan). The aforementioned authors investigated the tsunami hydrodynamics using a numerical model coupled with grain-size analysis.

Sediment sorting can be a helpful tsunami proxy as the majority of the tsunami deposits are classified as poorly sorted (Feldens et al., 2009; Paris et al., 2010; Sakuna et al., 2012; Tamura et al., 2015; Tyuleneva et al., 2018) with large amounts of reworked marine fossils from shallow areas and intraclastic materials (Cita et al., 1996; Abrantes et al., 2008) or well sorted (Ikehara et al., 2021). These variations make this statistical parameter only a supporting indicator of tsunami related deposits (Costa et al., 2021).

Sand mineralogical composition can also provide evidence of continental material (e.g., quartz, mica, feldspar, etc.) which indicates backwash processes (Ikehara et al., 2014) in offshore sediments. In addition, heavy mineral studies have been conducted to identify sediment sources and paleodynamics (Coalala, 2013). Due to the particularity of their properties, heavy minerals have become proxies for distinguishing tsunami deposition processes. In sandy tsunami layers, heavy minerals help to identify the boundaries of the sedimentary sequence because they are usually present at the base of the tsunami deposits (Morton et al., 2007) and mica at the top of tsunami deposits due to shape and suspended transport (Jagodziński et al., 2009). Costa et al. (2012) applied microtextured characteristics of the quartz grains to identify the percussion marks in the sediments provident from the tsunami event. In tsunami deposits, v-shaped patterns are usually found, showing the high energy involved in the hydrodynamics before the deposition. The lower the sediment

concentration is, in a turbulent flow, the deeper the marks and fresh surfaces, while high sediment concentrations express an increase in percussion marks (Costa et al., 2012). In the study of Kümmerer et al. 2020, microtextural analysis showed the increase of fresh surface and percussion mark in the tsunami samples compared to pre and post tsunami samples.

The dynamics of tsunami backwash can transport and deposit shells and microfossils from nearshore to offshore (Smedile et al., 2011; Toyofuku et al., 2014). Van den Bergh et al. (2003), studying a shallow marine embayment in Java, found significant shell fragments and carbonates derived from inland erosion. In addition, Feldens et al. (2009) detected a tsunami layer event in the Indian Ocean in 2004 through the presence of biogenic material such as grass and wood at Cape Pakarang. In Augusta Bay, multidisciplinary approach helped uncover tsunamigenic evidence by identifying epiphytic benthic foraminifera and increased grain size in the sedimentological record (Smedile et al., 2019).

The study of the geochemical composition of the sediments facilitates the interpretation of the source of sedimentary deposition in the offshore tsunami deposits, such as detecting allochthonous material (Tyuleneva et al., 2018). Gràcia et al. (2010) performed XRF-scan to measure the elements K, Ca, and Ti in turbidites in the deep-sea offshore Algarve waters to characterize detrital and biogenic deposition in turbidites. However, to characterize tsunami deposits, some ratios can be used (Chagué-Goff et al., 2017). Ti/Ca ratio is used to determine the characteristics of the sedimentary environment, which can be terrestrial or marine (Sakuna et al., 2012; Smedile et al., 2019; Riou et al., 2020a), and Ti/Sr ratio is often used, because the increase in marine sources is expressed by an increase in Sr (Cuven et al., 2013; Smedile et al., 2019). Later, Riou et al. (2020b) found the backwash deposits from the 2009 South Pacific tsunami and the 1960 Great Chile Tsunami with increased Ti/Ca ratio in the sedimentary section of the cores. Higher magnetic susceptibility values in tsunami deposits were also associated with layers enriched in volcanic rock fragments from inland with sediments of volcanic origin (van Den Bergh et al., 2003; Smedile et al., 2011). However, Abrantes et al. (2008) found a relationship between magnetic susceptibility and the deposition of reworked material from the tsunami event. In this study, Fe mimics the magnetic susceptibility while Ca had a similar pattern as the mean grain-size (Abrantes et al., 2008).

An approach applied by Bellanova et al. (2019), was the study of biomarkers such as n-alkanes and polycyclic aromatic hydrocarbons (PAHs) offshore Algarve in order to identify tsunami deposit. The results of this study revealed an increase in PAHs and n-alkanes (terrigenous material) related to the 1755 Lisbon tsunami.

Table 2 summarized some of the existing works dedicated to the offshore tsunami related deposits study with the following data: location, tsunami event, depth of the core location and methodology performed.

Table 2. List of some studies of the performed worldwide in order to identify and characterize continental shelf tsunami deposits.

Location (Country and Region)		Tsunami name and date	Depth (m)	Methodology	Reference
Pacific Ocean	Pago Pago Bay	Several events	15-60	Geophysics; Core description; Grain-size;	Riou et al. (2020a)
Pacific Ocean	Pago Pago Bay	2009 South Pacific Tsunami and 1960 Great Chilean Earthquake Tsunami	15-60	Geophysics; Grain-size; Digital image; XRF (Ti/Ca ratio);	Riou et al. (2020b)
India	Nagapattina	2004 Indian Ocean Tsunami	25	Grain-size; CaCO$_3$; Atomic Adsorption Spectrometer	Srinivasalu et al. (2010)
India	Nagapattina	2004 Indian Ocean Tsunami	5-10	Grain-size; Magnetic Susceptibility; Fourier Transformation Infrared Spectrometry	Veerasingam et al. (2014)
Indonesia	Teluk Banten	1883	2-30	Grain-size; X-ray; XRF; Magnetic Susceptibility;	van den Bergh et al. (2003)
Indonesia	Lhok Nga	2004 Indian Ocean Tsunami	<25	Boulder distribution offshore; Modelling	Paris et al. (2010)
Israel	Caesarea	-1550	15-20	Grain-size; Micropaleontology	Goodman-Tchernov et al. (2009)
Israel	Caesarea	Several events	3-15	Seismic survey	Goodman-Tchernov and Austin (2015)
Israel	Off Jisr al-Zarka	Several events	15.3	Grain-size; Fourier Transformation Infrared Spectrometry; X-Ray Diffraction; XRF; mineralogical	Tyuleneva et al. (2018)
Italy	Augusta Bay	Several events	72	Grain-size; X-ray imaging; Magnetic Susceptibility; Foraminifera; Geophysics;	Smedile et al. (2011)

Table 2: (cont.).

Location (Country and Region)		Tsunami name and date	Depth (m)	Methodology	Reference
Italy	Augusta Bay	Several events	60-110	X-ray; XRF, Grain-size, Micropaleontological; Magnetic Susceptibility	Smedile et al. (2019)
Japan	Hokkaido	2003 Tokachi-oki	38-112	Grain-size; Sedimentary Structure; Microfossil (Diatom, Foraminifera); Geophysical; XRD; Modelling.	Noda et al. (2007)
Japan	Sendai Bay	2011 Tohoku-Oki	122	Sediment composition; Mud content; XRD; Total Organic Carbon; C/N	Ikehara et al. (2014)
Japan	Off Shimokita	2011 Tohoku-Oki	55-211	Grain-size; Foraminifera; Organic Matter (C/N, biomarkers, Chl a)	Toyofuku et al. (2014)
Japan	Sendai Bay	2011 Tohoku-Oki	14-30	Grain-size; XRD	Tamura et al. (2015)
Japan	Kujukuri	Several events	120	Grain-size; Foraminifera; Organic Matter (C/N, biomarkers, Chl a); Sedimentary structure	Pilarczyk et al. (2020)
Portugal	Off Lisbon	1755 CE Lisbon Tsunami and 1969 CE	72	Grain-size; XRF; Magnetic Susceptibility	Abrantes et al. (2008)
Portugal	Off Algarve	1755 CE Lisbon Tsunami	96	Grain-size; Foraminifera; ; $CaCO_3$	Quintela et al. (2016)
Portugal	Off Algarve	1755 CE Lisbon Tsunami and potential event 3700 cal BP	50 – 300	Grain-size; Magnetic Susceptibility; Geophysics XRF; Biomarkers; Micropaleontology	Bellanova et al. (2019)
Portugal	Off Algarve	1755 CE Lisbon Tsunami	56-90	^{14}C and ^{210}Pb; Sediment Composition; Microtextural of the Quartz grains; Statistical analysis	Kümmerer et al. (2020)
Thailand	Khao Lak	2004 Indian Ocean Tsunami	10-70	Geophysics; Grain-size	Feldens et al. (2009)
Thailand	Khao Lak	2004 Indian Ocean Tsunami	9-57	Geophysics; Grain-size; MSCL; XRF; Magnetic Susceptibility;	Sakuna et al. (2012)
Thailand	Khao Lak	2004 Indian Ocean Tsunami	10-64	Structural description; Foraminifera	Milker et al. (2013)
Thailand	Khao Lak	2004 Indian Ocean Tsunami	9-15.3	Grain-size; Ti/Ca	Sakuna-Schwartz et al. (2015)

2.3. Tsunami mechanisms

Tsunami waves are generated by such mechanisms resultant from earthquakes, landslides, volcanic eruptions, and extra-terrestrial impacts (Dawson and Stewart, 2007). The tsunami event is separated into 4 main stages: (i) wave generation, (ii) propagation, (iii) inundation of the land area, and (iv) backwash, which can carry the eroding continental material (Li et al., 2013). The wavelength can extend hundreds of kilometers until it reaches shallow waters, where the tsunami wave can rise several meters and inundate inland areas (Ward, 2010). Tsunami mechanisms are responsible for changes in the geomorphology of the area, such as erosion and sediment accumulation (Figure 1). It suggests that the material associated with the offshore tsunami deposits may vary according to the erosional processes occurring in the coastal regions and during the propagation of the tsunami along the continental shelf and shelf edges (Le Roux and Vargas, 2005; Dawson and Stewart, 2007). For this reason, the backwash may include mixtures of various sedimentary components, such as terrestrial material, plant remains, and anthropogenic detritus from the coastal areas (Dawson and Shi, 2000; Goodman-Tchernov et al., 2009). Relatively, the backwash flow of the tsunami wave is a strong ocean current that transports and reworked sediments and, depending on the coastal topography, can reach different velocities (Hindson and Andrade, 1999; Dawson and Stewart, 2007). Thus, backwash flows can cause the accumulation of allochthonous material in offshore deposits (Paris et al., 2010), which is also susceptible to modification and erosion of the post-event deposition (Einsele et al., 1996). Backwash has been studied because it leaves significant changes in geomorphology and sedimentary structures (Le Roux and Vargas, 2005).

Some authors have attempted to determine the dynamic of the tsunami through the characteristics of the deposits. Indeed, some work on offshore tsunamis are based on foraminiferal studies. These can provide insight into sediment transport, velocity flux, and post depositional processes (Mamo et al., 2009). Tsunami waves can transport foraminifera to an unnatural environment and potentially rework or break these species, so a study of these microfossils coupled with a function for water depth it is possible to reconstruct the dynamics of the sedimentary distribution associated with tsunami deposits (Milker et al., 2013). Moreover, foraminifera species from intertidal zones were found in offshore sediment samples by Quintela et al. (2016), likely transported offshore by tsunami backwash.
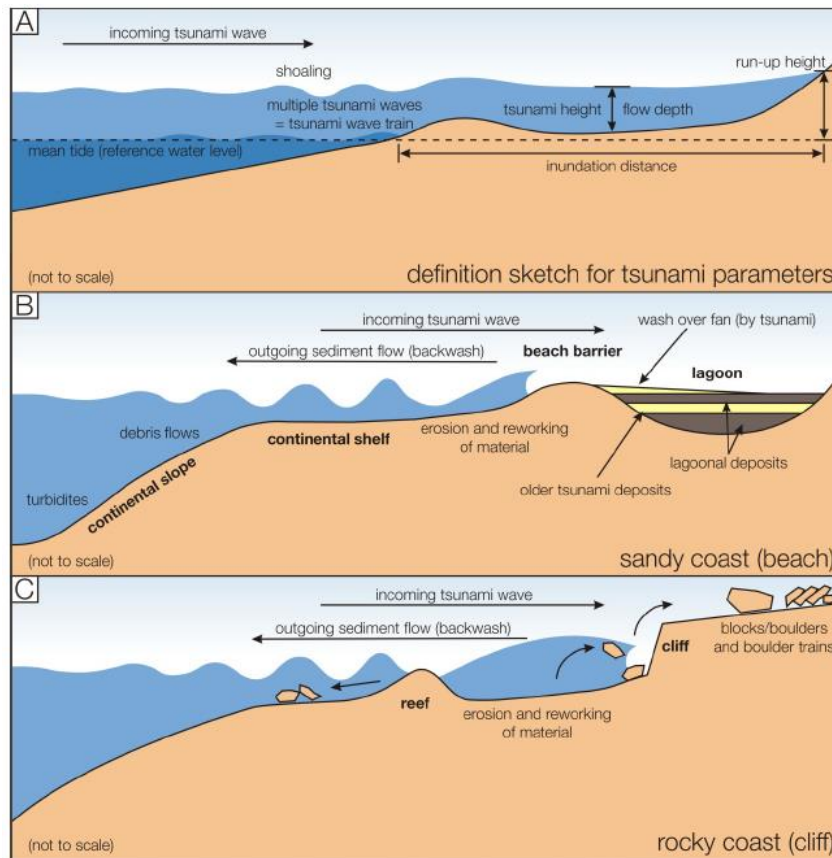
Figure 1. Conceptual tsunami model of sedimentation process. (A) A general definition of tsunami deposits. (B) Tsunami deposits in sandy coast; (C) Tsunami deposits in rock coasts (Koster, 2014).

2.4. The differentiation of tsunami deposits from other high energy events

Although offshore tsunamis and storms have different physical characteristics, both are capable of transporting and depositing sand layers. The differentiation of tsunami deposits from storm deposits is not a simple task because of the similarities in the deposits of these events. However, there are some differences, for example, storm deposits usually have better sorting than tsunami deposits, even if both are usually poorly sorted (Sakuna-Schwartz et al., 2015). Several studies have been conducted to differentiate between storm-associated and tsunami deposits (e.g., Morton et al., 2007; Ikehara et al., 2014; Sakuna-Schwartz et al., 2015). The difference between tsunami and storm deposits is related to wave dynamics. Tsunamis flow at depths greater than 10 m, while storm surges flow gradually at depths less than 3 m (Morton et al., 2007). Some authors differentiated the storms or flood to the tsunami deposits by the access of meteorological data (e.g., Veeransigam et al., 2014 and Ikehara et al., 2014). Ikehara et al. (2014), differentiated the 2011 Tohoku-Oki tsunami from storm as there was no data of significant storm or flood events at that time. Puga-Bernabéu and Aguirre (2017) found the differences between the high energy events through the study of the shell beds. In this study, tsunami deposits were

11

characterized by chaotic orientation with sharp fragments, while the storm deposited shells were horizontally distributed with rounded fragments. Tsunamis can distribute suspended sediments over a wide area. In contrast, storms transport sediments by traction and deposit the sediments close to the beach (Morton et al., 2007). Weiss and Bahburg (2006) have proposed theories based on linear waves to understand the depth where tsunami deposits are protected from storm waves, comparing the impact of tsunami and storm waves with the seafloor. They concluded that tsunami deposits are preserved at depths greater than 65 m, which means that in shallow water, tsunami deposits can be reworked by storm waves.

3. FRAMEWORK OF THE STUDY AREA

3.1. Geology and Geomorphology of the Algarve coastal area

The Algarve Basin is located in the Mesocenozoic terrains on the southern margin of Portugal, from Cape St. Vincent to the Guadiana River, composed of 3000 m of sediments based irregularly inland over the carboniferous terrains of the Portuguese zone (Terrinha et al., 2006). The sedimentary filling of the Algarve Basin occurred through several depositional stages related to tectonic events in association with the sea level variations (e.g.Terrinha et al., 2006). The earliest sediments are Triassic (Figure 2), and the Ludo formation represented the late filling of the basin during the post Miocene period (Moura and Boski, 1994).
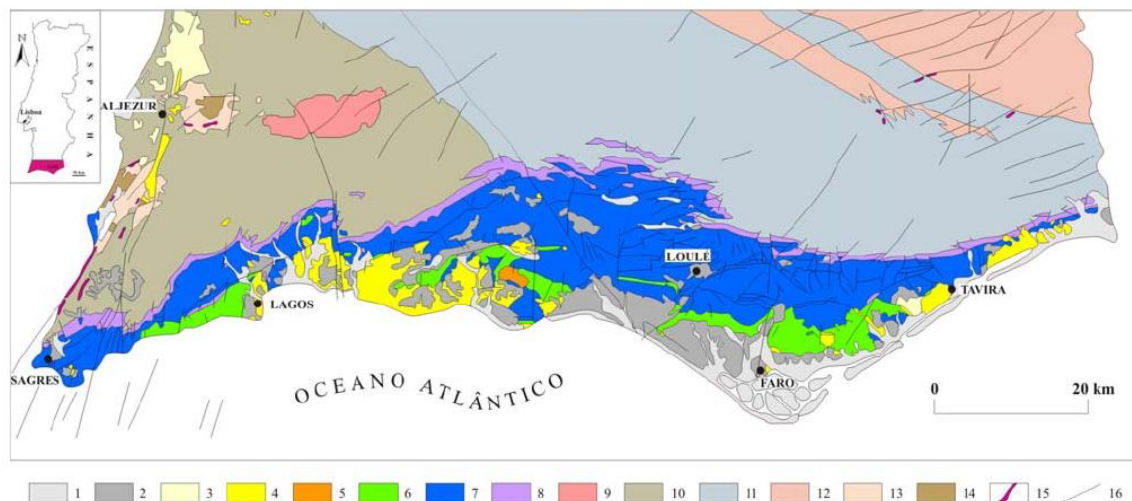
Figure 2. Geology of The Algarve Basin. 1- Holecene; 2- Pleistocene; 3- Pliocene; 4- Miocene; 5- Paleogene; 6- Cretaceous; 7- Jurassic; 8- Triassic/Hetangian; 9- Monchique Alkaline Complex; 10 To 14- Paleozoic; 15- Iodes; 16- Faults (Terrinha et al., 2006).

The Algarve is divided into 3 morphological sub-regions: (1) Serra (Upper Algarve); (2) Barrocal; and (3) Litoral, due to its geomorphological and geological diversity and its climatic and meteorologic characteristics (Bonnet, 1850 in Moura, 1998). The Algarve coast (Litoral) presents different geomorphological characteristics related to the geological setting and the wave incidence. Due to those aspects, the Algarve coast can be divided into three sectors: (i) west sector; (ii) southern west sector (barlavento); (iii) southern east sector (sotavento) (Moura, 1998). The study is located at the Sotavento sector, which is characterized by extensive beaches and sandy cliffs dating from the Pliocene and Pleistocene (Moura, 1998).

The cliffs from Ponta da Piedade to Olhos de Água are composed of carbonate and detrital rocks of the Miocene (limestones, calcarenites, siltstones) (Dias, 1988). Between Olhos da Água and Quinta do Lago, in which section we studied, the cliffs are composed of red clay-based sandstones, which are poorly consolidated and easily disintegrated. The sediments of the Vale do Lobo cliffs consist of fine to coarse sand, well sorted, and mineralogical composed by quartz, feldspars and iron oxide sands (Moura and Boski, 1994; Moura, 1998). The characteristic sand from the upper Pleistocene constitutes the sand of Faro - Quarteira da Formação do Ludo. These sands are composed of feldspar and iron-oxides, which give the tones of orange in the sediments (Moura, 1998). To the east of Vale do Lobo the coast is characterized by sandy type coast up to the Guadiana river. In this region, the coastline is characterized by long beaches, dunes, and the absence of cliffs.

3.2. The sedimentary cover of Algarve continental shelf

The Algarve continental shelf is narrow with an average width of 17 km (e.g. Lopes and Cunha, 2010), a gentle slope of 0.40º (Roque et al., 2010), and a well-defined edge and depths of 110 until 150 m. The continental slope is characterized by steeper inclination, which is interrupted by plateaus forming steps of 700 – 800 m deep, separated by the canyon heads cited above or by ditches (Moita, 1986).

The Algarve continental shelf is composed by Quaternary and Neogene formations, except the region near Cabo de São Vicente, where formations are Mesozoic (Magalhães, 1999). On the top of these formations, the sedimentary cover is composed of sands deriving mainly from the erosion of cliffs (Dias, 1988) and from a complex evolution since the last maximum glaciation (LMG) of the last 18 000 years (Rodrigues and Dias, 1989). The sediments are characterized by various types following the classification of Moita (1985) (Figure 3). In the inner shelf domain, the sand is bordering a muddy belt towards eastern, while in the west part, the shelf edge is marked by carbonate sands and a muddy sediments type dominance with 10 km wide between 50 and 100 m depth (Instituto Hidrográfico, 2012).
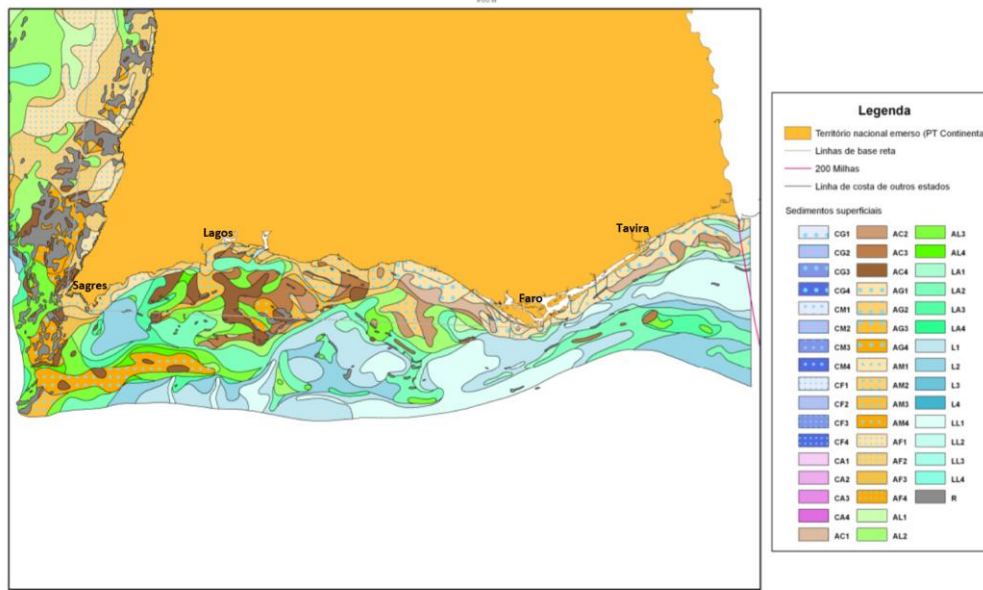
Figure 3. Sedimentary cover of The Algarve Continental Shelf (Instituto Hidrográfico, 2012) CG – Coarse Gravel; CM – Medium Gravel; CF – Fine Gravel; CA – Sandy Gravel; AC – Gravelly Sand; AG – Coarse Sand; AM – Medium Sand; AF – Fine Sand; AL – Muddy Sand (Silt < 25%); LA – Sandy Silt (25% < Silt < 50%); L – Silt (50% < Silt < 90%); LL – Silt (> 90%). 1 – Sediment Lithoclastic; 2 – Sediment Lithobioclastic; 3 – Sediment Biolithoclastic; 4 – Sediment Bioclastic.

3.3. The hydrodynamic regime of Algarve coast

In the southern coast of Portugal, the wave direction is dominated by west-southwest and southeast also known as "Levante" generated by regional winds (Costa et al., 2001). In storm conditions, the waves height can reach more than 3 m. However, registers from the south coast from 1986 to 2000 show that 65 % of the heights in the south are lower than 1 m, while waves greater than 3 m were only 2 % (Costa et al., 2001).

3.4. Study area

The investigation was carried out in an area located in Portugal's southern continental shelf, in the eastern part of the Algarve continental margin (Figure 4). The core selected for this study is the gravity core, MW107 (MW14-GC-107), collected from the Spanish research vessel Sarmiento de Gamboa, in 2014 in the scope of the Spanish national MOWER project (CTM 2012-39599-C03). The core was collected at 56.7 m depth, at 36.93° N, 7.99° W coordinates and has a 1.25 m length.
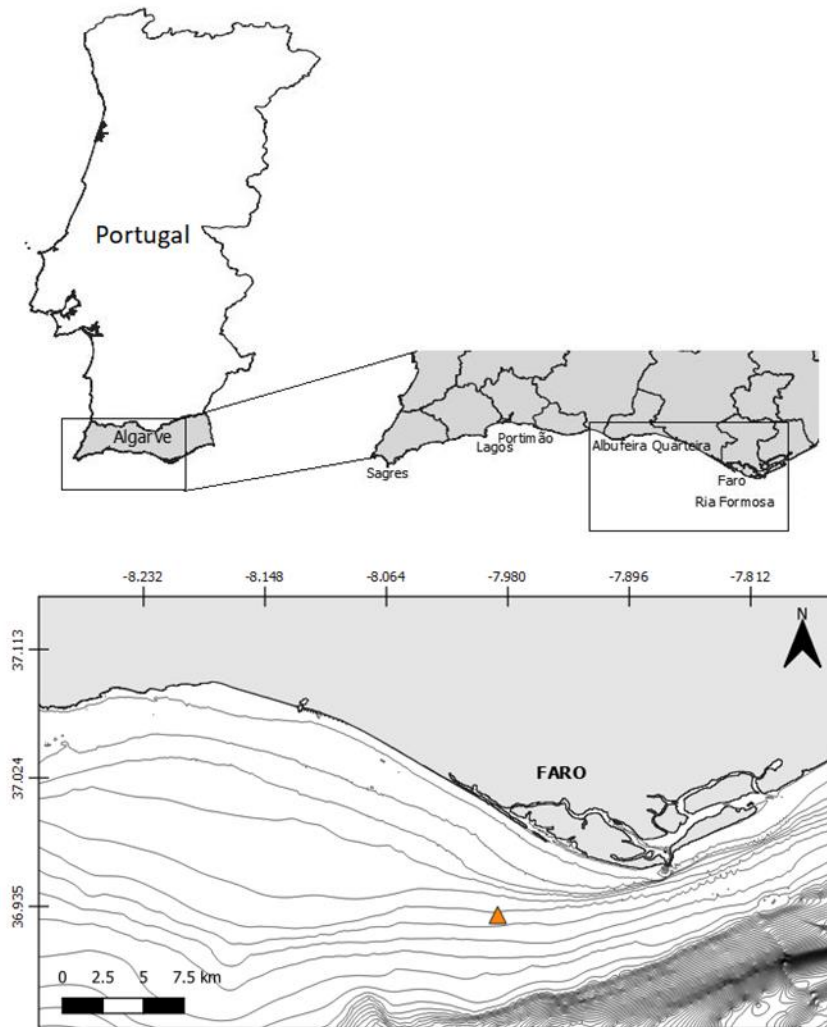
Figure 4. Location of the study area with core MW107 location (orange triangle), bathymetry with 10 m steps. (Bathymetry source: http://joa-quim.pt/mirone/data-links.html/algarve1-/grd, 22/11/2020).

4. METHODOLOGY

The methodology used in this work was essentially focused on the detailed sand mineralogical composition of the sandy sediments of the coastal area with the objective to search for some minerals that could be used as proxy for continental related material. The study was then focused with the search of these minerals in the studied continental shelf core layers. As referred above, these layers were defined in the ASTARTE project (subtask WP2.2). In the present work they were renamed for an easier reference as "layers", namely Layer 1, Layer 2, Layer 3, and Layer 4, and it was chosen to extend them 5 cm below and above of the ASTARTE defined layers (ADL) to observe any differences between them and the background normal sedimentation (Table 3). The applied methodology was divided by a fieldwork and laboratory work.

Table 3. Depth levels selected for this work were assembled in "layer" names (1 to 4). Levels distance in cm from the top. ADL=ASTARTE defined layers.

Layers Name	Section (cm)	5 cm Above (cm)	ADL (cm)	5 cm Below (cm)
Layer 4	13 - 27	13 - 17	18 -22	23 - 27
Layer 3	25 - 40	25 - 29	30 - 35	36 - 40
Layer 2	62 - 77	62 - 66	67 - 72	73 - 77
Layer 1	100 - 123	100 - 104	105 - 118	119 - 123

4.1. Field Work - Coastal sediments sampling

The fieldwork included the sediment sampling of 7 sites at the Algarve coastal area (Armação da Pêra, Baía Grande, Galé, Falésia Açoteias, Forte Novo, Vale do Lobo and Faro Beach) in March 2021 (Figure 5). For each site, superficial sediments were sampled in different zones of the beach (terrace, backshore, shoreface, beach face), cliff, and dune when existing and the coordinates were saved (Table 4, Figure 6).
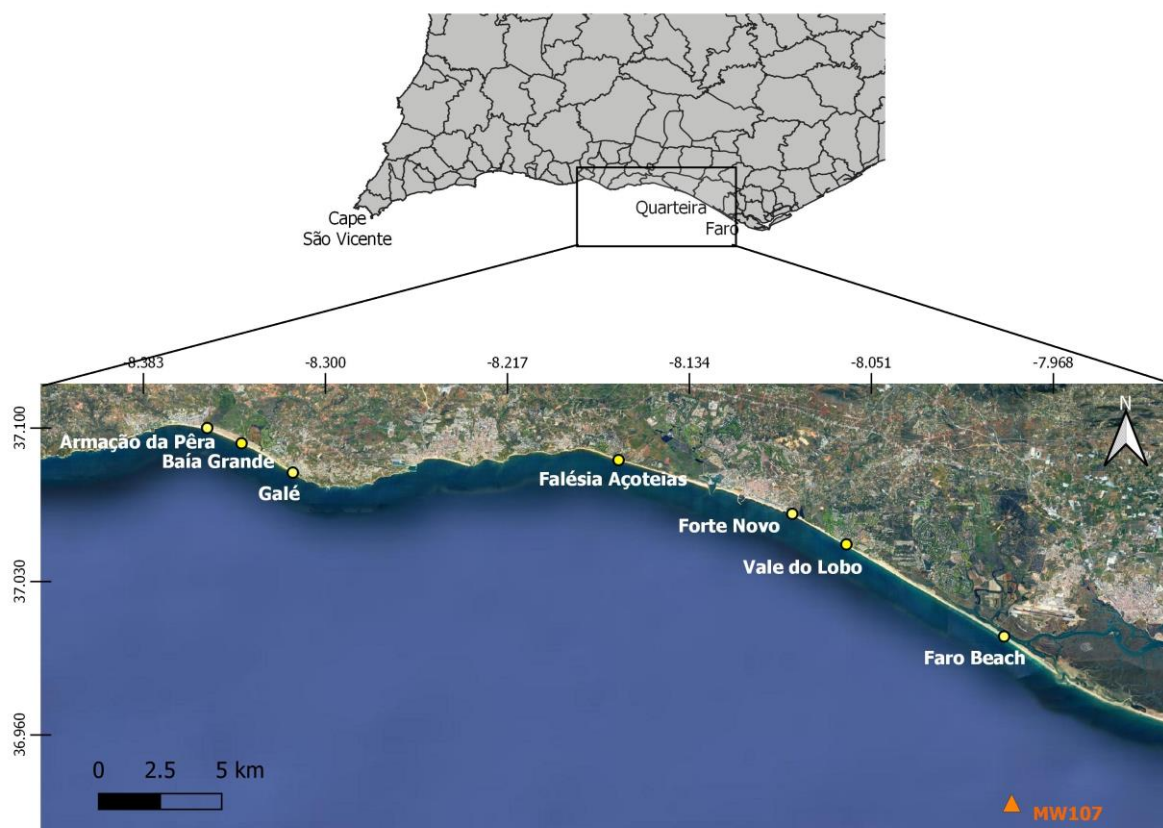
Figure 5. Location of the coastal studied section and the sampled beaches. The location of studied continental shelf core is represented by an orange triangle. Image source: Google Earth.

Table 4. Sites of the coastal samples, local of sampling and coordinates.

Site	Sampling	Coordinates	
Armação da Pêra	Beach (terrace)	37.1001°N	-8.3149°W
Baía Grande	Beach (backshore and beach face), Dune	37.0931°N	-83382°W
Galé	Beach (shoreface)	37.097°N	-8.3149°W
Falésia Açoteias	Beach (beach face), Cliff	37.0857°N	-8.1661°W
Forte Novo	Beach (backshore and beach face), Cliff	37.0606° N	-80874° W
Vale do Lobo	Cliff	37.0470° N	-8.0624° W
Faro beach	Dune	37.0050° N	-7.9905° W

18
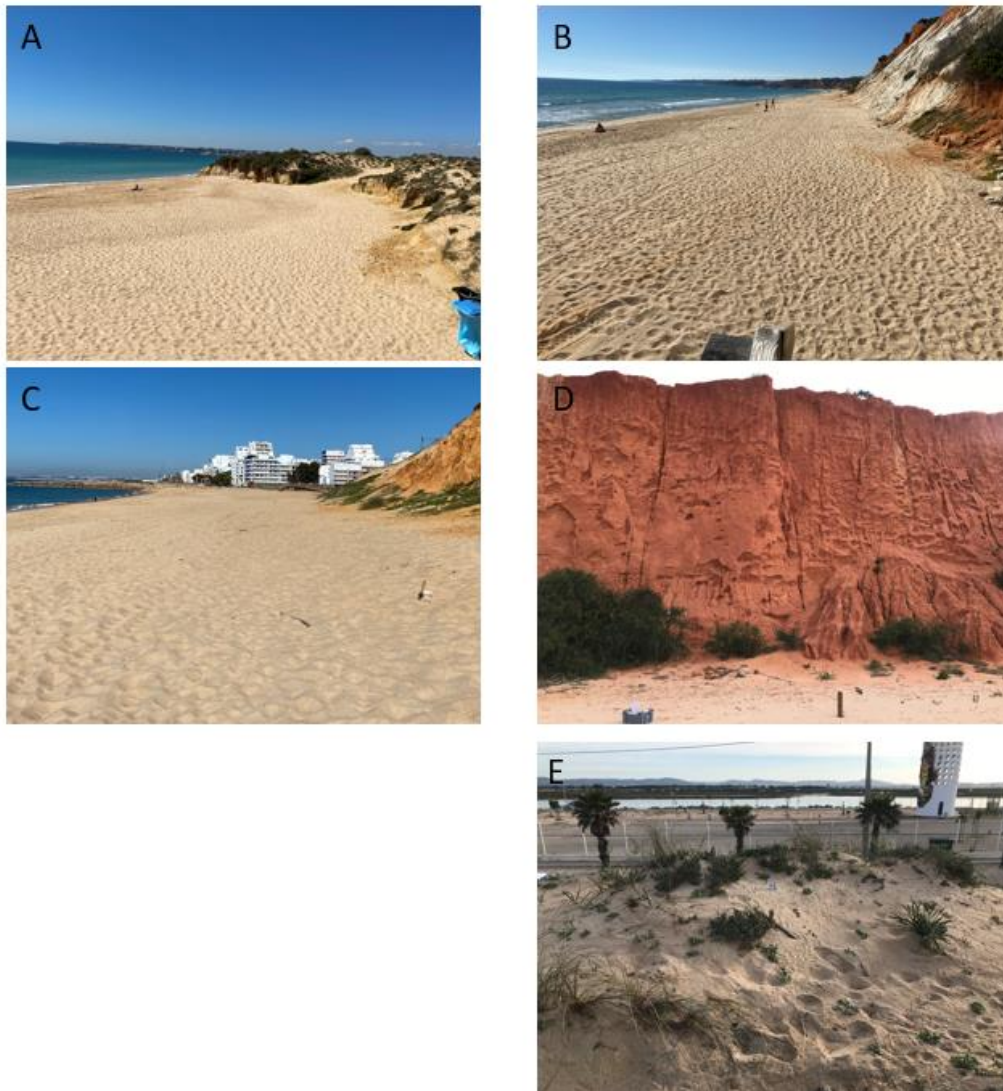
Figure 6. Photographs of sampling sites. (A) Baía Grande (Armação da Pêra), (B) Falésia Açoteias, (C) Forte Novo, (D) Vale do Lobo, (E) Faro Beach.

4.2. Laboratory Work – Sediment analysis

4.2.1. *Grain-size*

Grain-size analysis was performed on the coastal samples at the Geology laboratory at CIMA in the University of Algarve and at the Marine and Coastal Geology laboratory of IPMA in Tavira. The core samples were excluded from this analysis, as they had already been performed in the scope of the ASTARTE project.

The coastal samples were first dried in the oven (40°C). Thereafter, each sample was divided to obtain a smaller representative amount of the sample using the equipment the sample divider Retsch PT100. Grain-size analysis was performed by dry sieving according to the separation of 2000 μm, 1400 μm, 1000 μm, 710 μm, 500 μm, 355 μm,

250 μm, 180 μm, 125 μm, 90 μm and 63 μm meshes (Annex A). Once the grain-size separation was performed, they were weighted and the percentage computed (Annex A).

4.2.2. *Sand composition*

4.2.2.1. *Selected sand fractions*

As we were searching for a tracer of the coastal samples and in order to retaining the maximum information about the sand mineralogical composition of the studied core 3 sand fractions were analysed: 125 μm, 250 μm and 500 μm.

4.2.2.2. *Sand mineralogical composition*

The sand mineralogical identification was performed on the collected coastal samples and on the defined core layers (Drago et al., 2016, Table 3). Sand composition analysis was carried out in 12 coastal samples and in 68 layers of the MW107 core. The identification of the sand mineralogical composition of the sand was made under a binocular microscope Leica MZ16. For image record, it was used at Leica camera (model MC170HD) and LAS v4.12 software were used. For each sample, the 3 defined fractions above were studied, and 100 grains were counted per sample, resulting in 240 samples and 24,000 grains of sand observed (Annex B).

In each fraction of the coastal samples, sand grains were classified into 3 groups and 11 different subclasses. Terrigenous mineralogical compositions included quartz, mica, aggregates (lithic fragments), other terrigenous (feldspars, heavy minerals, and wood fragments). In the biogenic group, the subclasses included: molluscs, planktonic foraminifera, benthic foraminifera and other biogenic (pieces of organisms, ostracod, bryozoans). The authigenic group included only glauconite (Table 5). Following the analysis of the coastal sediments, two compositional classes were created to be applied as a coastal tracer in the sand composition analysis of the core sediments. These mineralogical compositions classes were: quartz covered by iron oxides; and orange clay aggregates with dark orange color (CMYK: 0, 69, 100, 0) that could be easily disintegrated. As they seem to be similar to some mineralogical components observed in coastal sediments, we decided to classify them separately, under the name of "iron-coated quartz" and "orange clay aggregates" (Annex B).

Table 5. Sand mineralogical composition used in this study.

Groups	Sand mineralogical compositions
Terrigenous	Quartz, Mica, Aggregates, Other Terrigenous, "Iron-coated quartz", "Orange clay aggregates",
Biogenic	Molluscs, Planktonic Foraminifera, Benthic Foraminifera, Other biogenic
Authigenic	Glauconite

4.3. Statistical Analyses

For the statistical analysis of the grain-size results we used "the method of the moments" (Folk and Ward, 1957). This method is composed of three moments: first, the mean grain-size; second, the variance (standard deviation), which measures the 'width' of a set of points. The third moment measures the skewness of the distribution. If the distribution is skewed to the left, has a negative skewness and indicates a higher percentage of fine sediments. While skewed to the right has a positive skewness and indicates high percentage of coarse sediments. As a fourth moment, kurtosis is used to determine if the distribution is tall and skinny or short and squat based on the same variance. In this work the statistical analysis it was focused in the mean grain-size and the standard deviation (sorting).

For computing these parameters and the statistical analysis of each sample, we used the GRADISTAT *software* (Blott and Pye, 2001). From the several methodological options it was chosen the "geometric method of moments", expressed in µm (Figure 7). For this study, the sediment classification according to Blott and Pye (2012) was adopted.

(b) Geometric method of moments

Mean	Standard deviation	Skewness	Kurtosis
$\bar{x}_g = \exp \dfrac{\Sigma f \ln m_m}{100}$	$\sigma_g = \exp \sqrt{\dfrac{\Sigma f (\ln m_m - \ln \bar{x}_g)^2}{100}}$	$Sk_g = \dfrac{\Sigma f (\ln m_m - \ln \bar{x}_g)^3}{100 \ln \sigma_g{}^3}$	$K_g = \dfrac{\Sigma f (\ln m_m - \ln \bar{x}_g)^4}{100 \ln \sigma_g{}^4}$

Sorting (σ_g)		Skewness (Sk_g)		Kurtosis (K_g)	
Very well sorted	<1·27	Very fine skewed	$<^-1\cdot30$	Very platykurtic	<1·70
Well sorted	1·27–1·41	Fine skewed	$^-1\cdot30$ to $^-0\cdot43$	Platykurtic	1·70–2·55
Moderately well sorted	1·41–1·62	Symmetrical	$^-0\cdot43$ to $^+0\cdot43$	Mesokurtic	2·55–3·70
Moderately sorted	1·62–2·00	Coarse skewed	$^+0\cdot43$ to $^+1\cdot30$	Leptokurtic	3·70–7·40
Poorly sorted	2·00–4·00	Very coarse skewed	$>^+1\cdot30$	Very leptokurtic	>7·40
Very poorly sorted	4·00–16·00				
Extremely poorly sorted	>16·00				

Figure 7. Geometric method of moments. Adapted from Blott and Pye (2001).

Based on the results of the laboratory analysis, statistical tests were performed in the open-source statistics software R to identify the similarities and differences between the sand mineralogical composition for each target layer. First of all, the data was performed under a Shapiro-Wilk test (Annex C) to analyze the normality of the data. Since the data was mainly not normal distributed, the non-parametric Kruskal-Wallis test was performed and p-values were calculated (p-values lower than 0.05 indicates the difference between the groups) in order to analyze the statistical significance of the variations of the sand mineralogical compositions between 3 groups named here as "Below ADL", "ADL", and "Above ADL" for each layer (Layer 1, Layer 2, Layer 3 and Layer 4) (Annex D). Below ADL is each cm of 5 cm below the ASTARTE defined layers, and above ADL is each cm of 5 cm above the ASTARTE defined layers.

Post-hoc Duun test was applied to determine which of the sample's pairs ("Below ADL", "ADL" and "Above ADL") were significantly different from each other. Afterward to reduce the error of the results a Bonferroni adjustment was performed on the Kruskal-Wallis results (Mangiafico, 2015).

Besides the statistical analysis, overall data from ASTARTE project (grain-size, carbonates, magnetic susceptibility, XRF) of each defined layer was also visually assessed in order to find any relation or similar behavior.

5. RESULTS

5.1. Grain-size analysis of coastal sediments

Grain-size analysis of the superficial sediments of the coastal sites shows that the samples from the cliff were classified according to Blott and Pye (2012) as "Very slightly gravelly sand", "Very slightly gravelly very slightly muddy sand" and "Very slightly muddy sand". Samples from the dunes sites were dominated by "sand", and the beach samples by "sand" and "Very slightly gravelly sand" (Figure 8).
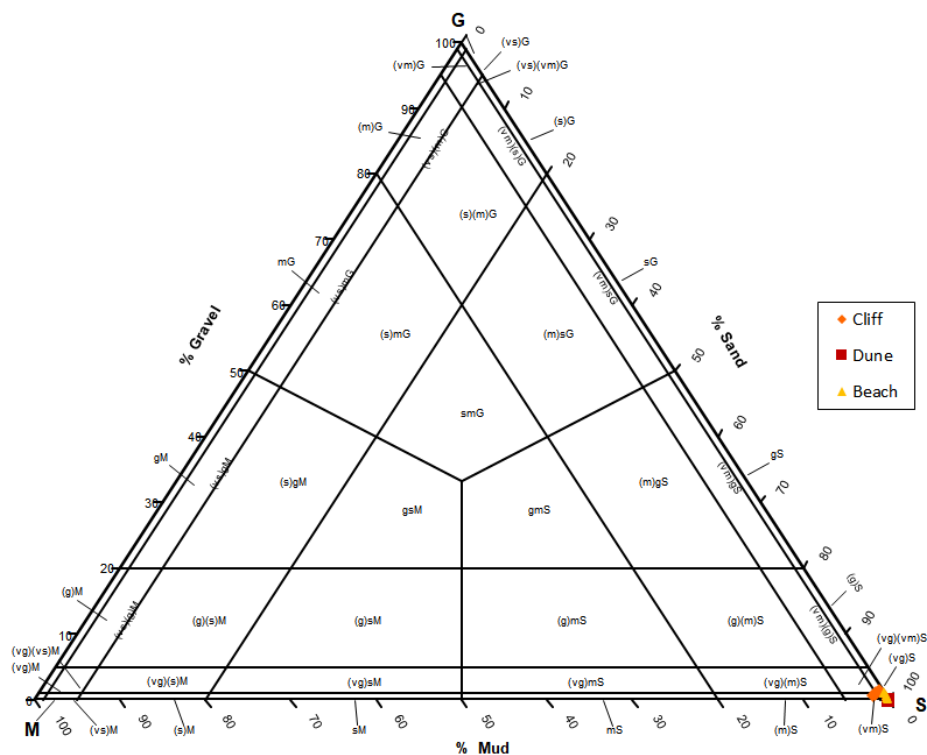
Figure 8. Classification of cliff, dune, and beach sediments (Blott and Pye 2012).

5.1.1. *Cliff*

The grain-size distribution of the selected sites at the cliff (Figure 9) shows that sediments samples of Falésia Açoteias were predominantly constituted by very coarse sand (55%), Forte Novo constituted by coarse sand (43%), and Vale do Lobo shows predominant constituted by medium sand (59%). In every sample the percentage of gravel and mud was below 1.5%.

Figure 9. Geographic location along the coast of the Algarve under the grain-size distribution. (1) Falésia Açoteias, cliff; (2) Forte Novo, cliff; (3) Vale do Lobo, cliff

The mean grain-size is higher (754 - 585 µm) in the samples of Falésia Açoteias and Forte Novo (Table 6), and the Vale do Lobo sample, the mean grain-size was finer (371 µm). In terms of sorting, the cliff sites were moderately sorted in Falésia Açoteias and poorly sorted in the samples of Forte Novo and Vale do Lobo.

According to Blott and Pye (2012), Falésia Açoteias and Vale do Lobo samples are "very slightly gravelly sand", "very slightly muddy sand", respectively, and Forte Novo "very slightly gravelly very slightly muddy sand".

Table 6. Sample classification according to Blott and Pye (2012), statistical parameters (mean grain-size and sorting).

Cliff	Classification	Mean grain-size (µm)	Sorting (µm)
Falésia Açoteias	Very slightly gravelly sand	754	1.77
Forte Novo	Very slightly gravelly very slightly muddy sand	585	2.16
Vale do Lobo	Very slightly muddy sand	371	2.02

5.1.2. *Dune*

The grain-size distribution of the selected sites at the dunes (Figure 10) shows that sediments samples from Baía Grande were predominantly constituted by medium sand (69%), and Faro Beach was predominantly constituted by coarse sand (67%). In every sample the percentages of gravel and mud was below than 1.5%.
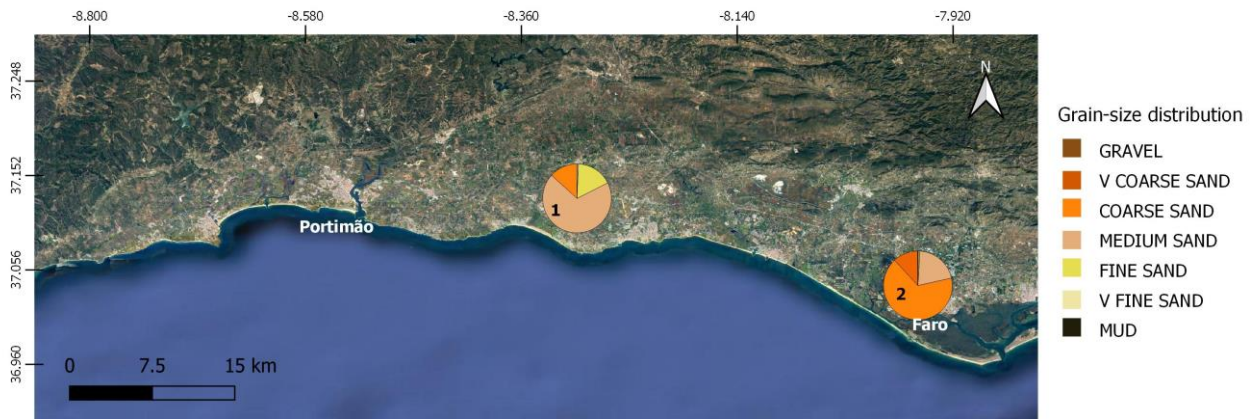
Figure 10. Geographic location along the coast of the Algarve under the grain-size distribution. (1) Baía Grande, dune; (2) Faro beach, dune

The mean grain-size is 340 μm in the sample of Baía Grande and, 658 μm at Faro Beach sample. The dune sediments were moderately well-sorted and classified as "sand" according to Blott and Pye (2012) (Table 7).

Table 7. Sample classification according to Blott and Pye (2012), statistical parameters (mean grain-size and sorting).

Dune	Classification	Mean grain-size (μm)	Sorting (μm)
Baía Grande	Sand	340	1.48
Faro Beach	Sand	658	1.5

5.1.3. *Beach*

The grain-size distribution of the selected sites at the beach sites shows that the sediments samples were predominant constituted by coarse sand, except in the samples from the beach face in Forte Novo and Baía Grande, which is predominantly constituted of

fine and medium sand, respectively (Figure 11). Mud was absent in all the sites, and gravel was almost absent or represented about below 1.5% of the entire samples.

Figure 11. Geographic location along the coast of the Algarve under the grain-size distribution. (1) Armação da Pêra, terrace; (2) Baía Grande, beachface; (3) Baía Grande, backshore; (4) Galé, shoreface; (5) Falésia Açoteias, beach face; (6) Forte Novo, beach face (7) Forte Novo, backshore.

The mean grain-size of the beaches sites are ranging from 448 – 568 µm (with the exception of Baía Grande (beach face) with lower mean grain-size of 338 µm, (Table 8, Figure 11), and they are moderately well sorted (Armação da Pêra; Baía Grande, backshore; Galé) to moderately sorted (Forte Novo, backshore; Forte Novo, beach face; Falésia Açoteias, beach face; Baía Grande, beach face). All the samples were classified as "sand", except Forte Novo (beach face) and Baía Grande (beach face), which were "very slightly gravelly sand"

Table 8. Sample classification according to Blott and Pye (2012), statistical parameters (mean grain-size and sorting).

Beach	Classification	Mean grain-size (µm)	Sorting (µm)
Armação da Pêra (terrace)	Sand	568	1.59
Baía Grande (beach face)	Very slightly gravelly sand	388	1.89
Baía Grande (backshore)	Sand	487	1.59
Galé (shoreface)	Sand	502	1.61
Falésia Açoteias (beach face)	Sand	533	1.96
Forte Novo (beach face)	Very slightly gravelly sand	532	1.67
Forte Novo (backshore)	Sand	448	1.63

5.2. Sand mineralogical composition of coastal sediments

5.2.1. *Cliff*

Overall, the sand mineralogical composition of the cliff samples shows predominance of terrigenous components. It could be highlighted the following characteristics:

- A predominance of quartz, in which the quartz hyaline was dominated in more than 90% of the samples from Falésia Açoteias in the 3 studied fractions and iron-coated quartz was predominantly in the samples from Forte Novo and Vale do Lobo especially in the fractions 250 and 500 µm where it was represented by more than 97% of the total sample of each fraction;
- The predominance of other terrigenous in the samples fraction 125 µm of Forte Novo and Vale do Lobo were represented by 60% and 80% respectively (Figure 12), which 52 % in Forte Novo and 79 % in Vale do Lobo were in particular orange clay aggregates.
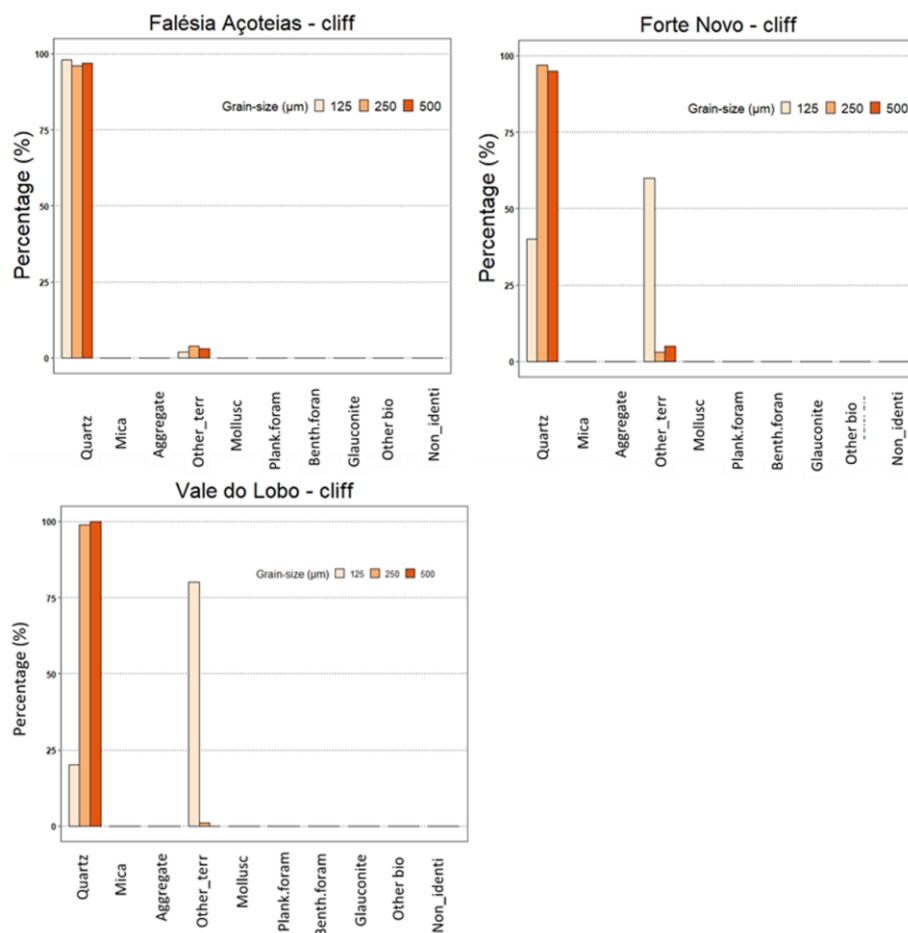
Figure 12. Sand mineralogical composition of the cliff samples.

27

5.2.2. *Dune*

Overall, the sand mineralogical composition of the dune samples shows predominance of terrigenous components. In the dune samples, it could be highlighted the following characteristics (Figure 13):

- In the samples from Baía Grande quartz was predominant in all studied fractions, where 63 % was quartz hyaline and around 30% iron-coated quartz. The biogenic components represented 2% of other biogenic;

- In the samples from Faro beach, quartz was predominant in the fractions 500 and 250 µm, were quartz hyaline represented 75% and 84 %, respectively and iron-coated quartz 21% and 10%. The sand fraction 125 µm showed a decrease in quartz, compared to the coarser fractions due to the increase of other terrigenous which was represented by 42 % with higher amount of heavy minerals.
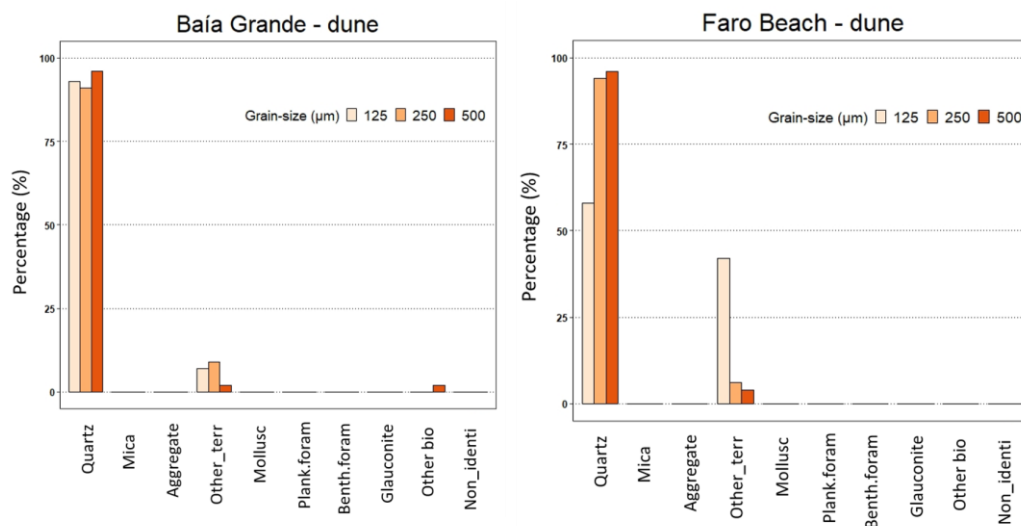
Figure 13. Sand mineralogical composition of the dune samples.

5.2.3. *Beach*

Overall, the sand mineralogical composition of the beach samples shows predominance of terrigenous components. In the beach samples, it could be highlighted the following characteristics (Figure 14):

- Quartz was the most predominant mineral in the beach samples represented by more than 75% of the total content, except in the samples of 125 µm at the sites of Forte Novo backshore and beach face. The quartz was predominant hyaline in all the beach samples represented ranging from 51 to 74 % and the iron-coated quartz from

7 to 36 %. The highest percentage of iron-coated quartz was found at the sample from Forte Novo backshore (36%) and more the 20% in some samples (Baía Grande beach face, Baía Grande backshore, Armação da Pêra, Forte Novo beach face, Forte Novo backshore), while the lowest percentage observed at Galé shoreface (7%);

- In the samples from Forte Novo backshore and beach face samples (125 μm), quartz contents were lower than 50% due to the significantly high contents of other terrigenous (heavy minerals and other minerals);

- Although terrigenous component is highly predominant in the beach samples, a lower percentage of biogenic components, particularly molluscs and other biogenic material, were observed at all beach samples, except in Armação da Pêra; The samples from the terrace of Armação da Pêra did not show molluscs in any of the fractions but was the only site that contained benthic foraminifera.
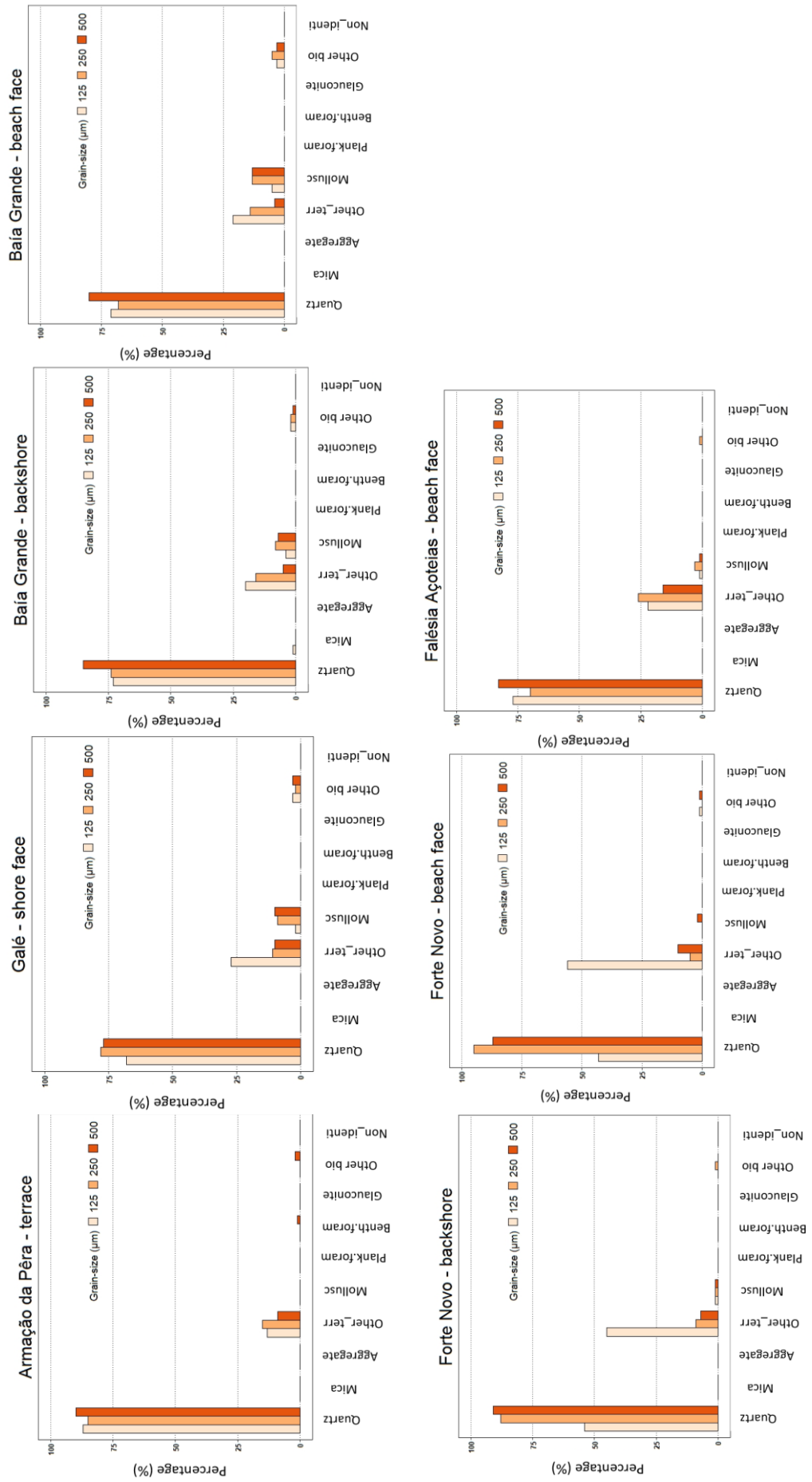
Figure 14. Sand mineralogical composition of the beach samples.

5.3. Sand mineralogical composition of core layers

As mentioned in the methodology, in the ASTARTE project (subtask WP2.2), the defined layers related to "potential high energy events" were renamed, from the base towards the top as defined Layer 1, 2, 3 and 4, respectively. And for differentiate them with the rest of the core, it was considered to study 5 cm above and 5 cm below of the ASTARTE defined layers.

5.3.1. *Layer 1*

The depths of Layer 1 are expressed in Table 9.

Table 9. Levels depths of Layer 1. ADL – ASTARTE defined layers.

Layer 1	
5 cm Above ADL	100 – 104 cm
ASTARTE Defined layer (ADL)	105 – 118 cm
5 cm Below ADL	119 – 123 cm

5.3.1.1. *125 μm sand fraction*

The terrigenous component is represented by 53% along the entire Layer 1 (Table 9), and the biogenic component is 47% (Figure 15). In this section, it could be highlighted the following characteristics:

- Mica shows an absence at the ADL reaching 0% (117 cm to 115 cm and 113 cm to 108 cm), and an increase ranging from 6% to 11% (107 cm to 100 cm and 123 to 118 cm);
- Aggregates show a small increase at the ADL (113 cm to 110 cm and 106 cm);
- Iron-coated quartz was found at different levels throughout the core, particularly at 117 cm (1%), 115 cm to 109 cm (1% each layer), and at 119 cm (2%) and 120 cm (1%).
- Orange clay aggregates was found at level 100 cm (1%);
- Wood fragments was found at level 107 cm;
- Benthic foraminifera and other biogenic showed a peak at levels 109 cm and 112 cm, respectively.

5.3.1.2. *250 μm sand fraction*

The terrigenous component was predominant (71%) along the entire Layer 1 (Table 9), while the biogenic component is present with a percentage of 29% (Figure 16). In this section, the sand mineralogical composition has the following main characteristics:

- Predominance of quartz in the entire Layer 1 ranging from 60% to 81% (123 cm to 100 cm);
- Iron-coated quartz was found at levels 120 cm (2%), 115 cm to 109 cm (1 – 2% each layer), 107 cm (1%) and 105 cm (1%), 104 cm (1%);
- The biogenic component was mainly molluscs and other biogenic. Molluscs show the maximum percentages at the ADL at 114 cm (24%) and a decreasing trend towards the top (113 cm to 112 cm, 109 cm to 106 cm);
- Wood fragments were found at level 101 cm.

5.3.1.3. *500 μm sand fraction*

This fraction was mostly composed of terrigenous components (81%) especially quartz (80%), while biogenic components represented a small percentage with 15% (Figure 17) for the whole Layer 1 (Table 9). Besides this, other characteristics can be highlighted:

- Mica was almost not found in the entire Layer 1 (123 cm – 100 cm), ranging from 0 to 1%, except in level 103 cm were mica shows increased to 9%;
- The other terrigenous component only contributed as high as 5% (Figure 17), more or less uniform but showing a maximum percentage at the base (123 cm and 120 cm);
- Iron-coated quartz was found at levels 114 cm (1%), 110 cm (2%), 109 cm (1%), 105 cm (2%), and 100 cm (1%).

Figure 15. Sand mineralogical compositions of Layer 1 fraction 125 μm. Black dashed line represents the ASTARTE defined layers.
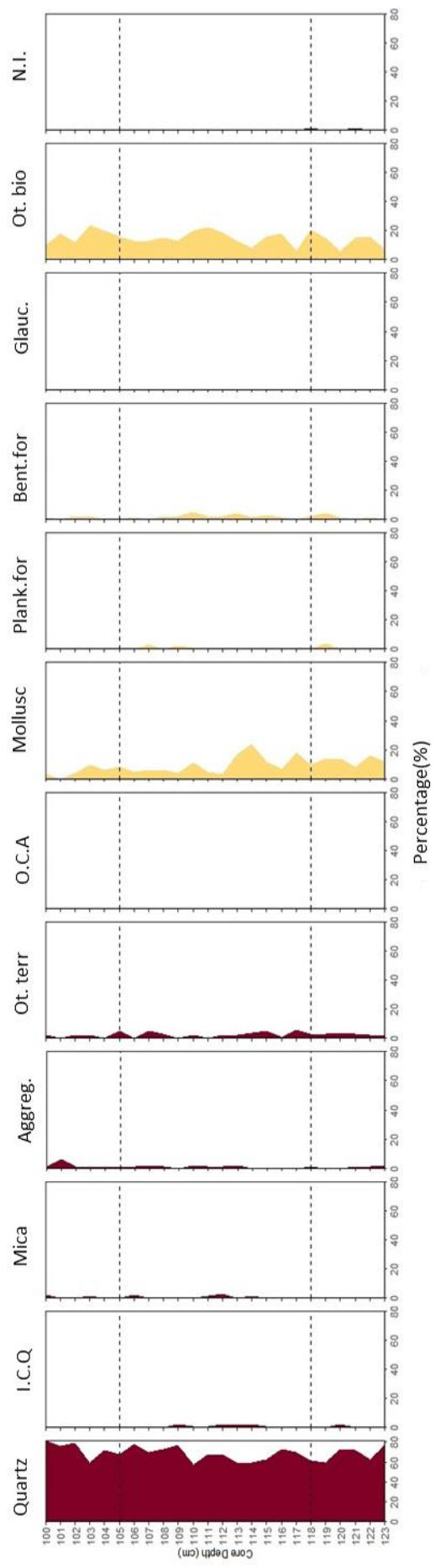
Figure 16. Sand mineralogical compositions of Layer 1 fraction 250 μm. Black dashed line represents the ASTARTE defined layers.
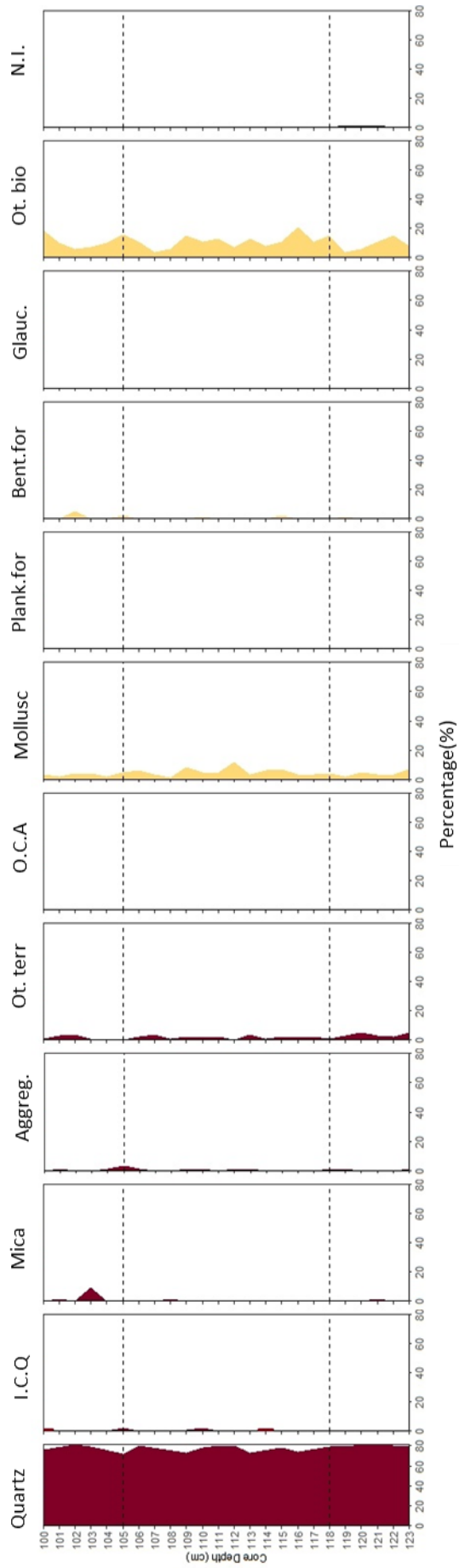
Figure 17. Sand mineralogical compositions of Layer 1 fraction 500 µm. Black dashed line represents the ASTARTE defined layers.

5.3.2. *Layer 2*

The depths of Layer 2 are expressed in Table 10.

Table 10. Levels depths of Layer 2. ADL – ASTARTE defined layers.

Layer 2	
5 cm Above ADL	62 – 66 cm
ASTARTE Defined layers (ADL)	67 – 72 cm
5 cm Below ADL	73 – 77 cm

5.3.2.1. *125 µm sand fraction*

The terrigenous component was represented by 54% (Figure 18) of the entire Layer 2 (Table 10), and the biogenic component 46%. In this section, it could be highlighted the following characteristics:

- Mica shows a slight increase on the top of the ADL reaching 5% at level 67 cm followed by an increase at level 66 cm (12 %);
- Other biogenic and benthic foraminifera were higher at levels 75 cm to 72 cm and 63 cm, while molluscs had the highest percentage at the boundary of the ADL and 66 cm, 65 cm, and 64 cm.

5.3.2.2. *250 µm sand fraction*

The terrigenous component was predominant in the Layer 2 (Table 10) represented by up to 68% of the entire section and biogenic component 31% (Figure 19). Nevertheless, some characteristics were highlighted:

- Quartz shows a slight decrease at the top of the ADL (69 cm to 67 cm), due to the increase aggregates and molluscs;
- Iron-coated quartz was found at level 72 cm (1%);
- A rapid decrease in the ADL of planktonic (0%) and benthic (2%) foraminifera and other biogenic (11%) at the level 70 cm;
- Wood fragments was found at level 71 cm.

5.3.2.3. *500 µm sand fraction*

The terrigenous assemblages were predominant (69%), while the biogenic component represented 30% (Figure 20) of the entire Layer 2 (Table 10). It could be highlighted the following characteristics:

- Mica was found only at level 65 cm (1%);

- Molluscs and other biogenic exhibit a similar pattern of decreasing towards the base of the ADL (72 cm to 67 cm).
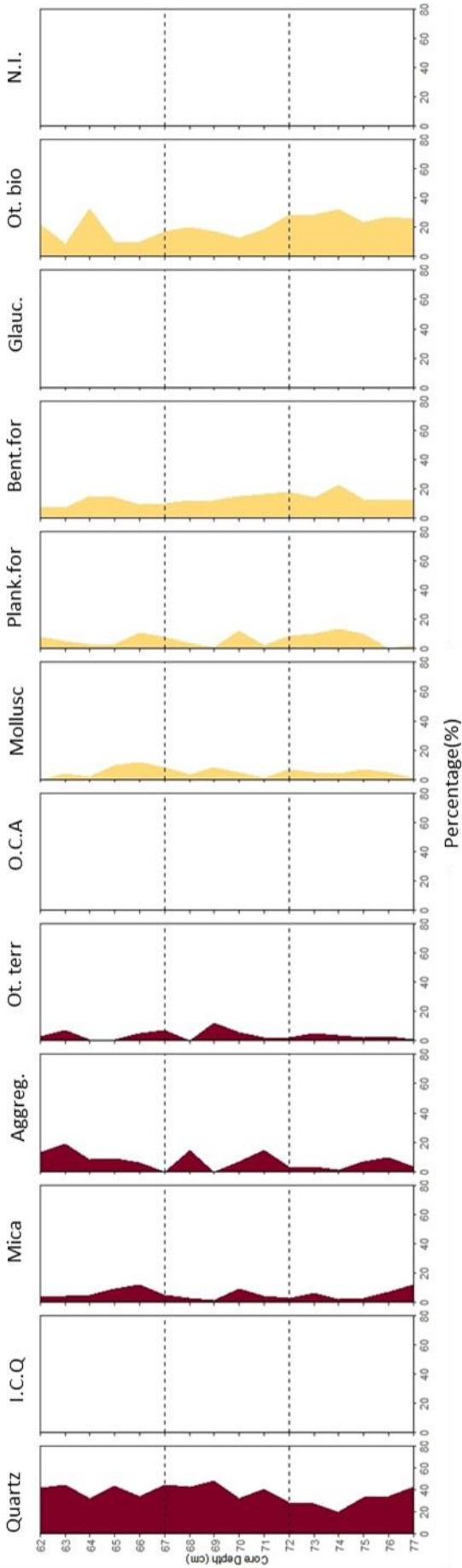
Figure 18. Sand mineralogical compositions of Layer 2 fraction 125 μm. Black dashed line represents the ASTARTE defined layers.
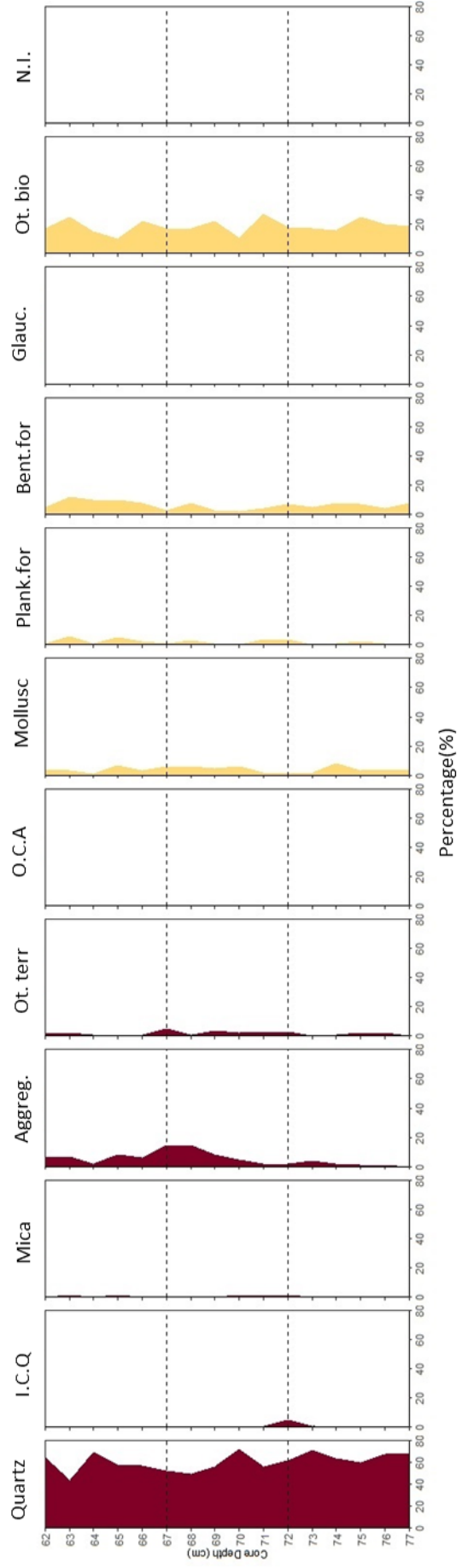
Figure 19. Sand mineralogical compositions of Layer 2 fraction 250 μm. Black dashed line represents the ASTARTE defined layers.

37
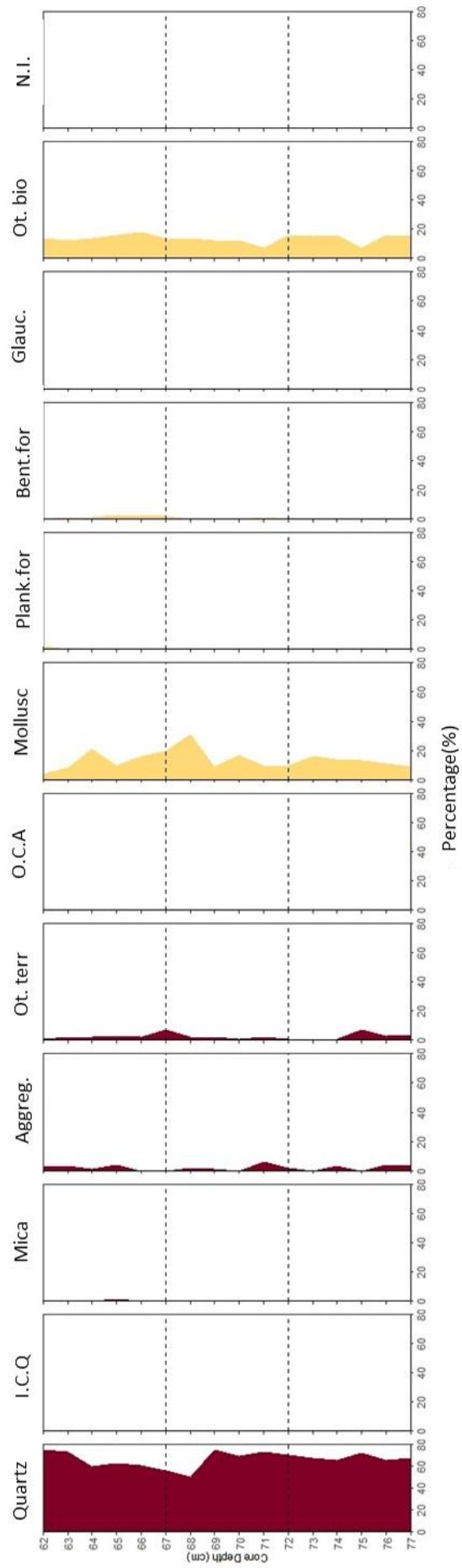
Figure 20. Sand mineralogical compositions of Layer 2 fraction 500 μm. Black dashed line represents the ASTARTE defined layers.

38

5.3.3. *Layer 3*

The depths of Layer 3 are expressed in Table 11.

Table 11. Levels depths of Layer 3. ADL – ASTARTE defined layers.

Layer 3	
5 cm Above ADL	25 – 29 cm
ASTARTE Defined layers (ADL)	30 – 35 cm
5 cm Below ADL	36 – 40 cm

5.3.3.1. *125 μm sand fraction*

The terrigenous component represented 58% of the entire Layer 3 (Table 11) and biogenic component 42% (Figure 21). In this section, it could be highlighted the following characteristics:

- The peak of the total terrigenous component shows an increase of 27% at level 32 cm;
- Mica was inexistent in the level 32 cm;
- Iron-coated quartz was found particularly at the levels 31 cm (1%) and 27 cm (1%);
- Orange clay aggregates were found at levels 39 cm to 32 cm, ranging from 24% to 1%. However, at level 32 cm, represented by 24% of the total sample in this level;
- Other terrigenous were higher at levels 39 cm (8%), 35 cm (7%), and 34 cm (7%);
- Molluscs and other biogenic shows an increase in the upper levels of the ADL reaching 20% and 26%, respectively at 31 cm depth;
- Planktonic and benthic foraminifera were higher at the base of the ADL (35 cm to 32 cm);
- Wood fragments were found at levels 35 cm and 28 cm.

5.3.3.2. *250 μm sand fraction*

The terrigenous component represented 61% of the entire Layer 3 (Table 11) and the biogenic component 39% (Figure 22). Besides this, the following characteristics could be highlighted:

- The peak of total terrigenous component (76%) at level 32 cm;
- Mica increased at level 30 cm (6%);
- Iron-coated quartz was found at level 35 cm (2%);

- Wood fragments were found at level 33 cm;
- Orange clay aggregates at the levels 38 cm (5%), 33 cm (1%), and 32 cm (2%).

5.3.3.3. *500 μm sand fraction*

The terrigenous component was represented by 63% of the entire Layer 3 (Table 11), while biogenic assemblages 37% (Figure 23). In this section, it could be highlighted the following characteristics:

- Mica shows an increase at levels 30 cm to 28 cm, reaching 6%;
- Other terrigenous present lower percentages in general and a slight increase in the base of the ADL at 35 cm to 32 cm (ranging from 2% to 3%).
- Iron-coated quartz was only found at level 34 cm (1%);
- The maximum percentage of molluscs was found at the ADL 34 cm and 31 cm levels (29% and 30%, respectively);
- Other biogenic and benthic foraminifera were higher at level 29 cm (28% and 14%, respectively).
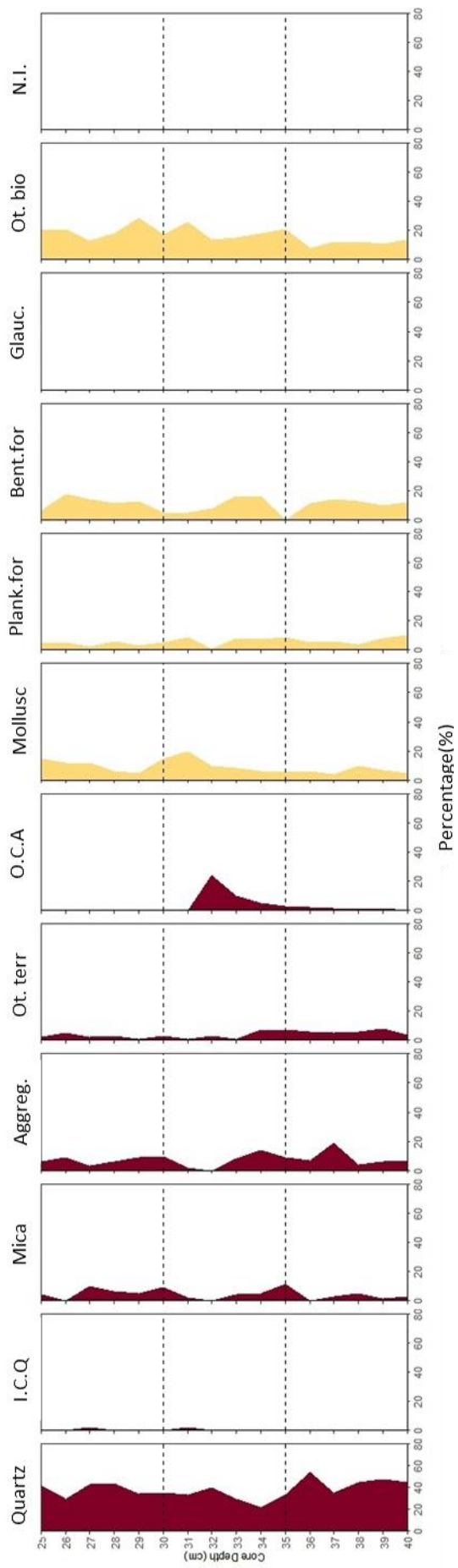
Figure 21. Sand mineralogical compositions of Layer 3 fraction 125 µm. Black dashed line represents the ASTARTE defined layers.
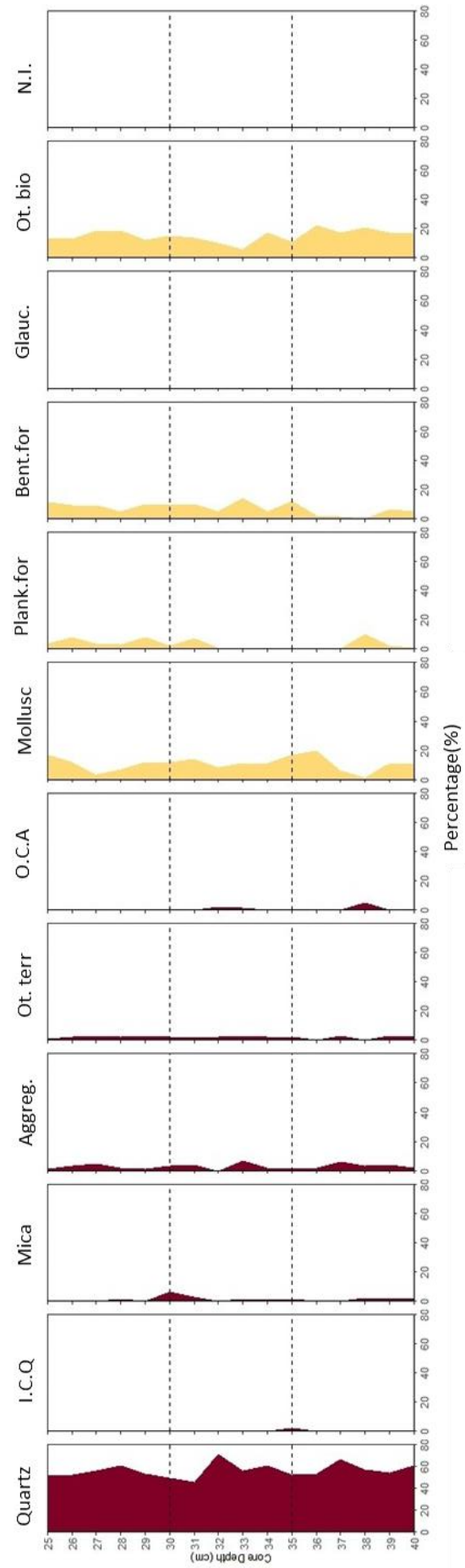
Figure 22. Sand mineralogical compositions of Layer 3 fraction 250 µm. Black dashed line represents the ASTARTE defined layers.

41
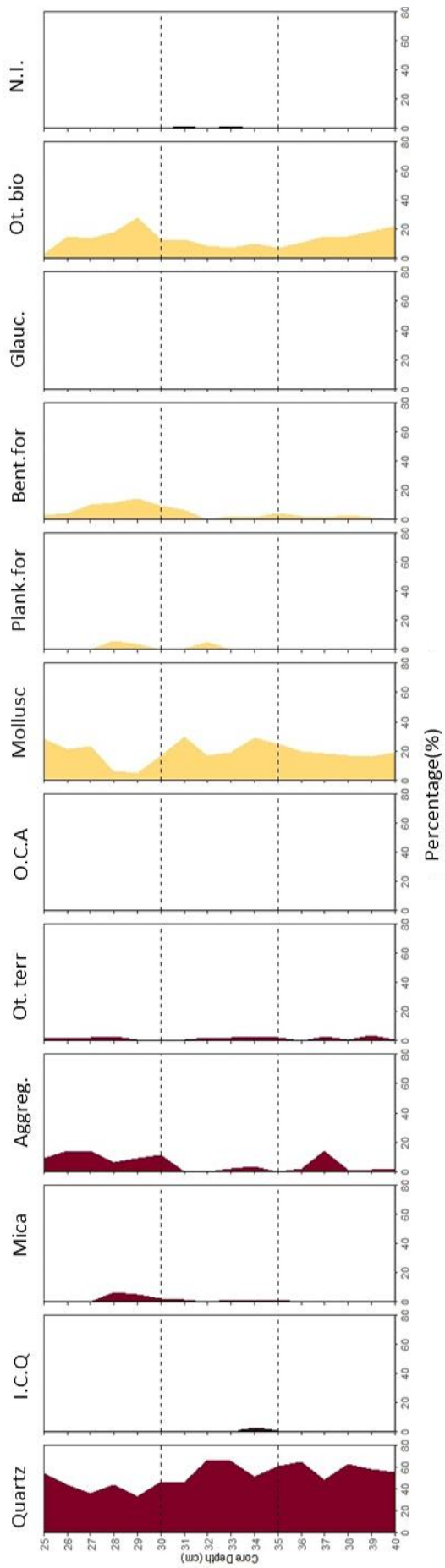
Figure 23. Sand mineralogical compositions of Layer 3 fraction 500 μm. Black dashed line represents the ASTARTE defined layers.

5.3.4. *Layer 4*

The depths of Layer 4 are expressed in Table 12.

Table 12. Levels depths of Layer 4. ADL – ASTARTE defined layers.

Layer 4	
5 cm Above ADL	13 – 17 cm
ASTARTE Defined layers (ADL)	18 – 22 cm
5 cm Below ADL	23 – 27 cm

5.3.4.1. *125 μm sand fraction*

The terrigenous component represented 49% of the entire Layer 4 (Table 12) and the biogenic component 51% (Figure 24). In this section, it could be highlighted the following characteristics:

- A rapid decrease of quartz, where quartz reached 20% at level 20 cm.
- Mica decreased at the ADL ranging from 0% to 1% at levels 22 cm to 18 cm and tends to increase at the levels 27 cm (10%) to 22 cm (3%) and 17 cm (7%) to 13 cm (5%);
- Iron-coated quartz found at level 27 cm (1%);
- The wood fragment was found at levels 24 cm, 23 cm, 22 cm, and 17 cm depth;
- Increase of molluscs at the top of the ADL (particularly at 19 cm) reaching 30%.

5.3.4.2. *250 μm sand fraction*

The terrigenous component is dominated in this Layer 4 (Table 12), represented by 61% of the entire section, while the biogenic component represented 38% (Figure 25). In Layer 4, it could be highlighted the following characteristics:

- Other terrigenous shows an increase in the edge of the ADL at level 18 cm (5%);
- Mica shows the maximum concentration at level 17 cm (3%);
- Molluscs, and other biogenic show a higher percentage at the top of the ADL from levels 20 cm to 18 cm;
- Benthic and planktonic foraminifera show an increase at levels 17 cm to 13 cm.

5.3.4.3. *500 μm sand fraction*

The terrigenous component was dominated in this layer, represented by 64% of the entire Layer 4 (Table 12), while the biogenic component represented 35% (Figure 26). In this section, it could be highlighted the following characteristics:

- Mica increases at the base of the ADL and at levels 17 cm and 16 cm (3% and 1%);
- Iron-coated quartz found at level 18 cm (1%);
- Molluscs presented the highest predominance with the maximum percentage in the levels 15 cm and 20 cm (34%) and a rapid decrease at 18 cm (12%);
- Benthic foraminifera and other biogenic were lower at the top of the ADL, while planktonic foraminifera were almost absent in the entire section, present only in levels 15 cm, 23 cm, and 24 cm with a small percentage.
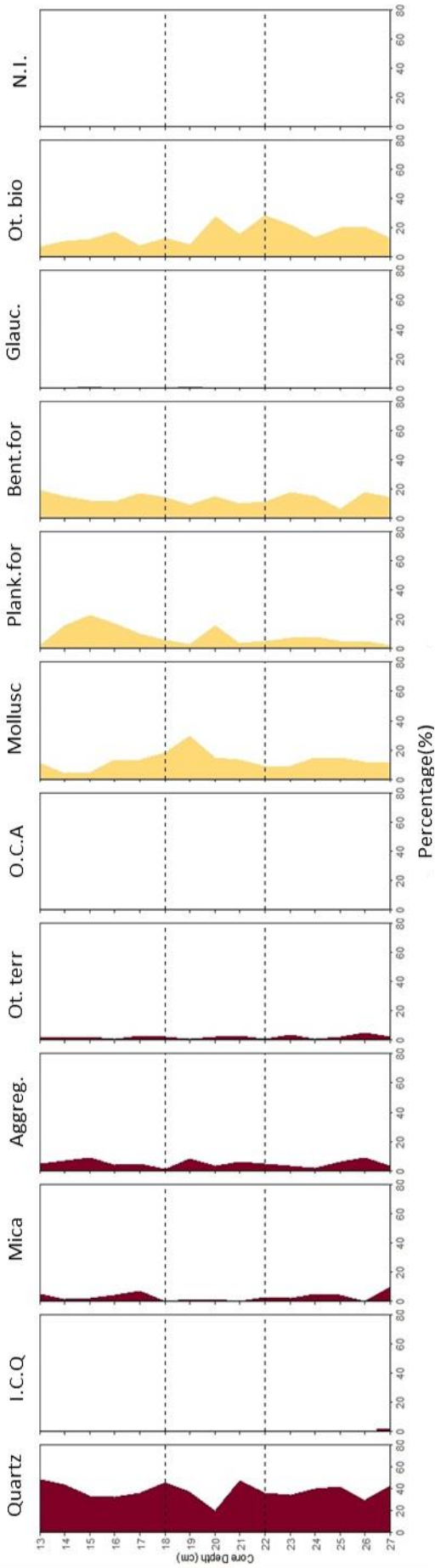
Figure 24. Sand mineralogical compositions of Layer 4 fraction 125 μm. Black dashed line represents the ASTARTE defined layers.
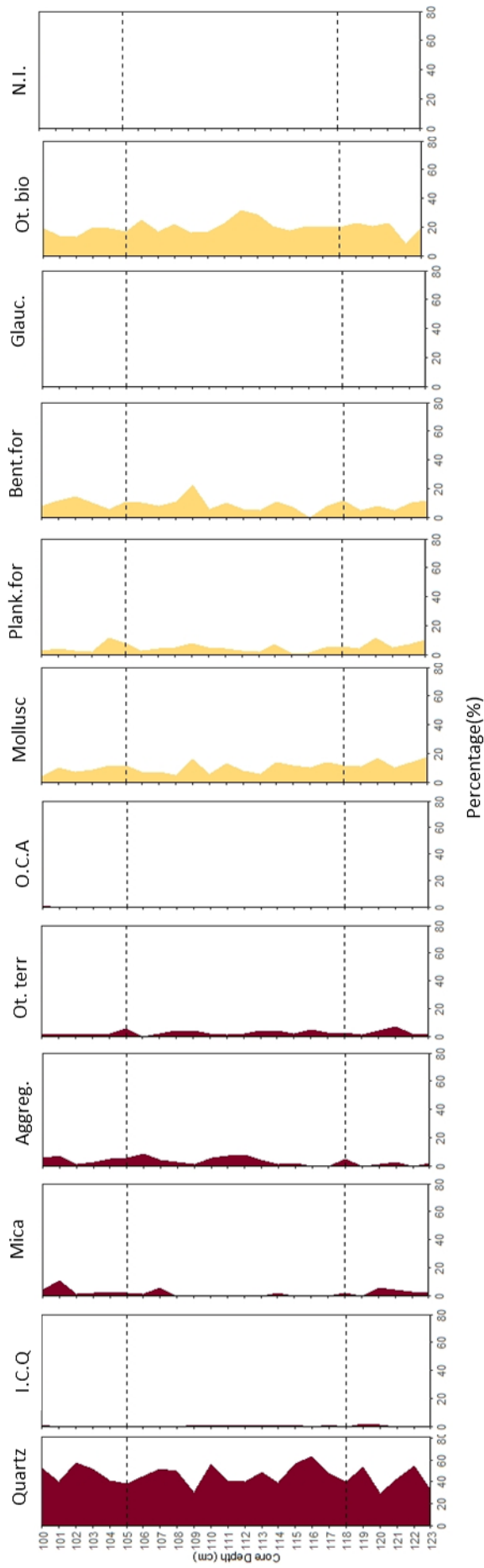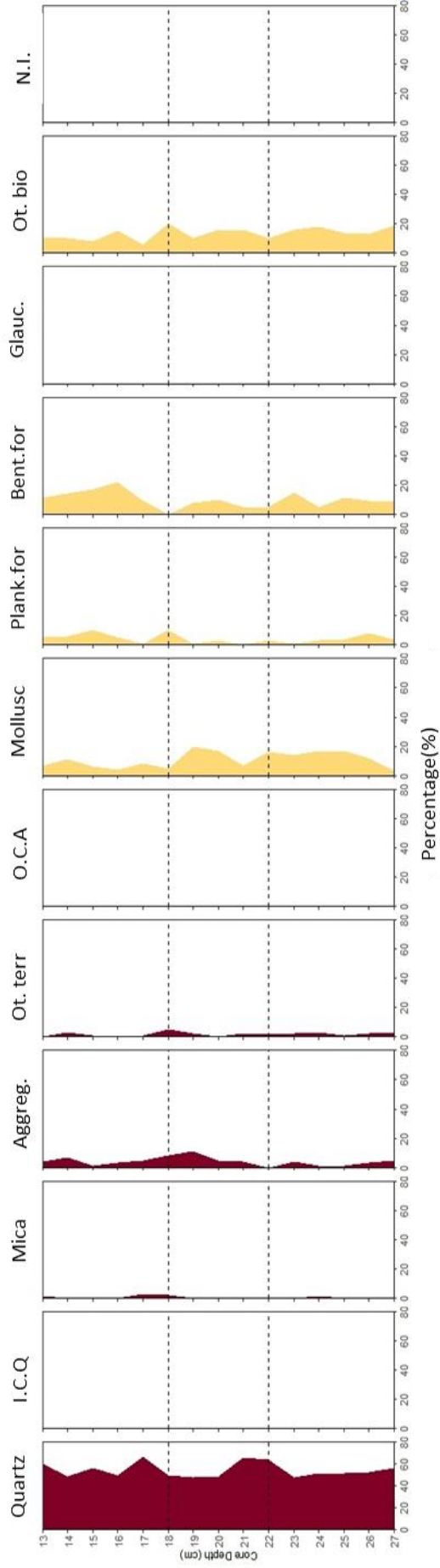

Figure 25. Sand mineralogical compositions of Layer 4 fraction 250 μm. Black dashed line represents the ASTARTE defined layers.
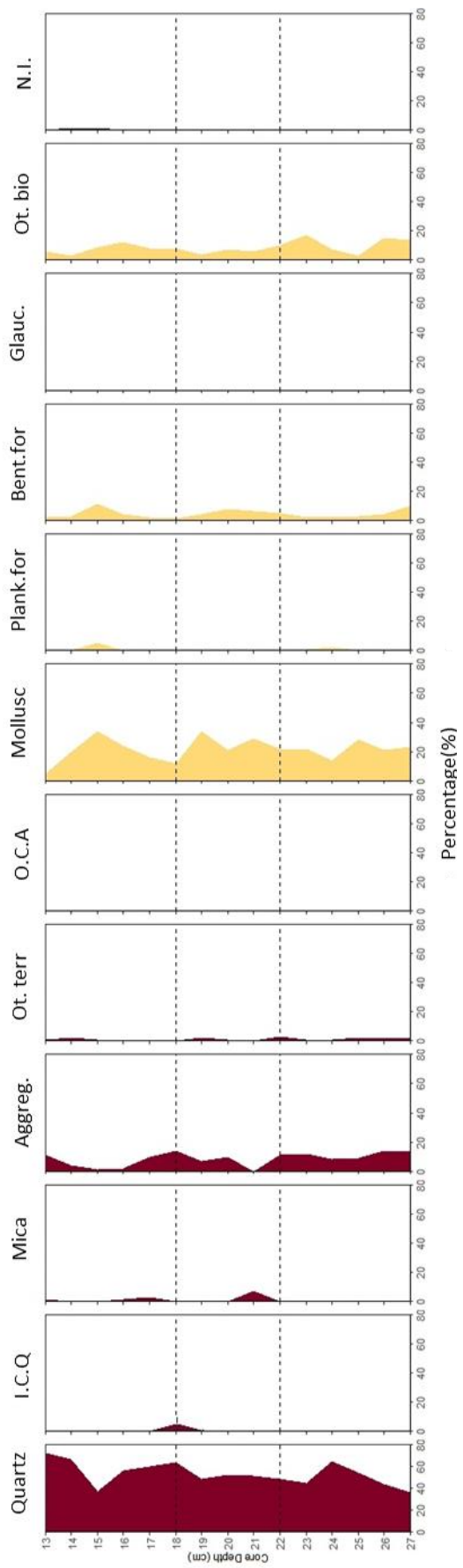
Figure 26. Sand mineralogical compositions of Layer 4 fraction 500 µm. Black dashed line represents the ASTARTE defined layers.

5.3.5. *Synthesis of the sand mineralogical composition results for Layer 1, 2, 3 and 4*

From the previous results, it was found similar patterns in all layers at the ASTARTE defined layers (ADL) of the studied core (Figure 27). Similar patterns included:

- The relative presence of continental related material from the local coastal area (iron-coated quartz and orange clay aggregates) in the ADL (117 cm, 115 cm, 114 cm, 113 cm, 112 cm, 111 cm, 110 cm, 109 cm, 107 cm, 105 cm), but also present in few levels above and below the ADL in the Layer 1 (120 cm, 119 cm, 104 cm, and 100 cm). At Layer 2 it was found at level 72 cm. At Layer 3 it was found from levels 39 cm to 31 cm. At Layer 4 was found at level 27 cm;

- In all the layers, except to Layer 1, the increase of molluscs was mainly at the upper part of the ADL, in Layer 2 (67 to 68 cm); Layer 3 (32 cm to 30 cm); and Layer 4 (20 cm to 18 cm);

- Mica showed a decline or even absence at the ADL and an increase at levels above or below the ADL at Layer 1 and Layer 4, while in layers 2 and 3, these variations were observed at the upper boundary of the ADL.

Core depth (cm)	Lower mica contents (ADL)	Increase of molluscs (ADL)	Fragments of wood	Iron coated quartz	Orange clay aggregates	
~20	X	X	(wood)	*		ADL Layer 4
~33	X	X	(wood)	*	***	ADL Layer 3
~68	X	X	(wood)	*		ADL Layer 2
~110	X		(wood)	***	*	ADL Layer 1

Figure 27. Summary of sand mineralogical composition results for all the layers. (wood symbol) - Fragment of wood. X – When agreed with the evidence. * It was used to describe the quantity (count) of the allochthonous material found. * 0 – 5; ** 5 – 10; *** more than 20. Dotted orange line – ASTARTE defined layers. ADL – ASTARTE defined layers

5.4. Statistical analyses

5.4.1. *Kruskal-Wallis*

5.4.1.1. *Layer 1*

The Kruskal-Wallis test of the levels of Layer 1 is summarized in Figure 28 and reveals that some of the sand mineralogical compositions were significantly different between the defined 3 groups ("Below ADL", "ADL", "Above ADL") (Annex D). The mineralogical composition quartz presents predominance in the levels of Layer 1 up to 80% (Figure 28(a)). The observation of the boxplot diagrams (Figure 28) for each sand mineralogical composition allowed to identify the differences between each group defined in this work. However, sand mineralogical composition shows minor significant differences between the 3 defined groups. The "ADL" is characterized by higher values of iron-coated quartz (0.5 – 0.8%) and other biogenic (18% – 19%) than the "Above ADL" and "Below ADL" levels. The results of iron-coated quartz demonstrated a significant difference and the Dunn test (Annex E), showed differences between "Above ADL" and "ADL" levels (p-value = 0.0328), also supporting the differences observed at the boxplot (Figure 28(b)). Other sand mineralogical composition that demonstrated that there was a significant difference is mica (p-value = 0.02767), and the Dunn test shows that mica was only significantly different between the levels corresponding to "Above ADL" and "ADL", as it suggested by p-value of 0.00756 and Bonferroni test 0.0227 (Figure 28(c)). Other terrigenous also shows a significant difference in the Kruskal-Wallis test (p-value = 0.02744), this difference was supported by the Bonferroni result of a p.adj of 0.0224. The results of the molluscs demonstrated a significant difference (p-value of 0.01933), and Bonferroni test exhibit a significant difference between "Above ADL" layers and "Below ADL" layers (p.adj = 0.0182). In the case of the molluscs it was observed a decrease in towards the top of Layer 1 (Figure 28(g)), expressed by the highest mean value of molluscs at the "Below ADL" levels and the lower at the "Above ADL" levels.
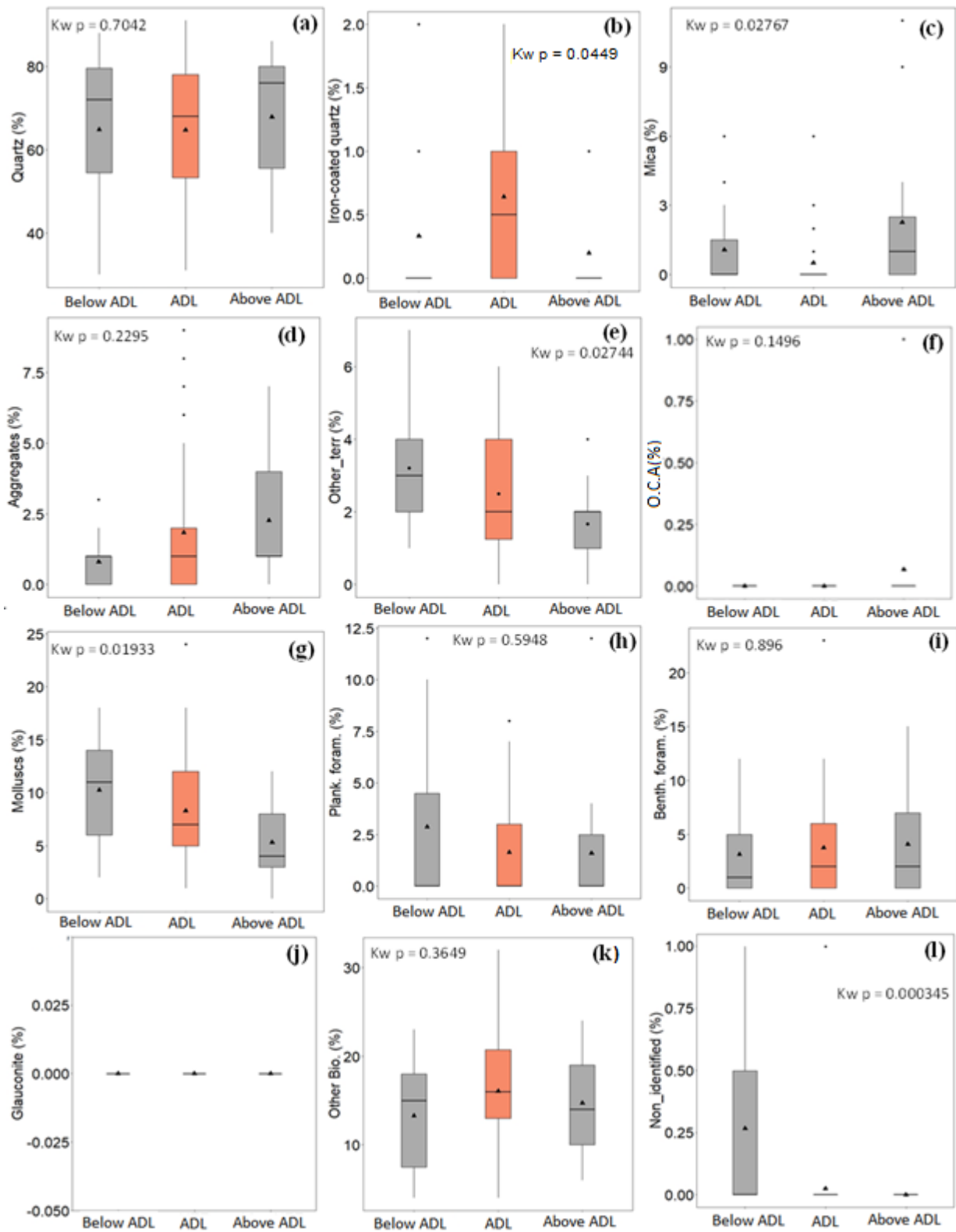
Figure 28. Boxplot with the comparison of sand mineralogical composition results throughout the 3 groups. Kw p - Kruskal-Wallis p-values results. Black triangles represent the mean values.

49

5.4.1.2. *Layer 2*

The Kruskal-Wallis test of the levels of Layer 2 is summarized in Figure 29. However, the sand mineralogical compositions variations were observed in the boxplot, there were no significant different results between the defined 3 groups ("Below ADL", "ADL", "Above ADL") for any of these elements. The sand mineralogical composition quartz showed the highest concentration in Layer 2 up to 60% (Figure 28(a)). The "ADL" levels were characterized by higher means values and medians values of iron-coated quartz and other terrigenous (Figure 29 (b) and Figure 29(e)), whereby iron-coated quartz was only present at the "ADL" levels. On the other hand, the values for mica reached the highest values in the levels "Below ADL" and "Above ADL" (Figure 29Figure 28(c)). In the case of mica, although the ranging of values was wider in the "Above ADL" levels, and the means values higher, the Kruskal-Wallis test shows not significant difference (p-value = 0.7144). For the other terrigenous, the mean value was slightly higher in "ADL" levels than the "Below ADL" and "Above ADL", however, the medians values did not show marked differences (p-value = 0.3865). The results of the molluscs component shows a slight increase in the mean and medians values of "ADL", but again p-value of 0.7506 is not significant (Figure 29 (g)).
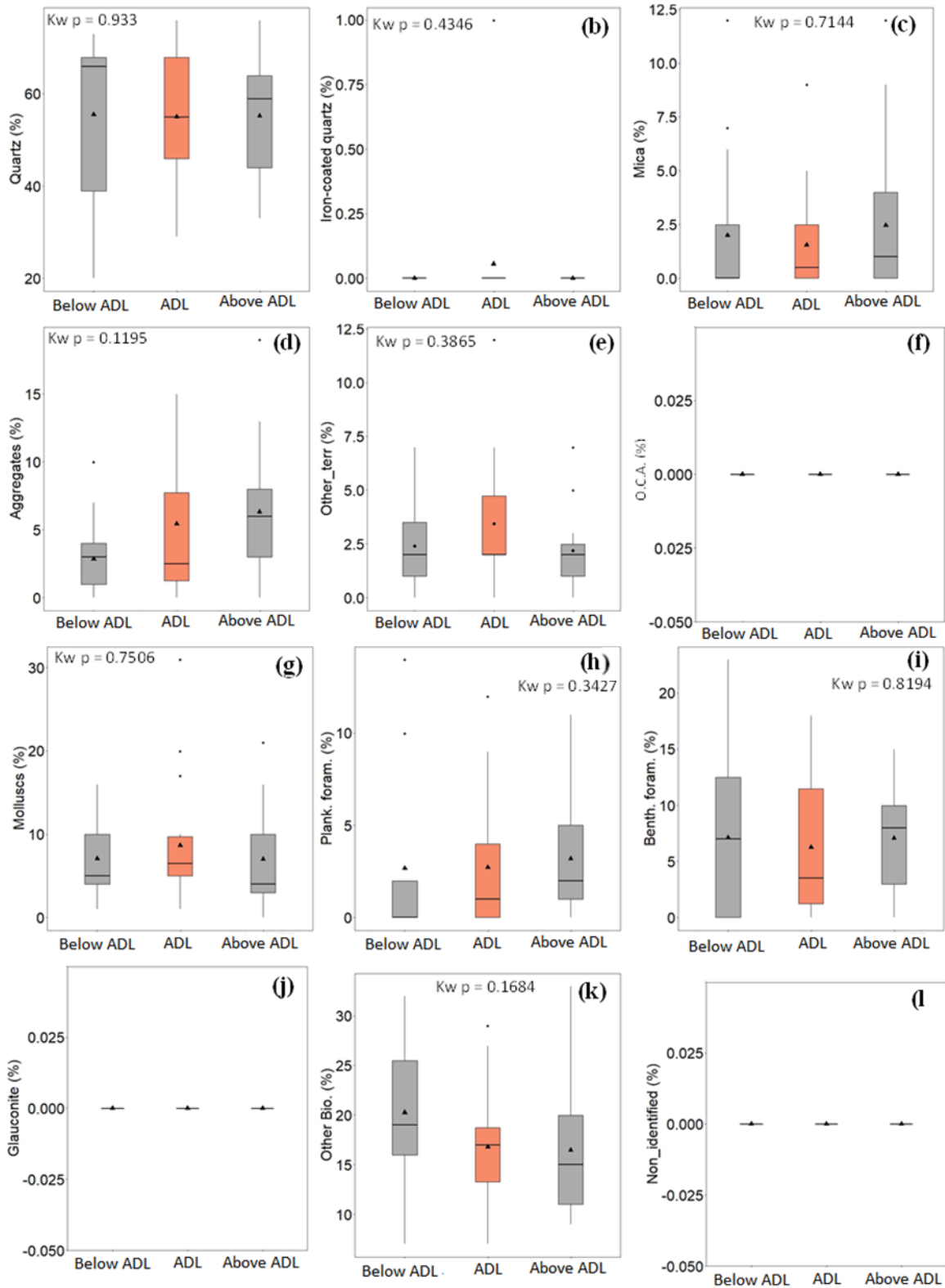
Figure 29. Boxplot with the comparation of sand mineralogical composition results throughout the 3 groups. Kw p - Kruskal-Wallis p-values results. Black triangles represent the mean values.

5.4.1.3. Layer 3

The Kruskal-Wallis test of the levels of Layer 3 is summarized in Figure 30 and reveals that only orange clay aggregates demonstrated significant difference between the defined 3 groups ("Below ADL", "ADL", "Above ADL"). The Dunn test (Annex E) results of orange clay aggregates showed a significant difference between "Above ADL" and "ADL"; "Above ADL" and "Below ADL" (p-value = 0.0187, 0.0481), supporting the differences observed at the boxplot (Figure 30(f)), in the "ADL" this element reached the maximum value of about 25%. Quartz was the most abundant assemblage between the sand mineralogical compositions up to 70% (Figure 30(a)). Iron-coated quartz did not show statistically significant difference (p-value = 0.79), although this sand mineralogical composition shows higher mean value in the "ADL" (Figure 30(b)). Regarding mica, the values reached a maximum in "Above ADL" (Figure 30(c)), but the statistical analysis did not show significance differences (p-value = 0.19411).
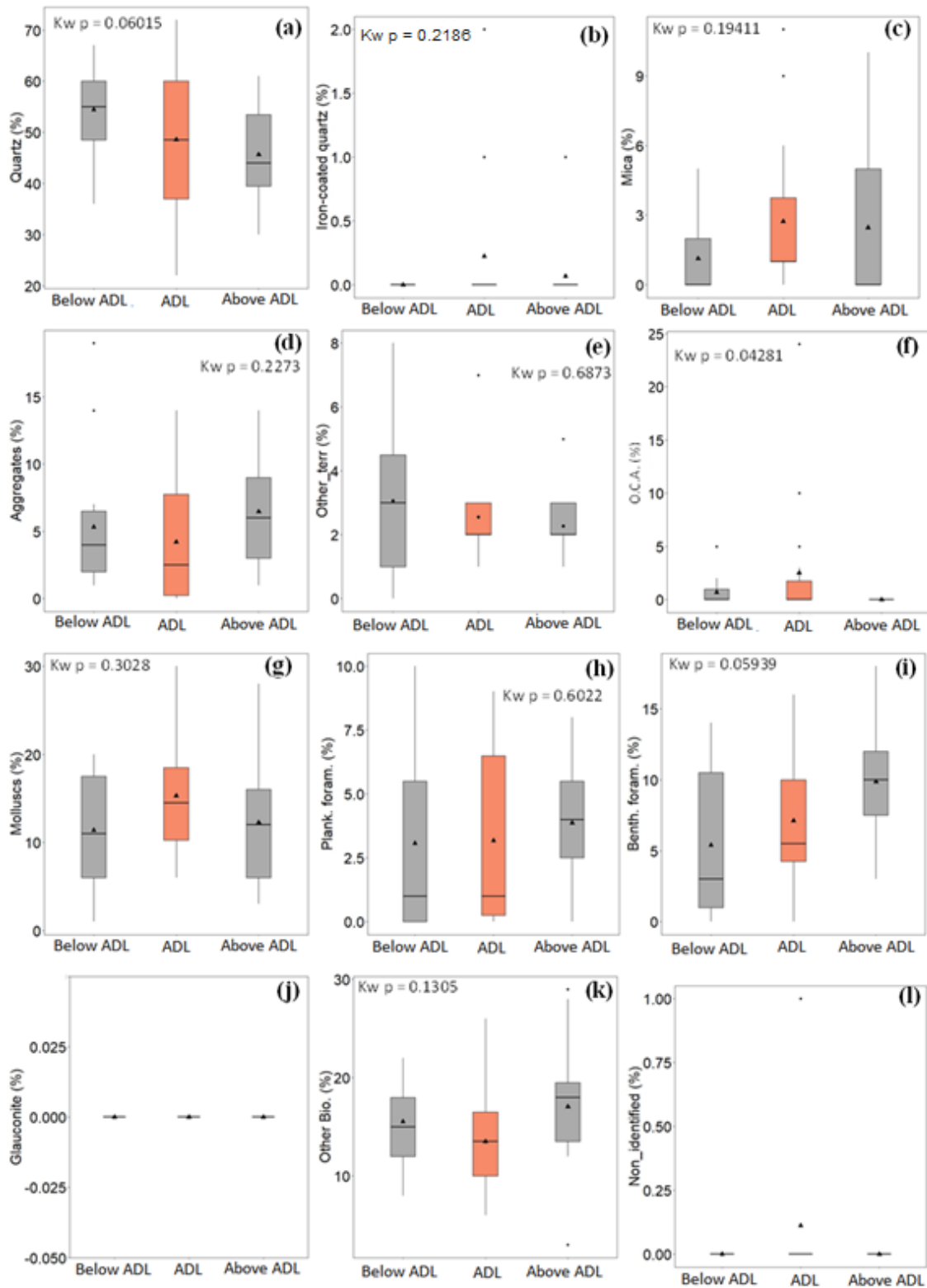
Figure 30. Boxplot with the comparison of sand mineralogical composition results throughout the 3 groups. Kw p - Kruskal-Wallis p-values results. Black triangles represent the mean values.

5.4.1.4. *Layer 4*

The Kruskal-Wallis test of the levels of Layer 4 is summarized in Figure 31 and reveals the sand mineralogical compositions demonstrated significant differences between the defined 3 groups ("Below ADL", "ADL", "Above ADL") it was only noted for other biogenic (p-value = 0.01529) (Figure 31(k)) and the Dunn test, flowed by Bonferroni test showed that other biogenic were significantly different between "Above ADL" and "Below ADL" (p-value = 0.00386; p.adj = 0.0116). The means value of iron-coated quartz was lower compared to the other sand mineralogical composition. However, only "Below ADL" and "ADL" levels were characterized with this assemblage. Although quartz shows higher means values and ranging of values wider in the "Above ADL" levels (Figure 31(a)), statistical analysis showed that was not significant difference between the 3 defined groups (p-value = 0.4575). The "ADL" levels were characterized by a lower content of mica, expressed by the lowest means, while "Above ADL" presented a higher ranging of values (Figure 31(c)), but Kruskal-Wallis did not show a significant difference (p-value = 0.186). In the case of molluscs, there is a visible difference between the 3 defined groups, explained by means and medians values higher in "ADL". Nevertheless, the Kruskal-Wallis test showed that this difference was not significant (p-value = 0.07208).
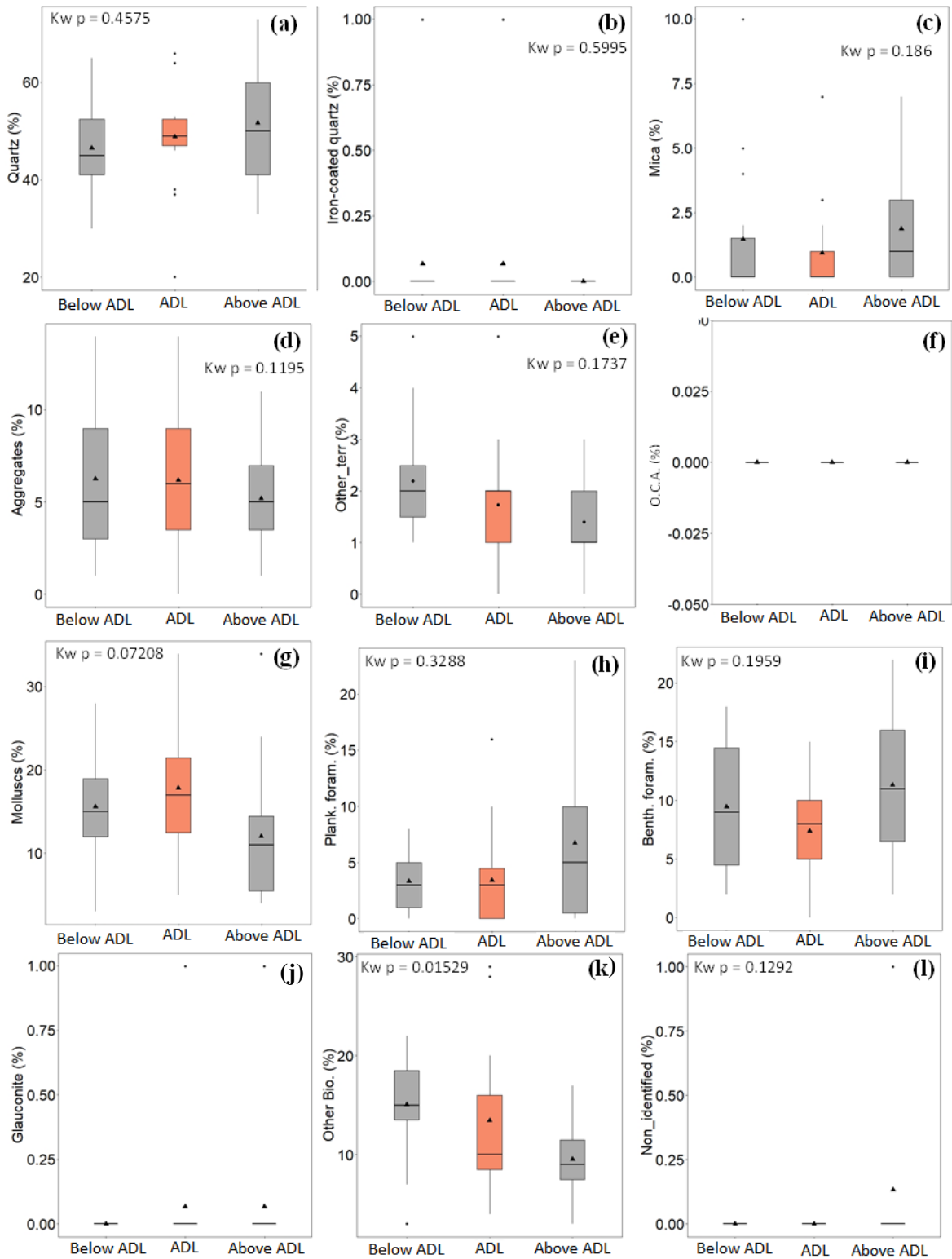
Figure 31. Boxplot with the comparation of sand mineralogical composition results throughout the 3 groups. Kw p - Kruskal-Wallis p-values results. Black triangles represent the mean values.

6. DISCUSSION

In geological studies of tsunami around the world, reliable identification methods for tsunami deposits have not yet been established. This is because it is difficult to recognize these events based on some predefined proxies. Plus, these deposits are usually evaluated in coastal areas because it is relatively easy to identify proxies at continental environment, originating from the sea. But, identifying proxies originating from the coastal in marine areas is definitely a higher challenge. Besides this, to distinguishing tsunami deposits from those from other high energy events, such as storms is not always easy (Costa et al., 2021). Thus, the best approach for the identification of offshore tsunami deposits, followed by this work, is based on a coherent multiproxy data (e.g. Smedile et al., 2011; Veerasingam et al., 2014; Tyuleneva et al., 2018; Riou et al., 2020).

This discussion structure includes in first the developed work in this thesis, focus on the sand mineralogical composition of the coastal and the studied core layers. Second is the results of the ASTARTE project (subtask WP2.2) and finally the multiproxy approach with all the proxies studied in this work and in some in ASTARTE project (subtask WP2.2).

6.1. Searching for continental related source sediment in the studied core

The sand mineralogical composition of the coastal samples of the Faro-Armação da Pêra section showed the prevalence of quartz (hyaline or iron-coated quartz) and orange clay aggregates (Figure 12, Figure 13, Figure 14). Considering that quartz is the most abundant mineral (Bevandić et al., 2020) and can be found in different environments, quartz hyaline cannot be considered an allochthonous material in the core samples. At the coastal sites, the sand mineralogical elements at Forte Novo and Vale do Lobo cliffs was predominantly of ferruginous sands (iron-coated quartz and orange clay aggregates). Regarding to the three different sand fractions observed in the coastal samples, the orange clay aggregates were mostly found in the 125 µm sand fraction (Figure 12), while the iron-coated quartz was predominant in the 250 µm and 500 µm sand fractions. In the studied core (MW107), these mineralogical elements (iron-coated quartz and orange clay aggregates) were detected in layers 1, 2, 3 and 4 (Figure 15, Figure 16, Figure 17, Figure 19, Figure 21, Figure 22, Figure 23 and Figure 26), probably because the cliffs are an ancient sedimentary source while the sediments of the beaches are constantly renewed. Orange clay aggregates was absent in Layer 2 and Layer 4, in contrast, iron-coated quartz

was found in all studied layers. However, the iron-coated quartz was present in more levels in Layer 1, the orange clay aggregates were more abundant in Layer 3, especially at level 32 cm, represented by 24 % of the total sample (Figure 21).

The presence of the continental related material from the coastal areas was different depending on the sand fraction observed. Iron-coated quartz was present in all the studied fractions, but more abundant in the 250 µm and 125 µm. The composition "orange clay aggregates" was only found in the sand fractions of 250 µm and 125 µm fractions, but more abundant in 125 µm (Figure 32).
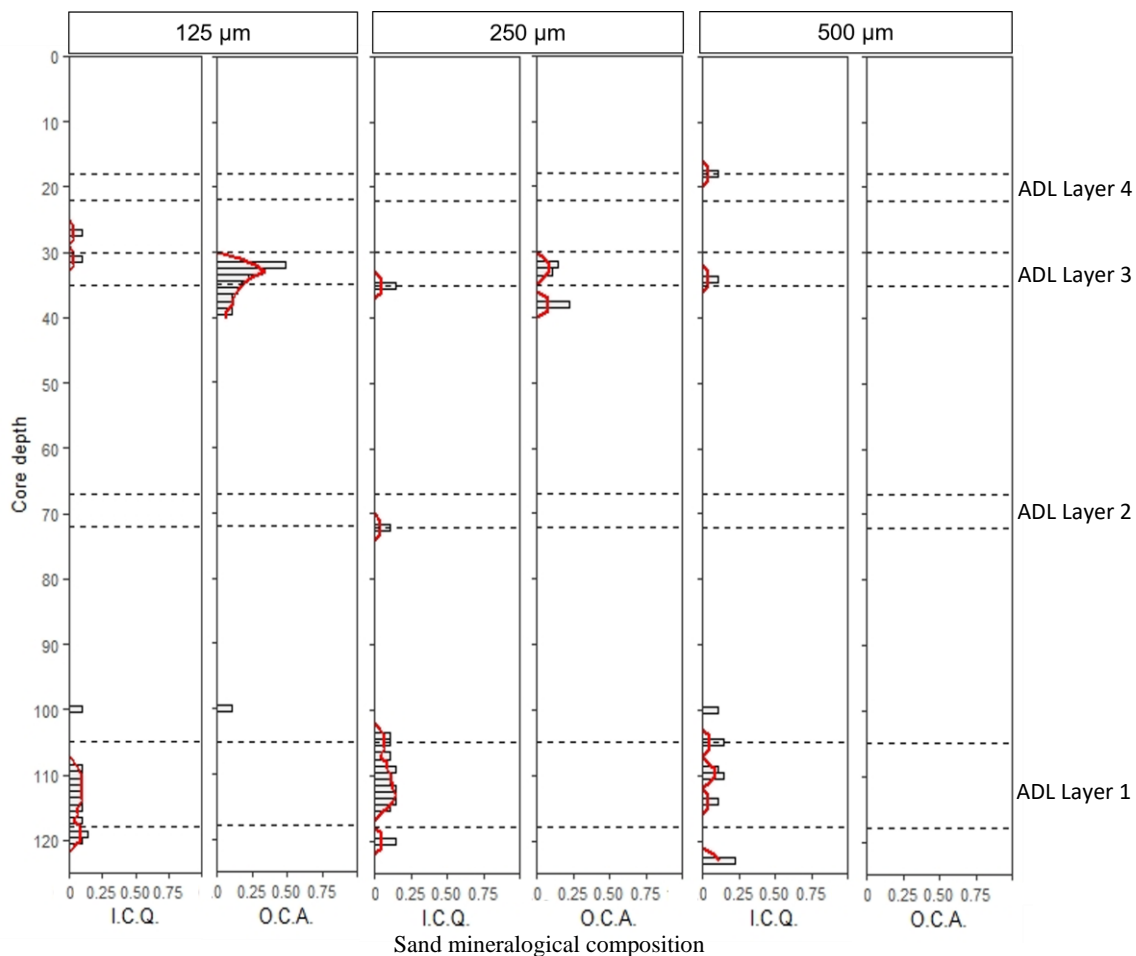
Figure 32. Presence of continental related sand composition in the core for each studied fraction. I.C.Q.– iron-coated quartz; O.CA.-orange clay aggregates; red line – moving average; dashed black line – ASTARTE defined layers. ADL – Astarte defined layers.

In a study of the estimated volume of sediments deposited by the 1755 Lisbon tsunami in Boca do Rio (Algarve) was suggested that a large dune was destroyed and a significant amount of sand it was transported offshore (Oliveira et al., 2009). In the case of the present work, the presence of the continental related material from the coastal areas in the core may suggest the contribution of the cliffs material in the studied core and their

occurrence is associated with transport seaward, which can be result of a high energy event or also to transport by the action of remobilization over the time by currents. Studies demonstrated that the high energy event (e.g. tsunami) erodes the coastal sediments during the uprush and transports this material during the backwash, which cause a mass transport towards offshore until lose the inertia and accumulates these material in a deposit offshore (Abrantes et al., 2008; Riou et al., 2020b). Considering that the studied core is located in 57 m depth, the distance between these cliffs sites and the core and the abundance of continental related material in the studied core, especially at Layer 1 and Layer 3 rise hypothesis of a high energy event transport capable of causing the erosion onshore and transport this material to the continental shelf is reasonable (Figure 33).
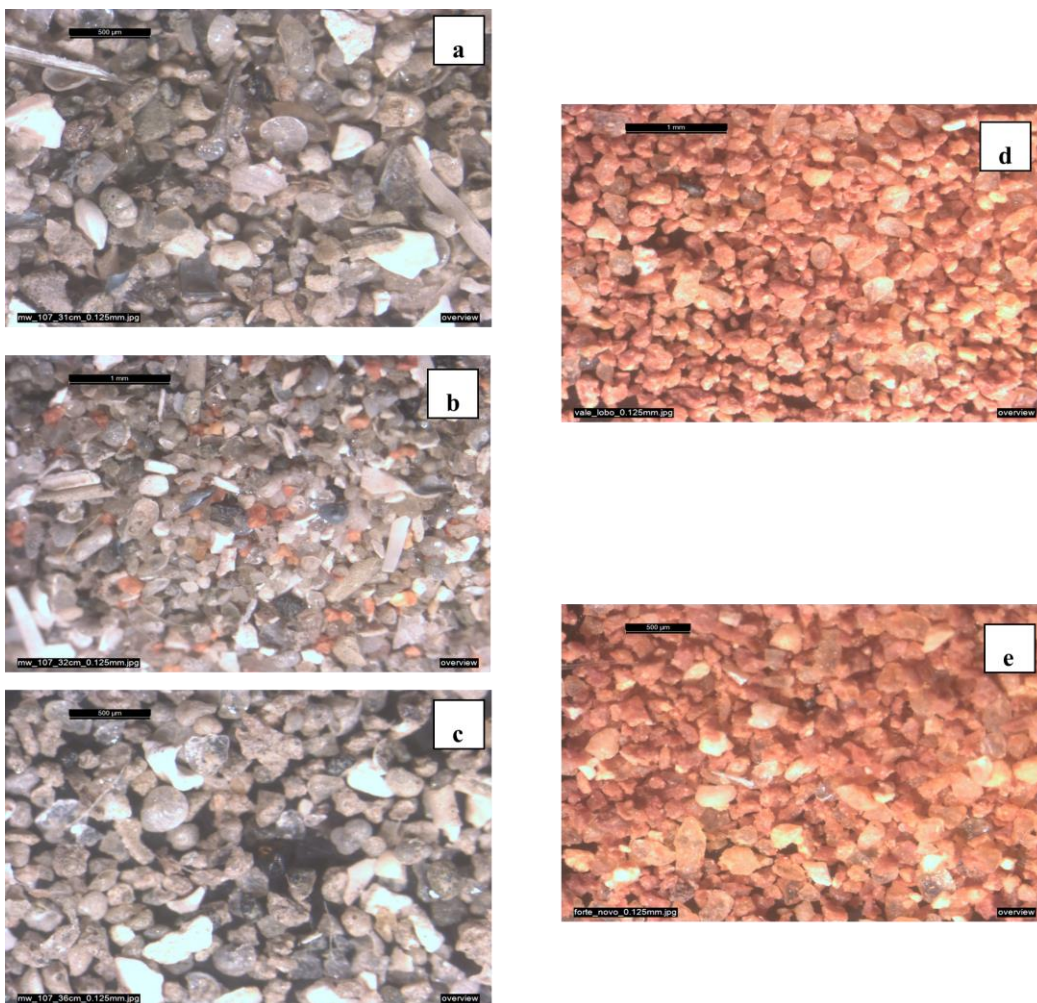
Figure 33. Photographs of the samples mineralogical composition 125µm fraction, a, b and c represent samples from the Layer 3, respectively at 31 cm, 32 cm and 36 cm; d and e are samples from Vale do Lobo cliff and Forte Novo cliff.

The variation of mica along the levels shows that in the ADL mica was almost absent or in very low percentage, except in uppermost part of the ADL (maximum 3 cm of

the limit with the top of ASTARTE defined layers) or in the 5 cm above the ADL, where mica presents the highest percentages. As mica is a mineral that is deposited in calm environments (e.g. Proske et al., 2011), its presence or absence can be indicative of the energy of the environment. A similar characteristic of the presence of mica was observed by Jagodziński et al. (2009), in tsunami deposits onshore Kho Khao Island (Thailand), and interpreted as mica has a particular planar shape which makes it more likely to be suspended in water and settled thereafter further offshore in the top or upper boundary of the tsunami sequence. The enrichment of mica was observed in top or in the uppermost part of the ADL (Figure 15, Figure 17, Figure 18, Figure 21, Figure 22, Figure 23, Figure 24, Figure 25 and Figure 26) and in the boxplot in the "Above Layer" samples of all the layers (Figure 28, Figure 29, Figure 30 and Figure 31). A good example is given at Layer 3, where the rapid decrease (absence) of mica at level 32 cm, coincides with the increase of continental related sediments (maximum peak of the orange clay aggregate).

In the "others terrigenous" elements we`ve considered, separately, wood fragments presence. They were found at the following levels in Layer 1 (107 cm and 101 cm), Layer 2 (71 cm), Layer 3 (35 cm and 28 cm), but especially in Layer 4, where wood fragments were present at 4 levels (24 cm, 23 cm, 22 cm and 17 cm). These findings were akin to those found offshore at Khao Lak, Thailand by Feldens et al. (2009) which reveal distinct characteristics in the tsunami deposits. According to these authors, the tsunamigenic deposit (transported by the backwash flow of the 2004 Indian Ocean tsunami) usually contains shells, wood fragments and grass of terrestrial origin. In the present study, the observation of this type of terrestrial material that is common inland, in the offshore tsunami deposits may suggests that these were transported by backwash flow (Sakuna et al., 2012).

In all layers the enrichment of molluscs was observed in the upper or in the top levels of the ADL, in Layer 3 (34 cm to 31 cm), in Layer 4 (20 cm and 19 cm), in Layer 2 (65 cm to 64 cm). In Layer 1, the increase of molluscs was observed in the within of the in the ADL (114 cm). Abrantes et al. (2008) and Toyofuku et al. (2014) interpreted the disturbed sedimentary bed formed by shells fragments the product of reworked and transported material by tsunami. Tyuleneva et al. (2018) also suggest that the enrichment of shells indicates an influx of new sediments and is the result of a turbulent flow capable of transporting the shells along with old costal sediments.

The statistical results show significant differences in Layer 1, Layer 3 and Layer 4 (Figure 28, Figure 30 and Figure 31). Layer 1 showed significant differences between the ADL and their 5 cm above and below for iron-coated quartz, mica, other terrigenous and non-identified. Conversely, Layer 2 did not show any significant differences between the levels above and below the in the ADL (Figure 29). In Layer 3 the statically significant differences was only for orange clay aggregates (Figure 30), and Layer 4 only for the other biogenic (Figure 31). Although the statistical results do not present significant differences for more sand mineralogical components between the studied groups determined for this analysis ("Above ADL", "ADL", "Below ADL"), it was possible to observe the differences of each sand mineralogical composition in the studied layers. The lack of significant differences between the 3 defined groups might be related to the result of the high energy event that mix the eroded material from inland with reworked material (Font et al., 2010).

6.2. High energy events layers defined in ASTARTE project

The layers were defined in the scope of the ASTARTE project based on grain-size parameters, XRF and magnetic parameters (Drago et al., 2016). Variations in mean grain-size, an increase of terrigenous or detrital geochemical proxies (XRF) and magnetic susceptibility as shown in the following Figure 34, and magnetic mineral phases in the Deliverable report 2.43 (http://194.117.20.221/index.php/deliverables.html).

The mean grain-size ranges from 212 µm (113 cm) to 12 µm (1 cm), fining up towards the top of the core, with an interruption at level 32 cm as the mean grain-size increases to 216 µm (Figure 34). The increase of the mean grain-size was observed in all the ADL; however, it was more pronounced at Layer 1 and Layer 3. The increase of grain-size is a feature frequently observed in tsunami deposits offshore (van den Bergh et al., 2003; Quintela et al., 2016; Tyuleneva et al., 2018). The textural components of the core were predominantly sand (from 17.1% to 75.2%) and silt (from 14.5% to 56.6%), followed by clay (from 5.9% to 24.8%) and gravel (from 0% to 14.9%), with an increase of sand and gravel in the ADL, these results agree with the increase of the mean grain-size both determined in the ASTARTE project.
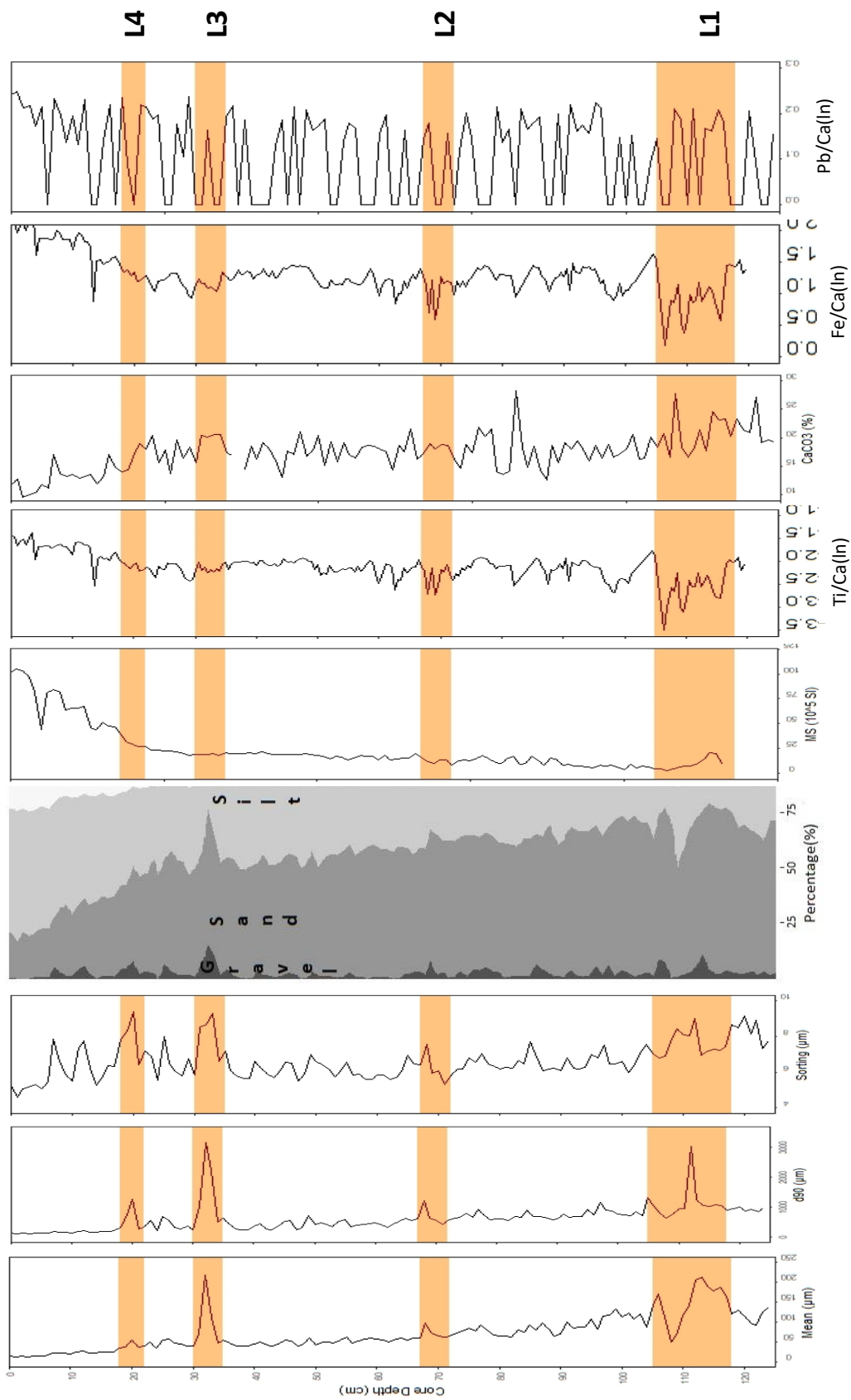
Figure 34. Multidisciplinary results from ASTARTE project. The grain-size was performed using laser diffraction for fraction < 500 μm and sieving for fractions <500 μm. The highlight in orange in the graphics represents the ASTARTE defined layers (ADL) of each Layer (L). MS – Magnetic susceptibility, Ti/Ca, Calcium carbonate, Fe/Ca (ln) and Pb/C(ln).

61

In particular, the statistical parameters based on grain-size analysis, such as sorting shows the samples to be very poorly sorted in the entire core. However, the ADL presented peaks in sorting with the maximum degree of very poorly sorted (Figure 34). Tyuleneva et al. (2018), recognized evidence of tsunami deposits with similar patterns offshore of Jirs al-Zarka in Israel with distinctive deviations in mean and sorting between the anomalous layers and the background layers. The D90 is an additional statistical parameter of the grain-size, these parameters presented peaks of increase at levels of Layer 1 (112 cm), Layer 2 (68 cm), Layer 3 (32 cm), and Layer 4 (20 cm) as the D90 shows 90% of the particle size distribution along the core. This increase might be related with a high energy event capable to transport the coarser sediments offshore (Sakuna-Schwartz et al., 2015).

The magnetic susceptibility studied in the ASTARTE project was obtained with the multi-sensor core logger. In general, magnetic susceptibility core values are low except for the 30 cm to the top (Figure 34), which displays maximum oscillation reaching 105.6 (10^{-5} SI) while the lower part of the core is characterized by lower values (2.3 (10^{-5} SI)). Although magnetic susceptibility shows uniform values from 100 cm to 18 cm, at the ADL was observed an increase of magnetic susceptibility values towards the top of each layer.

An increase of terrigenous proxies (Fe/Ca) are visible in all layers, except in Layer 4. Titanium/Calcium (Ti/Ca) ratios are usually used as proxy to investigate tsunami deposits to study the terrigenous input (Sakuna et al., 2012; Smedile et al., 2019; Riou et al., 2020b). XRF-log data results from the ASTARTE project reveal the increase in Ti/Ca ratio from the base towards the top, which might be associated with very coarse sand facies with higher amounts of carbonates from the top to the base of the core. The ratio of Ti/Ca was marked by peaks in the ADL of Layer 1, 2 and 3, which coincides with the increase of the calcium carbonate ($CaCO_3$) (Figure 34). The peaks of $CaCO_3$ it was observed at Layer 1 (107, 109 and 115 cm), Layer 2 (69 cm) and Layer 3 (34 cm to 31 cm). The peaks in carbonates at the ADL of Layer 1, 2 and 3 support the increase of the mean grain-size and increase of shells at the sand chaotic layers. Thus, the increase of bioclastic results in the Ti/Ca ratio, probably due to the input of shells fragments and the presence of reworked material (Abrantes et al., 2008), but may also be related to the weathering of carbonate rocks outcropping in the continental area (Figure 34). The Lead (Pb) is related to anthropogenic material presents higher values towards the top of the core (15 cm to 0 cm)

and also a discrete increase at layers with chaotic shells and coarse grain-size, such as in the ADL levels in Layer 1 (from 110 cm to 112 cm).

6.3. Multiproxy approach of high energy events in the studied core

Regarding the continental related material from the coastal sites (iron-coated quartz and orange clay aggregates), their presence in ASTARTE defined layers (ADL), especially at the Layer 1 and Layer 3 support the possible terrigenous contribution (Table 13).

Table 13. Summary of signatures of tsunami deposit offshore found in each ADL - ASTARTE defined layer. ✓ - when was present; - when was not present; cm - depth where was found the evidence.

Indicators	ADL Layer 1 105 - 118 cm	ADL Layer 2 67 - 72 cm	ADL Layer 3 30 - 35 cm	ADL Layer 4 18 - 22 cm
Rapid variation in Grain-size	118 cm - 113 cm	68 cm	32 cm	20 cm
Increase in sand content	118 cm - 113 cm	69 cm	32 cm	-
Poorly sorting	115 cm - 109 cm	68 cm	33 cm to 31 cm	20 cm -18 cm
Enrichment in CaCO3	115 cm, 109 cm,107 cm	69 cm	34 cm to 31 cm	-
Increase of terrigenous proxies (Fe/Ca)	✓	✓	✓	-
Low or absent presence of Mica	✓	✓	✓	✓
Presence of Iron-coated quartz	117 cm, 115 cm, 114 cm, 113 cm, 112 cm, 111 cm, 110 cm, 109 cm, 107 cm, 105 cm,	72 cm	35 cm, 34 cm, 31 cm	-
Presence of orange clay aggregates	-	-	39 cm to 32 cm	-
Enrichment in Molluscs	114 cm	66 cm to 64 cm	34 cm to 31 cm	20 cm, 19 cm, 15 cm
Presence of wood fragments	107 cm	71 cm	35 cm	22 cm

The depths with higher contents of iron-coated quartz and orange clay aggregates were similarly almost coincident with the depths of higher mean grain-size, especially at 32 cm depth (Layer 3). The increase of mean grain-size and of shells in the ASTARTE defined layers of Layer 1, 2, 3 and 4 and decrease of mica in ASTARTE defined layers support the hypothesis of a possible high energy event involved which transported continental related material offshore (Abrantes et al., 2008, Dawson and Stewart, 2008).

There are 3 types of events that drive continental material from onshore to offshore areas: (i) tsunami, (ii) storm and (iii) flash floods. The differentiation between the offshore deposits resulting from storms and tsunamis has been challenging because although they are generated by different mechanisms, they can be characterized by similar features in the

deposits, such as coarser grain-size (Costa et al., 2021). Offshore tsunami deposits are usually constituted by coarser sediments, which are also poorly sorted than the storm deposits (Goodman-Tchernov et al., 2009). Considering the distance from the location where the continental related sediments were predominated (Vale do Lobo and Forte Novo cliffs) and the presence of these sand mineralogical elements associated with coarser sediment levels in the core located at 56.7 m depth may it is associated with a high energy event capable of eroding and transporting the material from the coast to the continental shelf. Whereas deposition related to storm events are normally restricted to within 2 km of the coastline (Smedile et al., 2012) and the core MW107 is located at about 7 km from the coastline. As the depth increases, the seabed is less disturbed by storms and more for tsunami (Weiss and Bahburg, 2006). Kümmerer et al. (2020) studied the same core and defined after Weiss and Bahlburg (2006), assuming the boundary water depth where storm waves affect bottom sediments is 58 m (where is located the core MW107), the wave should be higher than 14 m to rework tsunami sediments. Since the registrations wave height of the study area is predominant lower than 1 m, and few waves greater than 3 m (2 %) (Costa et al., 2001), and the depth of closure in this area is around 10 m depth (Almeida et al., 2010), the storm events might be unlikely. Therefore, Kümmerer et al. (2020), considering the direction of the storm in the study area (southwest) and the depth, where is located the core, showed that the hypothesis of erosion of tsunami deposit by storm waves can be excluded. These observations may explain the evidence of terrigenous material in the defined layers. Terrigenous material from coastal areas can also be transported offshore by fluvial floods, however, the flood deposits offshore are generally less sorted and composed of finer sediments than the tsunami deposits, because of the high energy associated with the tsunami backwash capable of transporting coarser sediments (Sakuna-Schwartz et al., 2015). According to the location of the studied core, it is unlikely to have fluvial flood deposits due to the depth greater than the areas of fluvial discharges (Hindson and Andrade, 1999). However, the Algarve is one of the regions that has the lowest extreme events of fluvial flood reported (Zêzere et al., 2014). On the other hand, this region is frequently triggered by flash floods due to heavy precipitation events (Barbosa et al., 2018). Likewise, the heavy precipitation of December 1876 which caused several floods in the Iberian Peninsula (Trigo et al., 2014). However, fluvial floods events produce less pronounced imprints in the deposits than the tsunami events and are usually closer to the coast due to the lower energy involved (Sakuna-Schwartz et al., 2015).

The age model developed by Kümmerer et al. (2020) suggests that the core MW107 dates back to 4155 - 3785 BCE. If we compare the ASTARTE defined layers ages with existing studies, we can find some possible correlations between our layers ages and potential high energy events. For example, Layer 1 model age suggests ages from 4155 to 3448 BCE (Kümmerer et al., 2020), a similar age (3700 cal. BP) was found in a possible unknown tsunami event layers at 65 m depth off southwestern Algarve coast (Portugal) (Feist et al., 2019 in Reicherter et al., 2019; Bellanova et al., 2019, Feist et al., 2020). Bellanova et al. (2019), observed 25 cm thick well sorted sand layer with shells debris and increases of Si and Ca/Fe and peaks of n-alkanes, which suggests the input of terrestrial material. Feist et al. (2020) studied the same core and suggested a possible tsunami event non-identified in Portugal before and may be correlated to the Spanish tsunami layers identified by Koster and Reicherter (2014). These authors identified a layer event in the coast of Spain dated around 4000 years BP in the Golf of Cádiz. Tsunami deposits offshore were identified in the Andaman Sea in Thailand, with approximately 20 to 25 cm thickness with alternating layers of sand and mud (wide range of the grain-size distribution) and poorly sorted compared to the background sedimentation (Sakuna et al., 2012). In the present studied, the Layer 1 is characterized by grain-size variations along 22 cm thickness, which is alternating the particle size distribution of medium sand, very fine sand, medium sand, silt and medium sand. The layer at 112 cm depth is the coarser level at this layer with more than 10 % of gravel contents. Regarding the continental related material, iron-coated quartz was found in this layer at 12 levels (120 cm, 119 cm, 117 cm, 115 cm, 114 cm, 113 cm, 112 cm, 111 cm, 110 cm, 109 cm, 105 cm, and 100 cm) and fragments of wood (107 cm and 101 cm), which are frequently associated to the backwash (Feldens et al., 2009). The increase in particle size and carbonates coincide with the increase of terrigenous proxies (Fe/Ca) and presence of continental related material from the coastal area may suggest a potential high energy event related to this layer.

In the Layer 2, increases of grain-size and sand content was observed in the ASTARTE defined layers (Figure 34), however less marked than in Layer 1. The geochemical results show increases of carbonates and increases of terrigenous proxies (Fe/Ca). The continental related sand mineralogical elements (iron-coated quartz) was only found at 72 cm and wood fragments at 71 cm. The age of this layer is from 1468 to 662BCE (Kümmerer et al., 2020) did not coincide with any event from the tsunami catalogue and the proxies seems less marked than in the others studied layers.

The Layer 3 was marked by a rapid increase in grain-size, increased terrigenous proxies (Fe/Ca) and substantial presence of continental related material, such as orange clay aggregates at 32 cm (Figure 21). The presence of wood fragments and the absence of mica in the ASTARTE defined levels, support the argument of a high energy event that transported material from onshore to offshore. The Layer 3 is dated prior to 1755 CE (806 – 1461 CE) (Kümmerer et al., 2020), although the tsunami catalogues do not a present extreme event at this time, it is possible that this layer are from one event, as is common in tsunami deposits transport and redeposition of older material (Tyuleneva et al., 2018). Quintela et al. (2016), studied a core in the continental shelf of Algarve located 99 m depth. In this study the authors also considered levels below the levels dated for the 1755 CE, which could be possibly related to the 1755 CE Lisbon tsunami due to the enrichment of coastal foraminifera.

In the Layer 4 was observed the increase of mean grain-size, the presence of continental related sand mineralogical element (iron-coated quartz), and fragments of wood in several layers, which supports the terrigenous input in this layer. According to the model age of this core (Kümmerer et al., 2020), the age of potential levels of Layer 4 is from 1326 to 1794 CE, which might be associated with the 1755 Lisbon tsunami. Related to this tsunami event or evidence recorded already by other authors in the continental shelf of Portugal (Abrantes et al., 2008; Quintela et al., 2016, Kümmerer et al., 2020). Kümmerer (2019) also studied Layer 4. This author recognized in the sand composition analysis the enrichment of mica on the top of the tsunami layers and the presence of pieces of wood.

7. CONCLUSIONS

The work carried out in this study investigate evidence of terrigenous material transported from the coastal areas to the continental shelf based on the study of the sand mineralogical composition between the coastal sediments from Faro-Armação da Pêra and the ASTARTE defined layers (Drago et al., 2016), located in the continental shelf of Algarve in order to confirm the tsunamigenic origin of these layers. In total the sand mineralogical composition was studied in 36 samples from the coastal zone and 240 samples from the continental shelf. The characterization of the sedimentary (textural and mineralogical) from different coastal sites was an interesting approach for the identification of the source of the material possibly transported by high energy events into the continental shelf of Algarve.

Following is describe the key findings of these work applying the comparation of the sand mineralogical composition of the coastal area of Algarve and the continental shelf combined with the data results of the ASTARTE project (subtask WP2.2).

- The study of the sand mineralogical composition of the coastal sites highlighted the 2 main sand mineralogical elements in the coastal sites of Algarve. Iron-coated quartz and orange clay aggregates was applied as a proxy for continental related sediment mainly found in Vale do Lobo and Forte Novo cliffs sites. These sand mineralogical elements were found at the ASTARTE defined layers, especially in Layer 1 and Layer 3.

- The multiproxy approach applied in this work show that are three layers (Layer 1, Layer 3 and Layer 4) of the studied core potentially associated with high energy events in the continental shelf of Algarve. However, comparing the known tsunami events present in the catalogue with the studied sedimentary record is only one event that is apparently known in the core. According to the model ages for this core, the Layer 4 is the only one suitable for a historical tsunami in Portugal, the 1755 Lisbon tsunami.

- As the evidence supports the input of continental related material from the coastal area well matches with the increase of mean grain-size and the poorly sorting related to the layers above and below of the ASTARTE defined layers, and the increase of geochemical proxies, except at Layer 4, these results raise the hypothesis of the defined

layers could have been result of a high energy event such as tsunami, although the dates have coincided only for one know tsunami event.

- Layer 1: The Layer 1 revelated evidence such as a rapid increase in mean grain-size, enrichment in carbonates and terrigenous proxies (geochemical) and shells which coincides with the presence of iron-coated quartz is possibly associated to a potential high energy event. Therefore, this layer it may be related to an unknown event. The findings for this layer are in agreement with the study conducted by Feist et al., 2019 in Reicherter et al., 2019, Bellanova et al. 2019 and Feist et al. 2020.

- Layer 2: The Layer 2 showed lower variations compared to the other layers along the studied core. Despite this, some proxies that could be related to high energy event deposits were found, but it was notable that these findings were less pronounced than in the other layers. Also shown in the statistical analysis, which was the only layer that did not show any statistical differences between the 3 defined groups determined to the statistical analyses ("Below ADL", "ADL" and "Above ADL").

- Layer 3: The Layer 3 showed rapid increase in mean grain-size, poorly sorting, enrichment in carbonates and increase of terrigenous proxies (geochemical). Despite this, at Layer 3 great amount of continental related material was observed, similar to the elements of the sediments from the cliff sites of Vale do Lobo and Forte Novo, with increased mollusc fragments, absence of mica at the ASTARTE defined layers and presence of wood fragments. These arguments possibly suggest a high energy event layer and possibly a tsunami deposits, even considering that the age model of this layer was younger than the 1755 CE, the material carried by the tsunami wave backwash might be deposited on the older surface, due to the action of the tsunami waves eroding and remobilizing the seafloor sediments (Abrantes et al., 2008). Thereby the layers of 22 cm to 35 cm in this core might be related with a high energy event, which need detailed dating of these layers to be confirmed.

- Layer 4: The Layer 4 age coincides with the well known tsunami of 1755 and rapid increases in grain-size, presence of continental related material from the coastal area (iron-coated quartz) and wood fragments in several layers.

- The results found in this work show that the identification of the sand mineralogical composition of the coastal area can contribute to the identification of the terrigenous contribution related material transported offshore by possibly high energy events. The

studied also highlighted the importance of use a multiproxy approach, in order to explore the identification of potential high energy events in the sedimentary record.

- Following this work, further studies are recommended to study the sand mineralogical composition of the entire core, in order to confirm the background of the ASTARTE defined layer. Its also suggested to study more cores from the ASTARTE project (subtaskWP2.2) in order to obtain a lateral correlation. It is further recommended to date above and below the layers of potential high energy events, to determine if the material was deposit immediately after the event or if it is the result of subsequent remobilization and transport in the inner shelf should be conducted.

REFERENCES

Abrantes, F., Alt-Epping, U., Lebreiro, S., Voelker, A., Schneider, R., 2008. Sedimentological record of tsunamis on shallow-shelf areas: The case of the 1969 AD and 1755 AD tsunamis on the Portuguese Shelf off Lisbon. *Marine Geololgy,* 249, 283–293.

Almeida, L.P., Ferreira, Ó., Pacheco, A., 2010. Thresholds for morphological changes on an exposed sandy beach as a function of wave height. *Earth Surface Processes and Landforms*, 36, 4, 523-532.

Andrade, C., Freitas, M.C., Moreno, J., Craveiro, S.C., 2004. Stratigraphical evidence of Late Holocene barrier breaching and extreme storm in lagoonal sediments of Ria Formosa, Algarve, Portugal. *Marine Geology*, 339-362.

Andrade, C., Freitas, M.C., Oliveira, M.A., Costa, P.J.M., 2016. On the Sedimentological and Historical Evidences of Seismic-Triggered Tsunamis on the Algarve Coast of Portugal. *Plate Boundaries and Natural Hazards*, 1th edition, John Wiley & Sons, 219 -238.

Baptista, M.A., Miranda, P.M.A., Miranda, J.M., Mendes Victor, L., 1998a. Constrains of the source of the 1755 Lisbon tsunami inferred from numerical modelling of historical data on the source of the 1755 Lisbon tsunami. *Journal of Geodynamics*, 25. 159-174.

Baptista, M.A., Heitor, S., Miranda, J.M., Miranda, P., Mendes Victor, L., 1998b. The 1755 Lisbon tsunami; evaluation of the tsunami parameters. *Journal of Geodynamics*, 25: 143–157

Baptista, M.A., Miranda, J.M., Luis, J.F., 2006. In search of the 31 March 1761 earthquake and tsunami source. *Bulletin of the Seismological Society of America*, 96, 713-721.

Baptista, M.A., Miranda, J.M., 2007. The source of 1722 Algarve earthquake: evidence from MCS and Tsunami data. *Journal of Seismology*, 11, 371-380.

Baptista, M.A., Miranda, J.M., 2009. Revision of the Portuguese Catalog of Tsunami. *Natural Hazards and Earth System Science*, 9, 25-42.

Barbosa, S., Silva, A., Narciso, P., 2018. Analysis of the 1 November 2015 heavy rainfall episode in Algarve by using weather radar and rain gauge data. *Natural Hazards*, 93: S61-S76.

Bellanova, P., Reicherter, K., Costa, P.J.M., Feist, L., Freken, M., Schwarzbauer, J., Santisteban, J.I., Vött, A., Bosnic, U., Brückner, H., Schüttrumpf, H., Andrade, C., Duarte, J.F., Kuhlmann, J., 2019a. Uncharted archives – imprints of tsunami backwash deposits on the Algarve shelf (Portugal). EGU General Assembly 2020.

Bevandić, S., Blannin, R., Auwera, J.V., Delmelle, N., Caterina, D., Nguyen, F., Muchez, P., 2020. Geochemical and Mineralogical Characterisation of Historic Zn–Pb Mine Waste, Plombières, East Belgium. *Minerals*, 11, 8-24.

Bezzeghoud, M., Borges, J.F., 2003. Mecanismos Focais dos Sismos em Portugal Continenal. Focal Mechanisms of Earthquakes in Portugal. *Física de la Tierra,* 15, 229-245.

Blott, S.J., Pye, K., 2001. GRADISTAT: A grain size distribution and statistics package for the analysis of unconsolidated sediments. *Earth Surface Processes and Landforms*, 26 1237-1248.

Blott, S. J. & Pye, K., 2012. Particle size scales and classification of sediment types based on particle size distributions: review and recommended procedures. *Sedimentology* 59, 2071– 2096.

Chagué-Goff, C., Szczucinski, W., Shinozaki, T., 2017. Applications of geochemistry in tsunami research: A review. *Earth and Science Reviews*, 165, 203-2044.

Cita, M.B., Camerlenghi, A., Rimoldi, B., 1996. Deep-sea tsunami in the eastern Mediterranean new evidence and depositional models. *Sedimentary Geology*, 104, 155-173.

Coalala, N., 2013. *Environmental analysis of sedimentological parameters and heavy mineral sediments in the supply of the beaches in the region of Porto (Northern Portugal).* Master thesis Universidade do Porto, Porto, 137p.

Costa, M., Silva, R., Vitorino, J., 2001. Contribuição para o estudo do clima de agitação marítima na costa Portuguesa. 2ª Jornadas Portuguesas de Engenharia Costeira e Portuária. (In Portuguese).

Costa, P.J.M., 2012. *Sedimentological signatures of extreme marine inundations*. PhD thesis, Universidade de Lisboa, Portugal, 245p.

Costa, P.J.M., Andrade, C., Dawson, A.G., Mahaney, W.C., Freita, M.C., Paris, R., Taborda, R., 2012. Microtextural characteristics of quartz grains transported and deposited by tsunamis and storms. *Sedimentary Geology*, 275-276, 55-69.

Costa, P.J.M., Costas, S., Gonzàlez-Villanueva, R., Oliveira, M.A., Roelvink, D., Andrade, C., Freitas, M.c., Cunha, P.P., Martins, A., Buylaert, J.P., Murray, A., 2016. How did the AD 1755 tsunami impact on sand barriers across the southern coast of Portugal? *Geomorphology*, 268, 296-331.

Costa, P.J.M., Feist, L., Dawson, A.G., Stewart, I., Reicherter, K., Andrade, C., 2021. An overview on offshore tsunami deposits. In: *Tsunamiites, Second Edition, Chapter 11, Elsevier*, 183-192.

Cuven, S., Paris, R., Falvard, S., Miot-Noirault, E., Benbakkar, M., Schneider, J.L., Billy, I., 2013. High-resolution analysis of tsunami deposit: Case-study from the 1755 Lisbon tsunami in southwester Spain. *Marine Geology*, 337, 98-111.

Dawson, A.G., Hindson, R, Andrade, C., Freitas, C., Parish, R., Bateman, M., 1995. Tsunami sedimentation associated with the Lisbon earthquake of 1 November AD 1755: Boca do Rio, Algarve, Portugal. *The Holocene*, 5, 209–215.

Dawson, A.G., Shi, S., 2000. Tsunami Deposits. *Pure and Applied Geophysics*, 157, 857-897.

Dawson, A.G., Stewart, I., 2007. Tsunami deposits in the geological record. *Sedimentary Geology*, 200, 166-183.

Dawson, A.G., Stewart, I., 2008. Offshore tractive current deposition: the Forgotten tsunami sedimentation process. In: Shiki, T., Tsuji, Y., Yamazaki, T., Minoura, K. *Tsunamiites - Features and Implications*. Elsevier, Amsterdam, pp. 153e161.

Dias, J.M.A., 1988. Aspectos geológicos do Litoral Algarvio. *Geonovas* (Lisboa), 10, 113-128.

Drago T, Silva P, Lopes A, Magalhães V, Roque C, Rodrigues AI, Noiva J, Terrinha P, Mena A, Francés G, Koft, A., Völker, D., Omira, R., Baptista, M.A., 2016. Searching for tsunamis evidences on the Algarve (Southern Portugal) continental shelf sedimentary record. EGU General Assembly 2016, April, 2016 Vienna Austria.

Einsele, G., Chough, S.K., Shiki, T., 1996. Depositional events and their records – and introduction. *Sedimentary Geology,* 104, 1-9.

Feldens, P., Schwarzer, K., Szczucinski, W., Statteggerm K., Sakuna, D., Somgpongchaiykul, P., 2009. Impact of 2004 Tsunami on seafloor morphology and offshore sediments, Pakarang Cape, Thailand. *Polish Journal of Environment Studies*, 18, 63-68.

Feist, L., Frank, S., Bellanova, P., Laermanns, H., Cämmerer, C., Mathes-Schmidt, M., Biermanns, P., Brill, D., Costa, P.J.M., Teichner, F., Brückner, H., Schwarzbauer, J., Reicherter, K., 2019. The sedimentological and environmetal footprint of extreme wave events in Boca do Rio, Algarve coast, Portugal. *Sedimentary Geology*, 389, 147-160.

Feist, L., Reicherter, K., Costa, P.J.M., Bellanova, P., Santisteban, J.I., Bosnic, I.,Val-Peón, C., Schwarzbauer, J., Freken, M., Vött, A., Brückner, H., Schüttrumpf, H., Andrade, C., Duarte, J.F., Duarte, J.F., Kuhlmann, J., M152 scientific team, 2020. The continental shelf as an offshore archieve for tsunami deposits – an example from southwest Iberia (RV METEOR cruise M152). EGU General Assembly 2020.

Folk, R.L. and Ward, W.C., 1957. A Study in the Significance of Grain-Size Parameters. Journal of Sedimentary Petrology, 27, 3-26.

Font, E., Nascimento, C., Omira, R., Baptista, M.A., Silva, P.F., 2010. Identification of tsunami-induced deposits using numerical modeling and rock magnetism techniques: A study case of the 1755 Lisbon tsunami in Algarve, Portugal. *Physics of the Earth and Planetary Interiors*, 182, 187-198.

Font, E., Veiga-Pires, C., Pozo, M., Nave, S., Costas, S., Muñoz, F.R., Abadm M., Simões, N., Duarte, S., Rodríguez-Vidal, J., 2013. Benchmarks and sediment source(s) of the 1755 Lisbon tsunami deposit at Boca do Rio Estuary. *Marine Geology*, 343, 1-14.

Galbis, R. J., 1932. Catálogo sísmico de la zona compreendida entre los meriadianos 5° e y 20° W de Greenwich y los paralelos 45° y 25° N. Instituto Geográfico y Estadístico, Madrid, 807p.

Goodman-Tchernov, B.N., Dey, H.W., Reinhardt, E.G., McCoy, F., Mart, Y., 2009. Tsunami waves generated by the Santorini eruption reached Eastern Mediterranean shores. *Geology, 37*, 943–946.

Goodman-Tchernov, B.N., Austin, J.A., 2015. Deterioration of Israel's Caesarea Maritima's ancient harbor linked to repeated tsunami events identified in geophysical mapping of offshore stratigraphy. *Journal of Archaeology Science Reports*, 3, 444–454.

Gràcia, E., Vizciano,A., Escutia, C., Asioli, A., Rodés, Á., Pallàs, R., Garcia-Orellana, J.., Lebreiro, S., Goldfinger, C., 2010. Holocene earthquake record offshore Portugal (SW Iberia): testing turbidite paleoseismology in a slow-convergence margin. *Quaternary Science Reviews*, 29, 1156-1172.

Hindson, R.A., Andrande, C., 1999. Sedimentation and hydrodynamic process associated with the tsunami generated by the 1755 Lisbon earthquake. *Quartenary International,* 56, 27-38.

Instituto Hidrográfico, 2012. Cartografia dos sedimentos superficias da plataforma continental (Cabo de São Vicente ao Rio Guadiana). Escala 1:150 000, Folha SED 7/8, 1ª Edição.

Ikehara, K., Irino, T., Usamk, K., Jenkins, R., Omura, A., Ashi, J., 2014. Possible submarine tsunami deposits on the outer shelf of Sendai Bay, Japan resulting from the 2011 earthquake and tsunami off the Pacific coast of Tohoku. *Marine Geology*, 358, 120-127.

Ikehara, K., Irino, T., Saito, Y., 2021. The 2021 Tohoku-oki tsunami-induced sediment remobilization on the Sendai shelf, Japan, from a comparison of pre- and post-tsunami surface sediments. *Scientific reports*, *Nature portfolio*, 11:7864. 1-10.

Jagodziński, R., Sternal, B., Szczuciński, W., Lorene, S., 2009. Heavy minerals in 2004 tsunami deposits on Kho Khao Island, Thailand. *Polish Journal of Environmental Studies*, 18, 103-110.

Kortekaas, S., Dawson, A.G., 2007. Distinguishing tsunami and storm deposits: An example from Martinhal, SW Portugal. *Sedimentary Geology*, 200, 208-221.

Koster, F.B., 2014. *Modern approaches in paleotsunami research*. Master thesis, RWTH University of Aachen, Acheen, 128p.

Koster, B., Reicherter, K., 2014. Sedimentological and geophysical properties of a ca. 4000 year old tsunami deposit in southern Spain. *Sedimentary Geology*, 314, 1-16.

Kümmerer, V., 2019. *Anomalous layers in the southern Portuguese continental shelf sedimentary record: Potential evidence of the 1755 CE Lisbon tsunami*. Master thesis Universidade do Algarve, Faro, 82p.

Kümmerer, V., Drago, T., Veiga-Pires, C., Silva, P.E., Magalhães, V., Mena, A., Lopes, A., Rodrigues, A.I., Schmidt, S., Terrinha, P., Baptista, M.A., 2020. Exploring offshore sediment evidence of the 1755 CE tsunami (Faro, Portugal): Implications for the study of outer shelf tsunami deposits. *Minerals*, 731, 2-30.

Le Roux, J.P., Vargas, G., 2005. Hydraulic behavior of tsunami backflows: insights from their modern and ancient deposits. *Environmental Geology*, 49, 65-75.

Li, L., Qiu, Q., Huang, Z., 2013. Numerical modeling of the morphological change in Lhok Nga, west Banda Aceh, during the 2004 Indian Ocean tsunami: understanding tsunami deposits using a forward modeling method. *Natural Hazards*, 64, 1549-1574.

Lopes, F.C., Cunha, P.P., 2007. Tectono-sedimentary phases of the latest Cretaceous and Cenozoic compressive evolution of the Algarve margin (southern Portugal). *In*: Nichols, G., Williams, E.A., Paola, C. Sedimentary Processes, Environments and Basins – a tribute to Peter Friend.Wiley-Blackwell Publishing, Association of Sedimentologists Special Publication, 38, pp. 111-136. ISBN: 978-1-4051-7922-5.

Magalhães, F.M.Q.M., 1999. *Os sedimentos da plataforma continental Portuguesa: contrastes espaciais, perspectiva temporal, potencialidades econômicas*. Phd thesis Universidade de Lisboa, Lisboa, 287p.

Mamo, B., Strotz, L., Dominey-Howes, D., 2009. Tsunami sediments and their foraminiferal assemblages. *Earth-Science Reviews*, 96, 263-278.

Mangiafico, S.S., 2015. *An R Companion for the Handbook of Biological Statistic*, version 1.6.19. Available at: www.rcompanion.org/documents/RCompanionBioStatistics.pdf.

Milker, Y., Wilken, M., Schumann, J., Sakuna, D., Feldens, P., Schwarzer, K., Schmiedl, G., 2013. Sediment transport on the inner shelf off Khao Lak (Andaman Sea, Thailand) during the 2004 Indian Ocean tsunami and former storm events: evidence from foraminiferal transfer functions. *Natural Hazards Earth System Science*, 13, 3113-3128.

Miranda, J., Batlló, J.H., Ferreira, H. L., Matias, L.M., 2012. The 1531 Lisbon earthquake and tsunami. In*: Proceedings of the 15 World Conference on Earthquake Engineering*. Lisboa, Portugal, IAEE, 9.

Moita, I., 1985. Das Cartas Litológicas Submarinas ao Programa SEPLAT. Anais do Instituto Hidrográfico, 6: 43-45

Moita I., 1986. *Notícia explicativa da carta dos sedimentos superficiais da plataforma.* Folha SED 7 e 8. *Cabo de São Vicente ao rio Guadiana*. Instituto Hidrográfico, Lisboa, 19p.

Moreira, V.S., 1988. Historical and recent tsunamis in the European Area. Science of Tsunami Hazards, 6, 37-42.

Moreira, S., Costa, P.J.M., Andrande, C., Lira, P.C., Freitas, M.C., Oliveira, M.A., Reichart, G.J., 2017. High resolution geochemical and grain-size analysis of the AD 1755 tsunami deposit: Insights into the inland extent and inundation phases. *Marine Geology*, 290, 94-105.

Morton, R.A., Gelfenbaum, G., Jaffe, B.E., 2007. Physical criteria for distinguishing sand tsunami and storm deposits using modern examples. *Sedimentary Geology*, 200, 184-207.

Moura, D., Boski, T., 1994. Ludo Formation – A new lithostratigraphic unit in Quaternary of Central Algarve. *Gaia*, 9, 41-47.

Moura, D., 1998. *Litostratigrafia do Neogénico terminal e Plistocénico na Bacia Centro-Algarve. Evolução Paleoambiental*. Phd Thesis Universidade do Algarve, 252p.

Noda, A., Katayama., Sagayama, T., Suga, K., Uchida, Y., Satake, K., Abe, K., Okamura, Y., 2007. Evaluation of tsunami impacts on shallow marine sediments: An example from

the tsunami caused by the 2003 Tokachi-oki earthquake, northern Japan. *Sedimentary Geology,* 200, 314-327.

Oliveira, M.A., Andrade, C., Freitas, M.C., Costa, P.J., 2009. Modeling volume transfer between Beach-Foredune and the Backshore by the 1755 Lisbon Tsunami at Boca do Rio Lowland, Algarve (Portugal). Journal of Coastal Research, 56, 1547-1551.

Omira, R., Baptista, M.A., Miranda, J.M., 2011. Evaluating tsunami impact on the Gulf of Cadiz coast (Northeast Atlantic). *Pure and Applications Geophysics*, 168, 1033-1043.

Papadopoulos, G.A., Imamura, F., 2001. A proposal for a new tsunami intensity scale. *ITS 2001 Proceedings*, 5, 569- 577.

Paris, R., Fornier, J., Poizot, E., Etienne, S., Morin, J., Lavigne, F., Wassmer, P., 2010. Boulder and fine sediment transport and deposition by the 2004 tsunami in Lhok Nga (western Banda Aceh Sumatra, Indonesia): A couple offshore-onshore model. *Marine Geology*, 268, 43-54.

Pilarczyk, J.E., Sawai, Y., Matsumoto, D., Namegaya, Y., Nishida, N., Ikehara, K., Fujiwara, O., Gouramanis, C., Dura, T., Horton, B.P., 2020. Constraining sediment provenance for tsunami deposits using distributions of grain size and foraminifera from the Kujukuri coastline and shelf, Japan. *Sedimentology*, 67, 1373-1392 sed.12591, 1-20.

Puga-Bernabéu, A., Aguirre, J., 2017. Constrating storm-versus tsunami-related shell bed in shallow-water ramps. *Palaeogeography, Palaeoclimatology, Palaeoecology*, 471, 1-14.

Proske, U., Hanebuth, T.J.J., Gröger, J., Diêm, B.P., 2011. Late Holocene sedimentary and environmental development of the northern Mekong River Delta, Vietnam. *Quaternary International*, 230, 1-2, 57-66.

Quintela, M., Costa, P.J.M., Fatela, F., Drago, T., Hoska, N., Andrade, C., Freitas, M.C.., 2016. The AD 1755 tsunami deposits onshore and offshore of Algarve (south Portugal): Sediment transport interpretations based on the study of Foraminifera assemblages. *Quaternary International*, 408, 123-138..

Ramalho, I., Omira, R., El Moussaoui, S., Baptista, M.A., Zaghoul, M.N., 2018. Tsunami-induced morphological change – A model-based impact assessment of the 1755 tsunami in NE Atlantic from the Morocco coast. *Geomorphology*, 318, 78-91.

Riou, B., Chaumillion, E., Chagué, C., Sabatier, P., Schneider, J.L., Walsh, J.P., Zawadzki, A., Fierro, D., 2020a. Backwash sediment record of the 2009 South Pacific Tsunami and 1960 Great Chilean Earthquake Tsunami. *Scientific Reports*, 10, 4149.

Riou, B., Chaumillion, E., Schneider, J.L., Corrège, T., Chagué, C., 2020b. The sediment-fill of Pago Pago Bay (Tutuila Island, American Samoa) : New insights on the sediment record of past tsunamis. *Sedimentology*, 67, 1577-1600.

Reicherter, K., Vött, A., Feist, L., Costa, P.J.M., Schwarzbauer, J., Schüttrumpf, H., Holger, J., Raeke, A., Huhn-Frehers, K., 2019. METEOR-Berichte. Lisbon 1755, Cruise No. M152/1, 02.11.-14.11.2018, Funchal (Portugal)-Hamburg (Germany).

Rodrigues, A., Dias, J.M.A., 1989. Evolução Pós-Glaciária da Plataforma Continental Portuguesa a Norte do Cabo Mondego. Anais do Instituto Hidrográfico, n 10.

Roque, C., Hernández-Molina, F.J., Lobo, F., Somoza, L., Díaz-del-Río, V., Vázquez, J.T., Dias, j., 2010. Geomorphology of the Eastern Algarve proximal continental margin (South Portugal, SW Iberia Peninsula): sedimentary dynamics and its relationship with the last asymmetrical eustatic cycle. *Ciências da Terra*, 17, 7-28.

Sakuna, D., Szczucinski, W., Feldens, P., Schwazer, K., Khokiattiwong, S., 2012. Sedimentary deposits left by the 2004 Indian Ocean tsunami on the inner continental shelf offshore of Khao Lak, Andaman Sea (Thailand). *Earth, Planets Space*, 64, 931-943.

Sakuna-Schwartz, D., Feldens, P., Schwazer, K., Khokiattiwong, S., Stattegger, K., 2015. Internal structure of event layers preserved on the Andaman Sea continental shelf, Thailand: tsunami vs. storm and flash-flood deposits. *Natural Hazards and Earth System Sciences*, 15, 1181-1199.

Smedile, A., DE Martini, P.M., Pantosti, D., Belluci, L., Del Carlo, P., Gasperini, L., Pirrota, C., Polonia, A., Boschi, 2011. Possible tsunami signatures from an integrated study in Augusta Bay offshore (Eastern Sicily - Italy). *Marine Geology*, 281, 1-13.

Smedile, A., Molisso, F., Chagué, C., Iorio, M., Martini, P.M., Pinzi, S., Collins, P.E.F., Sagnotti, L., Pinzi, S., 2019. New coring study in Augusta Bay expands understanding of offshore tsunami deposits (Eastern Sicily, Italy). *Sedimentology*, 67, 1553-1576

Solares, J.M.M., Arroyo, A.L., 2004. The great historical 1755 earthquake. Effects and damage in Spain. *Journal of Seismology*, 8, 275p.

Srinivasalu, S., Jonathan, M.P., Thangadurai, N., Ram-Mohan, V., 2010. A study on pre- and post-tsunami shallow deposits off SE coast of India from the 2004 Indian Ocean tsunami: a geochemical approach. *Natural Hazards*, 52, 391-401.

Tamura, T., Sawai, Y., Ikehara, K., Nakashima, R., Hara, J., Kanai, Y., 2015. Shallow-marine deposits associated with the 2011 Tohoku-oki tsunami in Sendai Bay, Japan. *Journal of Quaternary Science*, 30, 293-297.

Terrinha, P., Rocha, R., Rey, J., Cachão, M., Moura, D., Roque, C., Martins, L., Valadares, V., Cabral, J., Azevedo, M. R., Barbero, L., Clavijo, E., Dias, R. P., Gafeira, H., Matias, H., Matias, L., Madeira, J., Marques da Silva, C., Munhá, J., Reblo, L., Ribeiro, C., Vicente, J., Youbbi, N., 2006. *A Bacia do Algarve: Estratigrafia, Paleogeografia e Tectónica. Geologia de Portugal no contexto da Ibéria*. Universidade de Évora, 247-316.

Terrinha, P., Noiva, J., Brito, P., Baptista, L.; Roque, C., Drago, T., Silva, P.F., Magalhães, V., Rodrigues, A.I., Lopes, A. New results of offshore record of tsunami deposits and MTDS in the NEAM region: The southwestern iberian margin case, April 2017. Available online: www.ASTARTE-project.eu (accessed on 30 November 2020).

Toyofuku, T., Duros, P., Fontanier, C., Mamo, B., Bichon, S., Buscail, R., Chabaud, G., Deflandre, B., Goubet, S., Grémare, A., Menniti, C., Fuji, M., Kawamura, K., Koho, K.A., Noda, A., Namegaya, Y., Oguri, K., Radakovitch, Murayama, M., Jan de Nooijer, L., Kurasawa, A., Ohkawara, N., Okutani, T., Sakuguchi, A., Jorissen, F., Reichart, G.J., Kitazato, H., 2014. Unexpected biotic resilience on the Japanese seafloor caused by the 2011 Tohoku-Oki tsunami. *Scientific Reports*, doi: 10.1038/srep07517.

Trigo, R.M., Varino, F., Ramos, A.M., Valente, M.A., Zêzere, J.L., Vaquero, J.M., Gouveia, C.M., Russo, A., 2014. The record precipitation and flood event in Iberia in December 1876: description and synoptic analysis. *Frontiers in Earth Science*, 2, 1-15.

Tyuleneva N., Braun, Y., Katz, T., Suchkov, I., Goodman-Tchernov, B., 2018. A new chalcolithic-era tsunami event identified in the offshore sedimentary record of Jisr al-Zarka (Israel). *Marine Geology*, 396, 67–78.

Van den Bergh, G.D., Boer, W., Hass, H., Van Werring, Tj.C.E., Van Wijhe, R., 2003. Shallow marine tsunami deposits in Teluk Banten (NW Java, Indonesia), generated by the 1883 Krakatau eruption. *Marine Geology*, 197, 13-34

Veerasingam, S., Venkatachalapathy, R., Basavalah, N., Ramkumar, T., Venkatramanan, S., Deenadaylan, K., 2014. Identification and characterization of tsunami deposits off southeast coast of India from the 2004 Indian Ocean tsunami: Rock and geochemical approach. *Journal of Earth System Science*, 123, 905-921.

Vigliotii, L., Andrade, C., Freitas, M.C., Capotondi, L., Gallerani, A., Belluci, L.G., 2019. Paleomagnetic, rock magnetic and geochemical study of 1755 tsunami deposit at Boca do Rio Algarve, Portugal). *Paleogeography, Paleoclimatology, Paleoecology*, 514, 500-566.

Ward, S.N., 2010. Tsunami. *Encyclopedia of Solid Earth Geophysics*. Springer, 1-18.

Weiss, R., Bahlburg, H., 2006. A note on the preservation of offshore tsunami deposits. *Journal of Sedimentary Research*, 76, 1267-1273.

Zêzere, J.L., Pereira, S., Tavares, A.O., Bateira, C., Trigo, R.M., Quaresma, I., Santos, P.P., Verde, J., 2014. DISASTER: a GIS database on hydro-geomorphologic disasters in Portugal. *Natural Hazards*, 72, 503-532.

Zitellini, N., Mendes, L.A., Cordoba, D., Danobeitia, J., Nicolich, R., Pellis, G., Ribeiro, A., Sartori, R., Torelli, L., Bartolome, R., Bortoluzzi, G., Calafato, A., Carrilho, F., Casoni, L., Chierici, F., Corela, C., Correggiari, A., Della Vedova, B., Gracia, E., Jornet, P., Landuzzi, M., Ligi, M., Magagnoli, A., Marozzi, G., Matias, L., Penitenti, D., Rodrigues, P., Rovere, M., Terrinha, P., Vigliotti, L., Ruiz Zahinos, A., 2001. The quest for the Africa–Eurasia plate boundary west of the Strait of Gibraltar, *Earth and Planetary Science Letters*, 82, 285-296.

Zitellini, N., Rovere, M., Terrinha, P., Chierici, F., Matias, L., Bigsets, T., 2004. Neogene through Quaternary tectonic reactivation of SW Iberian passive margin. *Pure Applied Geophysics*, 161, 565-587.

Annex

Annex A: Grain-size analysis

Cliff sites

Grain-size (μm)	forte_novo_cliff	falesia_acoteias_cliff	vale_lobo_cliff
2000	1.11	1.33	0.7
1400	5.44	9.16	0.9
1000	16.01	18.80	1.8
710	21.1	24.70	5.7
500	21.9	30.73	18.5
355	16.1	11.60	32.3
250	9.9	2.05	27
180	3.03	0.42	5.2
125	2.07	0.36	3
90	1.27	0.15	2.1
63	1.02	0.20	1.3
<63	1.05	0.50	1.5

Dune sites

Grain-size (μm)	baia_grande_duna	faro_beach_duna
2000	0.004	0.1
1400	0.0014	1.7
1000	0.13	10
710	1.34	31.7
500	11.9	34.9
355	32.57	17.5
250	36.4	3.1
180	14.69	0.6
125	2.2	0.1
90	0.45	0.1
63	0.13	0.1
	0.18	0.1

Beach sites

Grain-size (µm)	armacao _pera_	gale_sho reface	falesia_acoteias _beachface	forte_novo _beachface	fortenovo_ backshore	baia_gran de_backsh ore	baia_grande _beachface
2000	0.558	0.3322	0.359	0.9711	0.1839	0.5524	1.2035
1400	1.71	0.8792	2.7872	2.6312	1.0552	1.3327	3.0962
1000	8	5.2255	12.5628	6.7905	3.7275	4.5722	5.893
710	19.738	18.7775	28.5076	15.9701	10.1742	14.1223	9.0875
500	33.129	24.3084	17.2272	26.4934	24.1656	24.2975	10.6856
355	22	24.5927	8.1477	28.1884	30.7822	28.8137	14.6924
250	10.789	21.7344	11.8651	15.2147	21.768	22.2091	28.6807
180	3.405	3.3749	11.7748	2.2771	5.6404	3.646	20.0976
125	0.589	0.5337	5.9711	1.4025	2.44	0.6614	6.2049
90	0.045	0.11	0.7242	0.31	0.2975	0.0979	0.354
63	0.014	0.08	0.08	0.052	0.1156	0.01	0.005
	0.023	0.06	0.0241	0.0749	0.0842	0.01	0.0084

Annex B: Sand mineralogical composition

Table with the counts of the sand mineralogical composition. Size = grain-size (μm);
Q = Quartz; ICQ = Iron-coated quartz; Mi = Mica, Ag = Aggregates, OT = Other
terrigenous; OA = Orange clay aggregates; MO = molluscs; PL=planktic foraminifera; BE=
benthic foraminifera; GL = Glauconite; OB = Other biogenic; NI = non-identified; ADL =
above layers.

size	depth	Layer	sample	Q	ICQ	MI	AG	OT	OA	MO	PL	BE	GL	OB	NI
125	13	L4	above ADL	49	0	5	5	2	0	11	2	19	0	7	0
125	14	L4	above ADL	44	0	1	7	2	0	4	16	15	0	11	0
125	15	L4	above ADL	34	0	2	9	2	0	5	23	12	1	12	0
125	16	L4	above ADL	33	0	4	4	1	0	13	17	11	0	17	0
125	17	L4	above ADL	37	0	7	5	3	0	13	10	17	0	8	0
125	18	L4	ADL	46	0	0	1	2	0	18	6	14	0	13	0
125	19	L4	ADL	38	0	1	8	1	0	30	3	9	1	9	0
125	20	L4	ADL	20	0	1	3	2	0	15	16	15	0	28	0
125	21	L4	ADL	48	0	0	6	3	0	13	4	10	0	16	0
125	22	L4	ADL	37	0	3	5	1	0	9	5	11	0	29	0
125	23	L4	Below ADL	35	0	2	3	4	0	9	7	18	0	22	0
125	24	L4	Below ADL	40	0	5	2	1	0	15	8	15	0	14	0
125	25	L3	above ADL	42	0	4	6	2	0	15	5	6	0	20	0
125	26	L3	above ADL	30	0	0	9	5	0	12	5	18	0	21	0
125	27	L3	above ADL	43	1	10	3	2	0	12	2	14	0	13	0
125	28	L3	above ADL	44	0	6	6	3	0	6	6	11	0	18	0
125	29	L3	above ADL	35	0	5	9	1	0	5	3	13	0	29	0
125	30	L3	ADL	36	0	9	10	3	0	15	5	5	0	17	0
125	31	L3	ADL	34	1	2	2	1	0	20	9	5	0	26	0
125	32	L3	ADL	40	0	0	0	3	24	10	1	8	0	14	0
125	33	L3	ADL	30	0	4	8	1	10	8	8	16	0	15	0
125	34	L3	ADL	22	0	5	14	7	5	6	7	16	0	18	0
125	35	L3	ADL	34	0	11	9	7	3	6	9	0	0	21	0
125	36	L3	Below ADL	55	0	0	7	6	2	6	5	11	0	8	0
125	37	L3	Below ADL	36	0	3	19	5	1	4	6	14	0	12	0
125	38	L3	Below ADL	45	0	5	4	6	1	10	4	13	0	12	0
125	39	L3	Below ADL	48	0	1	6	8	1	7	8	10	0	11	0
125	40	L3	Below ADL	45	0	3	7	4	0	5	10	12	0	14	0
125	62	L2	above ADL	42	0	4	13	3	0	0	8	8	0	22	0
125	63	L2	above ADL	45	0	4	19	7	0	4	5	7	0	9	0
125	64	L2	above ADL	33	0	5	8	1	0	2	3	15	0	33	0
125	65	L2	above ADL	44	0	9	9	1	0	10	3	14	0	10	0
125	66	L2	above ADL	35	0	12	6	5	0	12	11	9	0	10	0
125	67	L2	ADL	45	0	5	0	7	0	8	8	10	0	17	0
125	68	L2	ADL	43	0	3	15	0	0	3	4	12	0	20	0
125	69	L2	ADL	49	0	1	0	12	0	8	1	12	0	17	0

125	70	L2	ADL	33	0	9	7	6	0	5	12	15	0	13	0
125	71	L2	ADL	41	0	4	15	2	0	1	2	16	0	19	0
125	72	L2	ADL	29	0	3	3	2	0	7	9	18	0	29	0
125	73	L2	Below ADL	28	0	6	3	5	0	5	10	14	0	29	0
125	74	L2	Below ADL	20	0	2	1	4	0	4	14	23	0	32	0
125	75	L2	Below ADL	34	0	3	7	2	0	7	10	13	0	24	0
125	76	L2	Below ADL	35	0	7	10	3	0	5	0	13	0	27	0
125	77	L2	Below ADL	43	0	12	3	1	0	1	2	12	0	26	0
125	100	L1	above ADL	53	1	4	6	1	1	4	3	8	0	19	0
125	101	L1	above ADL	40	0	11	7	2	0	10	4	12	0	14	0
125	102	L1	above ADL	58	0	1	1	2	0	7	3	15	0	13	0
125	103	L1	above ADL	52	0	2	3	2	0	9	2	10	0	20	0
125	104	L1	above ADL	41	0	3	5	2	0	12	12	6	0	19	0
125	105	L1	ADL	38	0	2	6	6	0	12	8	11	0	17	0
125	106	L1	ADL	45	0	1	9	0	0	7	3	10	0	25	0
125	107	L1	ADL	52	0	6	4	2	0	7	4	8	0	17	0
125	108	L1	ADL	50	0	0	3	4	0	5	5	11	0	22	0
125	109	L1	ADL	31	1	0	1	4	0	16	8	23	0	16	0
125	110	L1	ADL	57	1	0	6	2	0	6	5	6	0	17	0
125	111	L1	ADL	41	1	0	7	1	0	13	4	10	0	23	0
125	112	L1	ADL	40	1	0	8	2	0	8	3	6	0	32	0
125	113	L1	ADL	49	1	0	4	4	0	6	2	5	0	29	0
125	114	L1	ADL	39	1	2	1	4	0	14	7	11	0	21	0
125	115	L1	ADL	57	1	0	2	2	0	12	1	7	0	18	0
125	116	L1	ADL	63	0	0	0	5	0	10	1	0	0	21	0
125	117	L1	ADL	48	1	0	0	3	0	14	5	8	0	21	0
125	118	L1	ADL	40	0	2	5	3	0	12	6	12	0	20	0
125	119	L1	Below ADL	54	2	0	0	1	0	11	4	5	0	23	0
125	120	L1	Below ADL	30	1	6	1	4	0	17	12	8	0	21	0
125	121	L1	Below ADL	43	0	4	3	7	0	10	5	5	0	23	0
125	122	L1	Below ADL	55	0	3	0	2	0	14	7	10	0	9	0
125	123	L1	Below ADL	34	0	2	2	2	0	18	10	12	0	20	0
250	13	L4	Below ADL	60	0	1	4	0	0	7	6	11	0	11	0
250	14	L4	Below ADL	49	0	0	7	3	0	11	6	14	0	10	0
250	15	L4	Below ADL	57	0	0	1	1	0	6	10	17	0	8	0
250	16	L4	above ADL	50	0	0	3	1	0	4	5	22	0	15	0
250	17	L4	above ADL	67	0	3	5	1	0	8	1	9	0	6	0
250	18	L4	ADL	50	0	2	8	5	0	5	10	0	0	20	0
250	19	L4	ADL	48	0	0	11	2	0	20	1	8	0	10	0
250	20	L4	ADL	49	0	0	5	0	0	17	3	10	0	16	0
250	21	L4	ADL	66	0	0	4	2	0	7	0	5	0	16	0
250	22	L4	ADL	64	0	0	0	2	0	16	3	5	0	10	0
250	23	L4	Below ADL	48	0	0	4	2	0	14	1	15	0	16	0
250	24	L4	Below ADL	52	0	1	1	3	0	17	3	5	0	18	0
250	25	L3	above ADL	52	0	0	1	1	0	17	4	11	0	14	0
250	26	L3	above ADL	53	0	0	3	2	0	12	8	9	0	13	0
250	27	L3	above ADL	57	0	0	5	3	0	3	4	9	0	19	0
250	28	L3	above ADL	61	0	1	2	2	0	7	3	5	0	19	0

250	29	L3	above ADL	54	0	0	1	3	0	12	8	10	0	12	0
250	30	L3	ADL	50	0	6	3	2	0	12	2	10	0	15	0
250	31	L3	ADL	46	0	3	4	2	0	14	7	10	0	14	0
250	32	L3	ADL	72	0	0	0	2	2	8	1	5	0	10	0
250	33	L3	ADL	57	0	1	7	3	1	11	0	14	0	6	0
250	34	L3	ADL	61	0	1	2	2	0	11	1	5	0	17	0
250	35	L3	ADL	53	2	1	1	2	0	17	1	12	0	11	0
250	36	L3	Below ADL	54	0	0	2	0	0	20	0	2	0	22	0
250	37	L3	Below ADL	67	0	0	6	3	0	6	0	1	0	17	0
250	38	L3	Below ADL	58	0	2	3	0	5	1	10	0	0	21	0
250	39	L3	Below ADL	55	0	2	4	3	0	11	2	6	0	17	0
250	40	L3	Below ADL	61	0	1	2	2	0	11	1	5	0	17	0
250	62	L2	above ADL	65	0	0	6	2	0	4	1	5	0	17	0
250	63	L2	above ADL	44	0	1	7	2	0	3	6	12	0	25	0
250	64	L2	above ADL	70	0	0	2	1	0	1	1	10	0	15	0
250	65	L2	above ADL	59	0	1	8	0	0	7	5	10	0	10	0
250	66	L2	above ADL	58	0	0	6	1	0	3	2	8	0	22	0
250	67	L2	ADL	53	0	0	15	5	0	6	1	3	0	17	0
250	68	L2	ADL	50	0	0	15	1	0	6	3	8	0	17	0
250	69	L2	ADL	57	0	0	8	4	0	5	1	3	0	22	0
250	70	L2	ADL	73	0	1	5	2	0	6	0	2	0	11	0
250	71	L2	ADL	57	0	1	2	3	0	2	4	4	0	27	0
250	72	L2	ADL	62	1	1	2	3	0	2	4	7	0	18	0
250	73	L2	Below ADL	72	0	0	4	0	0	2	0	5	0	17	0
250	74	L2	Below ADL	64	0	0	2	1	0	8	1	8	0	16	0
250	75	L2	Below ADL	60	0	0	1	2	0	3	2	7	0	25	0
250	76	L2	Below ADL	68	0	0	1	2	0	4	1	4	0	20	0
250	77	L2	Below ADL	69	0	0	0	0	0	4	0	8	0	19	0
250	100	L1	above ADL	81	0	2	1	2	0	3	0	1	0	10	0
250	101	L1	above ADL	76	0	0	6	0	0	0	0	0	0	18	0
250	102	L1	above ADL	79	0	0	1	2	0	4	0	2	0	12	0
250	103	L1	above ADL	60	0	1	1	2	0	10	0	2	0	24	0
250	104	L1	above ADL	72	1	0	1	0	0	6	0	0	0	20	0
250	105	L1	ADL	68	1	0	1	5	0	8	1	0	0	16	0
250	106	L1	ADL	78	0	2	1	0	0	5	0	1	0	13	0
250	107	L1	ADL	70	1	0	2	5	0	6	3	0	0	13	0
250	108	L1	ADL	73	0	0	1	3	0	6	0	2	0	15	0
250	109	L1	ADL	77	2	0	0	0	0	4	2	2	0	13	0
250	110	L1	ADL	58	1	0	2	2	0	11	1	5	0	20	0
250	111	L1	ADL	68	1	1	1	0	0	5	0	2	0	22	0
250	112	L1	ADL	68	2	3	1	2	0	3	0	2	0	19	0
250	113	L1	ADL	60	2	0	2	2	0	17	0	4	0	13	0
250	114	L1	ADL	60	2	1	0	4	0	24	0	1	0	8	0
250	115	L1	ADL	63	1	0	0	5	0	12	0	3	0	16	0
250	116	L1	ADL	73	0	0	0	1	0	7	0	1	0	18	0
250	117	L1	ADL	70	0	0	0	6	0	18	0	0	0	6	0
250	118	L1	ADL	62	0	0	1	3	0	10	0	2	0	21	1
250	119	L1	Below ADL	60	0	0	0	3	0	14	4	4	0	15	0

250	120	L1	Below ADL	73	2	0	0	4	0	14	0	1	0	6	0
250	121	L1	Below ADL	72	0	0	1	3	0	8	0	0	0	15	1
250	122	L1	Below ADL	63	0	0	1	2	0	16	1	1	0	16	0
250	123	L1	Below ADL	77	0	0	2	2	0	12	0	0	0	7	0
500	13	L4	above ADL	73	0	1	11	1	0	5	0	3	0	6	0
500	14	L4	above ADL	67	0	0	4	2	0	20	0	3	0	3	1
500	15	L4	above ADL	38	0	0	1	1	0	34	5	11	0	9	1
500	16	L4	above ADL	57	0	1	2	0	0	24	0	4	0	12	0
500	17	L4	above ADL	60	0	3	10	1	0	16	0	2	0	8	0
500	18	L4	ADL	64	1	0	14	0	0	12	0	1	0	8	0
500	19	L4	ADL	49	0	0	7	2	0	34	0	4	0	4	0
500	20	L4	ADL	53	0	0	10	1	0	21	0	8	0	7	0
500	21	L4	ADL	52	0	7	0	0	0	29	0	6	0	6	0
500	22	L4	ADL	49	0	0	11	3	0	22	0	5	0	10	0
500	23	L4	Below ADL	45	0	0	12	1	0	22	1	2	0	17	0
500	24	L4	Below ADL	65	0	0	8	1	0	14	2	3	0	7	0
500	25	L3	above ADL	55	0	0	9	2	0	28	0	3	0	3	0
500	26	L3	above ADL	44	0	0	14	2	0	21	0	4	0	15	0
500	27	L3	above ADL	37	0	0	14	2	0	23	0	10	0	14	0
500	28	L3	above ADL	44	0	6	6	3	0	6	6	11	0	18	0
500	29	L3	above ADL	34	0	5	9	1	0	5	4	14	0	28	0
500	30	L3	ADL	47	0	2	11	1	0	17	0	9	0	13	0
500	31	L3	ADL	47	0	1	0	1	0	30	1	6	0	13	1
500	32	L3	ADL	67	0	0	0	2	0	17	5	0	0	9	0
500	33	L3	ADL	66	0	1	2	2	0	19	0	2	0	7	1
500	34	L3	ADL	52	1	1	3	3	0	29	0	1	0	10	0
500	35	L3	ADL	61	0	1	0	2	0	25	0	4	0	7	0
500	36	L3	Below ADL	65	0	0	2	0	0	20	0	2	0	11	0
500	37	L3	Below ADL	49	0	0	14	3	0	18	0	1	0	15	0
500	38	L3	Below ADL	63	0	0	1	1	0	17	0	3	0	15	0
500	39	L3	Below ADL	59	0	0	1	4	0	16	0	1	0	19	0
500	40	L3	Below ADL	56	0	0	2	1	0	19	0	0	0	22	0
500	62	L2	above ADL	76	0	0	3	1	0	4	2	0	0	14	0
500	63	L2	above ADL	74	0	0	3	2	0	8	0	1	0	12	0
500	64	L2	above ADL	60	0	0	1	2	0	21	1	1	0	14	0
500	65	L2	above ADL	63	0	1	4	3	0	10	0	3	0	16	0
500	66	L2	above ADL	61	0	0	0	2	0	16	0	3	0	18	0
500	67	L2	ADL	57	0	0	0	7	0	20	0	2	0	14	0
500	68	L2	ADL	51	0	0	2	2	0	31	0	0	0	14	0
500	69	L2	ADL	76	0	0	1	2	0	9	0	0	0	12	0
500	70	L2	ADL	70	0	0	0	1	0	17	0	0	0	12	0
500	71	L2	ADL	74	0	0	6	2	0	10	0	1	0	7	0
500	72	L2	ADL	71	0	0	2	1	0	10	0	0	0	16	0
500	73	L2	Below ADL	68	0	0	0	1	0	16	0	0	0	15	0
500	74	L2	Below ADL	66	0	0	3	1	0	14	0	0	0	16	0
500	75	L2	Below ADL	73	0	0	0	7	0	13	0	0	0	7	0
500	76	L2	Below ADL	66	0	0	4	3	0	11	0	0	0	16	0
500	77	L2	Below ADL	68	0	0	4	4	0	9	0	0	0	15	0

500	100	L1	above ADL	76	1	0	0	1	0	3	0	0	0	19	0
500	101	L1	above ADL	83	0	1	1	3	0	2	0	0	0	10	0
500	102	L1	above ADL	81	0	0	0	4	0	4	0	5	0	6	0
500	103	L1	above ADL	79	0	9	0	1	0	4	0	0	0	7	0
500	104	L1	above ADL	86	0	0	1	1	0	2	0	0	0	10	0
500	105	L1	ADL	72	2	0	3	0	0	5	0	2	0	16	0
500	106	L1	ADL	80	0	0	1	2	0	6	0	0	0	11	0
500	107	L1	ADL	89	0	0	0	4	0	3	0	0	0	4	0
500	108	L1	ADL	91	0	1	0	1	0	1	0	0	0	6	0
500	109	L1	ADL	73	1	0	1	2	0	8	0	0	0	15	0
500	110	L1	ADL	78	2	0	1	2	0	5	0	1	0	11	0
500	111	L1	ADL	80	0	0	0	2	0	5	0	0	0	13	0
500	112	L1	ADL	80	0	0	1	0	0	12	0	0	0	7	0
500	113	L1	ADL	79	0	0	1	4	0	3	0	0	0	13	0
500	114	L1	ADL	84	1	0	0	1	0	6	0	0	0	8	0
500	115	L1	ADL	78	0	0	0	2	0	7	0	2	0	11	0
500	116	L1	ADL	74	0	0	0	2	0	3	0	0	0	21	0
500	117	L1	ADL	84	0	0	0	2	0	3	0	0	0	11	0
500	118	L1	ADL	79	0	0	1	1	0	4	0	0	0	15	0
500	119	L1	Below ADL	88	0	0	1	3	0	2	0	1	0	4	1
500	120	L1	Below ADL	83	0	0	0	5	0	5	0	0	0	6	1
500	121	L1	Below ADL	81	0	1	0	3	0	3	0	0	0	11	1
500	122	L1	Below ADL	80	0	0	0	2	0	3	0	0	0	15	0
500	123	L1	Below ADL	79	0	0	1	5	0	7	0	0	0	8	0
125	0	C1	falesia_acoteias_cliff	95	3	0	0	2	0	0	0	0	0	0	0
125	0	C2	baia_grande_dune	63	30	0		7	0	0	0	0	0	0	0
125	0	C3	arma_pera_terr_alto	67	20	0	0	13	0	0	0	0	0	0	0
125	0	C4	praia_faro_dune	49	9	0	0	42	0	0	0	0	0	0	0
125	0	C5	forte_novo_cliff	0	40	0	0	8	52	0	0	0	0	0	0
125	0	C6	vale_lobo_cliff	0	20	0	0	1	79	0	0	0	0	0	0
125	0	C7	falesia_acoteia_beachface	62	15	0	0	22	0	1	0	0	0	0	0
125	0	C8	forte_novo_backshore	44	10	0	0	45	0	1	0	0	0	0	0
125	0	C9	forte_novo_beachface	34	9	0	0	56	0	0	0	0	0	1	0
125	0	C10	gale_shoreface	55	13	0	0	27	0	2	0	0	0	3	0
125	0	C11	baia_grande_beachface	50	21	0	0	21	0	5	0	0	0	3	0
125	0	C12	baia_grande_backshore	58	15	1	0	20	0	4	0	0	0	2	0
250	0	C1	falesia_acoteias_cliff	90	6	0	0	4	0	0	0	0	0	0	0
250	0	C2	baia_grande_dune	59	32	0		9	0	0	0	0	0	0	0
250	0	C3	arma_pera_terr_alto	50	35	0	0	15	0	0	0	0	0	0	0
250	0	C4	praia_faro_dune	84	10	0	0	6	0	0	0	0	0	0	0
250	0	C5	forte_novo_cliff	0	97	0	0	3	0	0	0	0	0	0	0
250	0	C6	vale_lobo_cliff	0	99	0	0	1	0	0	0	0	0	0	0
250	0	C7	falesia_acoteia_beachface	57	13	0	0	26	0	3	0	0	0	1	0
250	0	C8	forte_novo_backshore	59	29	0	0	9	0	1	0	1	0	1	0
250	0	C9	forte_novo_beachface	74	21	0	0	5	0	0	0	0	0	0	0
250	0	C10	gale_shoreface	67	11	0	0	11	0	9	0	0	0	2	0
250	0	C11	baia_grande_beachface	51	17	0	0	14	0	13	0	0	0	5	0
250	0	C12	baia_grande_backshore	59	15	0	0	16	0	8	0	0	0	2	0

500	0	C1	falesia_acoteias_cliff	90	7	0	0	3	0		0	0	0	0	0
500	0	C2	baia_grande_dune	66	30	0	0	2	0	0	0	0	0	2	0
500	0	C3	arma_pera_terr_alto	70	20	0	0	9	0	0	0	1	0	0	0
500	0	C4	praia_faro_duna	75	21	0	0	4	0	0	0	0	0	0	0
500	0	C5	forte_novo_cliff	0	95	0	0	5	0	0	0	0	0	0	0
500	0	C6	vale_lobo_cliff	0	100	0	0	0	0	0	0	0	0	0	0
500	0	C7	falesia_acoteia_beachface	66	17	0	0	16	0	1	0	0	0	0	0
500	0	C8	forte_novo_backshore	55	36	0	0	7	0	1	1	0	0	0	0
500	0	C9	forte_novo_beachface	55	32	0	0	10	0	2	0	0	0	1	0
500	0	C10	gale_shoreface	70	7	0	0	10	0	10	0	0	0	3	0
500	0	C11	baia_grande_beachface	59	21	0	0	4	0	13	0	0	0	3	0
500	0	C12	baia_grande_backshore	66	19	0	0	5	0	7	2	0	0	1	0

Annex C: Normality test – Shapiro-Wilk

L1	test
Quartz	0.00116
Ironcoatedquartz	3.85E-11
Mica	1.66E-13
Aggregate	6.55E-10
Other_terr	0.00058
Orange_clay	2.20E-16
Molluscs	1.66E-03
Plankforam	5.46E-11
Benthforam	6.22E-09
Glauconite	
Otherbio	2.25E-01
Non_identified	2.20E-16

L2	test
Quartz	0.01534
Ironcoatedquartz	2.44E-15
Mica	5.69E-09
Aggregate	3.25E-05
Other_terr	5.05E-06
Orange_clay	
Molluscs	6.08E-05
Plankforam	2.58E-07
Benthforam	2.86E-03
Glauconite	
Otherbio	7.89E-02
Non_identified	

L3	test
Quartz	0.6581
Ironcoatedquartz	1.16E-13
Mica	2.85E-07
Aggregate	4.79E-04
Other_terr	6.95E-05
Orange_clay	2.08E-13
Molluscs	6.25E-02
Plankforam	7.30E-05
Benthforam	3.25E-02
Glauconite	
Otherbio	6.84E-01
Non_identified	1.09E-14

L4	test
Quartz	0.8433
Ironcoatedquartz	3.72E-14
Mica	1.35E-08
Aggregate	4.16E-02
Other_terr	4.33E-04
Orange_clay	
Molluscs	7.26E-02
Plankforam	2.66E-06
Benthforam	1.82E-01
Glauconite	3.72E-14
Otherbio	1.13E-01
Non_identified	3.72E-14

Annex D: Kruskal-Wallis

L1	KW
Quartz	7.04E-01
Ironcoatedquartz	0.0449
Mica	0.02767
Aggregate	0.2295
Other_terr	0.02744
Orange_clay	0.1496
Molluscs	0.01933
Plankforam	5.95E-01
Benthforam	0.896
Glauconite	
Otherbio	0.3649
Non_identified	0.000345

L2	KW
Quartz	9.33E-01
Ironcoatedquartz	0.4346
Mica	0.7144
Aggregate	0.1195
Other_terr	0.3865
Orange_clay	
Molluscs	0.7506
Plankforam	3.43E-01
Benthforam	0.8194
Glauconite	
Otherbio	0.1684
Non_identified	

L3	KW
Quartz	6.02E-02
Ironcoatedquartz	0.2186
Mica	0.19411
Aggregate	0.2273
Other_terr	0.6873
Orange_clay	0.04281
Molluscs	0.3028
Plankforam	6.02E-01
Benthforam	0.05939
Glauconite	
Otherbio	0.1305
Non_identified	0.1822

L4	KW
Quartz	4.58E-01
Ironcoatedquartz	0.5995
Mica	0.186
Aggregate	0.1195
Other_terr	0.1737
Orange_clay	
Molluscs	0.07208
Plankforam	3.29E-01
Benthforam	0.1959
Glauconite	0.5995
Otherbio	0.01529
Non_identified	0.1292

Annex E: Post-hoc Dunn Test and Bonferroni Adjustment

ADL – ASTARTE defined layers

Sand mineralogical composition	Pairs		stat	p	p.adj	p.sig
				Layer 1		
Iron-coated quartz	AboveADL	BelowADL	0.275	0.784	1	
	AboveADL	ADL	2.13	0.0328	0.0985	
	BelowADL	ADL	1.8	0.0717	0.215	
Mica	AboveADL	BelowADL	-1.46	0.143	0.43	
	AboveADL	ADL	-2.67	0.00756	0.0227	*
	BelowADL	ADL	-0.895	0.371	1	
Other terr.	AboveADL	BelowADL	2.68	0.00745	0.0224	*
	AboveADL	ADL	1.76	0.0777	0.233	

	Pairs		stat	p	p.adj	p.sig
	BelowADL	ADL	-1.48	0.138	0.413	
	AboveADL	BelowADL	2.74	0.00607	0.0182	*
Mollusc	AboveADL	ADL	2.14	0.0321	0.0962	
	BelowADL	ADL	-1.19	0.235	0.705	
	AboveADL	BelowADL	2.85	0.00433	0.013	*
N.I.	AboveADL	ADL	0.309	0.757	1	
	BelowADL	ADL	-3.15	0.00161	0.00483	**

Layer 3						
Sand mineralogical composition	Pairs		stat	p	p.adj	p.sig
	AboveADL	BelowADL	-1.98	0.0481	0.144	
Orange_clay	AboveADL	ADL	-2.35	0.0187	0.056	
	BelowADL	ADL	0.288	0.773	1	

Layer 4						
Sand mineralogical composition	Pairs		stat	p	p.adj	p.sig
	AboveADL	BelowADL	2.89	0.00386	0.0116	*
Other bio	AboveADL	ADL	1.54	0.124	0.372	
	BelowADL	ADL	-1.35	0.177	0.53	

Annex F: R script

```
library(psych)
library(ggplot2)
library(cowplot)
data <- gretldata
###        Data set        ###############################################################
coastal <-  subset(data, Place =="Coastal")
mw107 <- subset (data, MW == "107")
L1 <- subset(mw107, Layer == "L1")
L2 <- subset(mw107, Layer == "L2")
L3 <- subset(mw107, Layer == "L3")
L4 <- subset(mw107, Layer == "L4")
######     Normality test – Shapiro        #############################################
shapiro.test(L1$Quartz)
shapiro.test(L1$Ironcoatedquartz)
shapiro.test(L1$Mica)
shapiro.test(L1$Aggregates)
shapiro.test(L1$Other_terr)
shapiro.test(L1$Orange_clay)
shapiro.test(L1$Mollusc)
shapiro.test(L1$Plankforam)
shapiro.test(L1$Benthforam)
shapiro.test(L1$Glauconite)
shapiro.test(L1$Otherbio)
shapiro.test(L1$Non_identified)
```

```
####        Kruskal wallis test        ###############################################
library(FSA)
kruskal.test(Quartz ~ sample, data = L1)
kruskal.test(Ironcoatedquartz ~ sample, data = L1)
kruskal.test(Mica ~ sample, data = L1)
kruskal.test(Aggregate ~ sample, data = L1)
kruskal.test(Other_terr ~ sample, data = L1)
kruskal.test(Orange_clay ~ sample, data = L1)
kruskal.test(Mollusc ~ sample, data = L1)
kruskal.test(Plankforam ~ sample, data = L1)
kruskal.test(Benthforam ~ sample, data = L1)
kruskal.test(Glauconite ~ sample, data = L1)
kruskal.test(Otherbio ~ sample, data = L1)
kruskal.test(Non_identified ~ sample, data = L1)
#####    Post-hoc        ############################################################
library(rstatix)
dunn_test(Quartz ~ sample, data = L1, p.adjust.method = "bonferroni")
dunn_test(Ironcoatedquartz ~ sample, data = L1, p.adjust.method = "bonferroni")
dunn_test(Mica ~  sample, data = L1, p.adjust.method = "bonferroni")
dunn_test(Aggregate ~ sample, data = L1, p.adjust.method = "bonferroni")
dunn_test(Other_terr ~ sample, data = L1, p.adjust.method = "bonferroni")
dunn_test(Orange_clay ~ sample, data = L1, p.adjust.method = "bonferroni")
dunn_test(Mollusc ~ sample, data = L1, p.adjust.method = "bonferroni")
dunn_test(Plankforam ~ sample, data = L1, p.adjust.method = "bonferroni")
dunn_test(Benthforam ~ sample, data = L1, p.adjust.method = "bonferroni")
dunn_test(Otherbio ~ sample,data = L1, p.adjust.method = "bonferroni")
dunn_test(Non_identified ~ sample, data = L1, p.adjust.method = "bonferroni")
##Plot boxplot              #########################################################
L1$sample <- factor(L1$sample, levels = c("BelowADL", "ADL", "aboveADL"))
qtz <- ggplot(L1, aes(as.factor(sample), Quartz)) +
geom_boxplot(width = 0.3, fill =  c("white"), alpha = 0.8 , colour = "black") +
theme_bw () +
theme(panel.background = element_blank(),
panel.grid.major = element_blank(),
    panel.grid.minor = element_blank()) +
scale_x_discrete(name = NULL) +
scale_y_continuous("Quartz (%)") +
theme(text = element_text(size = 18))+
stat_summary(fun=mean, geom="point", shape=17, size=2, color="orangered1")
iq <- ggplot(L1, aes(as.factor(sample), Ironcoatedquartz)) +
geom_boxplot(width = 0.3, fill =  c("white"), alpha = 0.8 , colour = "black") +
theme_bw () +
theme(panel.background = element_blank(),
panel.grid.major = element_blank(),
    panel.grid.minor = element_blank()) +
scale_x_discrete(name = NULL) +
scale_y_continuous("I.Q.C (%)") +
theme(text = element_text(size = 18))+
stat_summary(fun=mean, geom="point", shape=17, size=2, color="orangered1")
mica <- ggplot(L1, aes(as.factor(sample), Mica)) +
geom_boxplot(width = 0.3, fill =  c("white"), alpha = 0.8 , colour = "black") +
theme_bw () +
theme(panel.background = element_blank(),
panel.grid.major = element_blank(),
    panel.grid.minor = element_blank()) +
scale_x_discrete(name = NULL) +
```

```
scale_y_continuous("Mica (%)") +
theme(text = element_text(size = 18))+
stat_summary(fun=mean, geom="point", shape=17, size=2, color="orangered1")
ag <- ggplot(L1 aes(as.factor(sample),Aggregate)) +
geom_boxplot(width = 0.3, fill = c("white"), alpha = 0.8 , colour = "black") +
theme_bw () +
theme(panel.background = element_blank(),
panel.grid.major = element_blank(),
    panel.grid.minor = element_blank()) +
scale_x_discrete(name = NULL) +
scale_y_continuous("Aggregate (%)") +
theme(text = element_text(size = 18))+
stat_summary(fun=mean, geom="point", shape=17, size=2, color="orangered1")
ot <- ggplot(L1 aes(as.factor(sample),Other_terr)) +
geom_boxplot(width = 0.3, fill = c("white"), alpha = 0.8 , colour = "black") +
theme_bw () +
theme(panel.background = element_blank(),
panel.grid.major = element_blank(),
    panel.grid.minor = element_blank()) +
scale_x_discrete(name = NULL) +
scale_y_continuous("Other_terr (%)") +
theme(text = element_text(size = 18))+
stat_summary(fun=mean, geom="point", shape=17, size=2, color="orangered1")
ot2 <- ggplot(L1, aes(as.factor(sample), Orange_clay)) +
geom_boxplot(width = 0.3, fill = c("white"), alpha = 0.8 , colour = "black") +
theme_bw () +
theme(panel.background = element_blank(),
panel.grid.major = element_blank(),
    panel.grid.minor = element_blank()) +
scale_x_discrete(name = NULL) +
scale_y_continuous("Orange_clay (%)") +
theme(text = element_text(size = 18))+
stat_summary(fun=mean, geom="point", shape=17, size=2, color="orangered1")
mo <- ggplot(L1 aes(as.factor(sample), Mollusc)) +
geom_boxplot(width = 0.3, fill = c("white"), alpha = 0.8 , colour = "black") +
theme_bw () +
theme(panel.background = element_blank(),
panel.grid.major = element_blank(),
    panel.grid.minor = element_blank()) +
scale_x_discrete(name = NULL) +
scale_y_continuous("Mollusc (%)") +
theme(text = element_text(size = 18))+
stat_summary(fun=mean, geom="point", shape=17, size=2, color="orangered1")

pla<- ggplot(L1 aes(as.factor(sample), Plankforam )) +
geom_boxplot(width = 0.3, fill = c("white"), alpha = 0.8 , colour = "black") +
theme_bw () +
theme(panel.background = element_blank(),
panel.grid.major = element_blank(),
    panel.grid.minor = element_blank()) +
scale_x_discrete(name = NULL) +
scale_y_continuous("Plankforam  (%)") +
theme(text = element_text(size = 18))+
stat_summary(fun=mean, geom="point", shape=17, size=2, color="orangered1")
bent<- ggplot(L1 aes(as.factor(sample), Benthforam)) +
geom_boxplot(width = 0.3, fill = c("white"), alpha = 0.8 , colour = "black") +
```

```
theme_bw () +
theme(panel.background = element_blank(),
panel.grid.major = element_blank(),
     panel.grid.minor = element_blank()) +
scale_x_discrete(name = NULL) +
scale_y_continuous("Benthforam (%)") +
theme(text = element_text(size = 18))+
stat_summary(fun=mean, geom="point", shape=17, size=2, color="orangered1")
ob<- ggplot(L1, aes(as.factor(sample), Otherbio)) +
geom_boxplot(width = 0.3, fill =  c("white"), alpha = 0.8 , colour = "black") +
theme_bw () +
theme(panel.background = element_blank(),
panel.grid.major = element_blank(),
     panel.grid.minor = element_blank()) +
scale_x_discrete(name = NULL) +
scale_y_continuous("Otherbio (%)") +
theme(text = element_text(size = 18))+
stat_summary(fun=mean, geom="point", shape=17, size=2, color="orangered1")
gl<- ggplot(L1, aes(as.factor(sample), Glauconite)) +
geom_boxplot(width = 0.3, fill =  c("white"), alpha = 0.8 , colour = "black") +
theme_bw () +
theme(panel.background = element_blank(),
panel.grid.major = element_blank(),
     panel.grid.minor = element_blank()) +
scale_x_discrete(name = NULL) +
scale_y_continuous("Glauconite (%)") +
theme(text = element_text(size = 18))+
stat_summary(fun=mean, geom="point", shape=17, size=2, color="orangered1")
ni<- ggplot(L1 aes(as.factor(sample), Non_identified)) +
geom_boxplot(width = 0.3, fill =  c("white"), alpha = 0.8 , colour = "black") +
theme_bw () +
theme(panel.background = element_blank(),
panel.grid.major = element_blank(),
     panel.grid.minor = element_blank()) +
scale_x_discrete(name = NULL) +
scale_y_continuous("N.I. (%)") +
theme(text = element_text(size = 18))+
stat_summary(fun=mean, geom="point", shape=17, size=2, color="orangered1")
```

Annex G: Age estimations ASTARTE Project (Subtask WP2.2)

Depth (cm)	Material	Conventinal Age	Calibrated Age
28.5	Shell	1380 +/- 40 BP	Cal 900 - 960 AD
68.5	Shell	3380+/- 40 BP	Cal 1740 - 1620 BCE
90.5	Shell + gastropods	5260+/- 30 BP	Cal 4230 - 4200 BCE Cal 4170 - 4090 BCE Cal 4080 - 3980 BCE
110.5	Shell	5600 +/- 30 BP	Cal 3945 to 3590 BCE